JPL Publication 92-7

Theory of Post-Block II VLBI Observable Extraction

Stephen T. Lowe

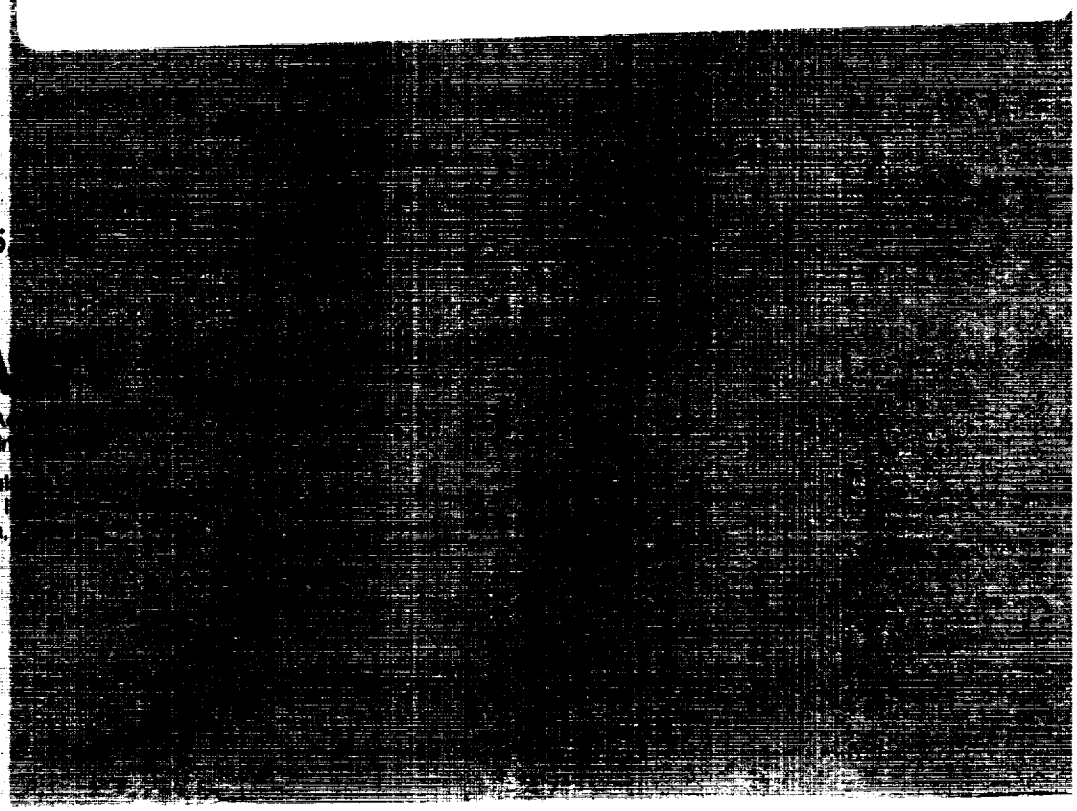

July 15

National A
Space Adm

Jet Propul
California I
Pasadena,

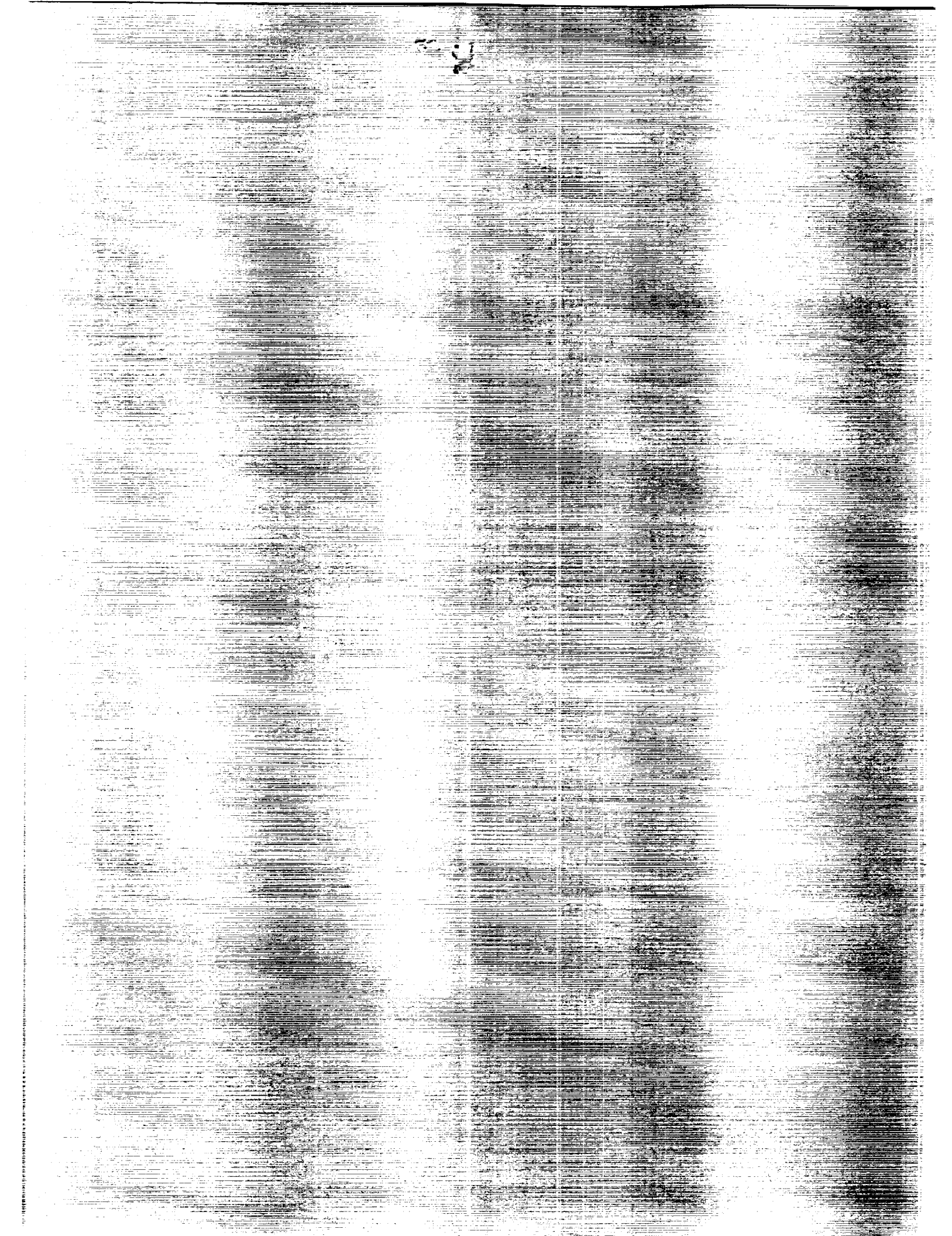

JPL Publication 92-7

Theory of Post-Block II VLBI Observable Extraction

Stephen T. Lowe

July 15, 1992

National Aeronautics and
Space Administration

Jet Propulsion Laboratory
California Institute of Technology
Pasadena, California

The research described in this publication was carried out by the Jet Propulsion Laboratory, California Institute of Technology, under a contract with the National Aeronautics and Space Administration.

Abstract

This report describes the algorithms used in the post-Block II fringe-fitting software called "Fit." The steps needed to derive the VLBI charged-particle corrected group delay, phase delay rate, and phase delay (the latter without resolving cycle ambiguities) are presented beginning with the set of complex fringe phasors as a function of observation frequency and time. The set of complex phasors is obtained from the JPL/CIT Block II correlator. The output of Fit is the set of charged-particle corrected observables (along with ancillary information) in a form amenable to the software program "Modest."

Acknowledgments

Much of this work is a result of my collaboration with Robert Treuhaft on detecting planetary gravitational deflection. That project motivated my writing Fit, and I thank Bob for a great deal of insight and feedback over the 2–3 years we worked on that project. Dave Fort deserves thanks for his numerous explanations and checks of the Block II software and hardware which were necessary for a working version of Fit. I would also like to thank Chris Jacobs and Robert Coker for their feedback on Fit's performance and some editing of this report, and Ojars Sovers for his help with Modest.

Table of Contents

Figure Captions

List of Tables

Section 1

Introduction

This report presents the theoretical basis for the post-Block II fringe fitting data analysis used in very long baseline interferometry (VLBI). The overall goal of this analysis is to extract unbiased physical observables for each observation scan, namely the charged particle corrected bandwidth synthesis (BWS) delay, phase delay rate and phase delay (when cycle ambiguity resolution is possible), directly from the Block II correlation coefficients. These observables are typically combined with those from other scans and passed to the fitting program Modest[1] (formerly called Masterfit) for further analysis.

By design, much of the material in this report is independent of a specific software implementation. However, where choices in computer memory allocation or processing time influence the analysis, this report will refer specifically to the program Fit and its solutions to the various data analysis problems. As experience with Mark III data increases and as better computational resources become available, detailed improvements will be developed and implemented in Fit. Although some details of the implementation may change as future improvements are made, the majority of the material presented here should remain current.

The Block II processor is a VLBI correlator developed at JPL and the California Institute of Technology. A detailed description of this processor can be found in references 2 and 3. The Block II is capable of correlating both Mark II and Mark III data formats[3], although this report will concentrate on the Mark III data type because its higher data rate makes it much more desirable for high accuracy work (Fit is able to process Mark II data and much of the material presented in this report is valid for both data types).

Some aspects of post-Block II data analysis have been described in reference 2; however, at the time of its writing, the Block II was expected to include a hardware device named Tensor. This device was designed to perform the Fast Fourier Transforms needed in the data analysis described in sections 6 through 11 in this report and section 13 in the reference. Work on Tensor was abandoned before its completion, leaving the post-Tensor

software, named Restore, without an input route, except for a software emulator of the Tensor hardware. This software emulator was designed for debugging Tensor during its construction, and not for data analysis. Thus, except for the software emulator of the Tensor hardware in combination with Restore, no route from the Block II processor to VLBI observables existed.

Because Tensor's function would eventually have to be performed by post-correlation software, the opportunity to drop many restrictions and approximations required for such a hardware device was exploited. This report presents these new analysis steps, along with all those needed to obtain the final observables from the Block II output, and their theoretical justification. The material presented here can be roughly divided into three tasks: a) obtaining an a priori estimate of residual delay, phase delay rate and phase for each observation band, b) calculating accurate corrections to the a priori estimates using phase tracking and linear least-squares parameter estimation, and c) combining these estimates with the correlator model and applying charged-particle corrections to obtain the final observables. Each of these tasks is divided into several topics which are covered in detail by each section of this report. Sections 2–5 cover some preliminary calculations necessary to the analysis, sections 6–11 discuss the a priori calculation, sections 12–15 are concerned with parameter estimation, sections 16–18 pertain to the final observable estimates and section 19 covers the Modest interface. Appendices A and B describe specific calculations in more detail than that found in the text, appendix C gives the mathematical definitions of special variables used extensively in the least-squares analysis and charged-particle calibration, and appendix D presents a complete list of variable definitions.

The Phase Sign Convention Used in this Report

Because observables extracted from the Block II output are passed to Modest, the sign convention of both must be treated explicitly. The Block II's phase sign convention is station 1 phase minus station 2 phase, while Modest's is the reverse. Most expressions in this report are valid in either sign convention as long as all quantities are in the same system. However, the Block II convention is implicitly assumed for all residual observables because

these are derived more directly from the correlator output; total observables, because they are passed to Modest, are assumed to be in the Modest system. This separation of the two sign conventions corresponds to that used by Fit. In this report, the Block II system is used up through section 15 and the Modest convention is used in sections 16 to 20.

Section 2

Correlation Coefficients and Error Analysis

This section presents expressions for the complex correlation coefficients and their errors as a function of the number of Block II accumulation counts: the Block II counts are the raw inputs to Fit. Expressions relating correlation coefficient errors to phase and amplitude errors are also given. Finally, the variance of instrumental phase calibration phasors and their effect on the calibrated cross-correlation data are derived.

The Frequency Domain Correlation Coefficient and its Variance

The delayed bitstreams from each station at the correlator are multiplied together and counterrotated[2] in quadrature for a number of lags, typically eight. A Fourier Transform (FT) is performed to transform these lag-domain correlation coefficients to the frequency domain. These final frequency domain correlation coefficients are the primary correlator output passed to Fit. The frequency domain correlation coefficients for bin b, $\vec{\rho}_b(t)$, can be written

$$\vec{\rho}_b(t) = \frac{1}{N_L} \sum_{l=0}^{N_L-1} \vec{\rho}_l(t) e^{-2\pi i \frac{bl}{N_L}} \qquad [2.1]$$

where the sum over lag shows the FT explicitly, $\vec{\rho}_l(t)$ is the complex correlation coefficient for lag l after fringe counterrotation at time t and N_L is the number of lags. Both b and l are integers ranging from 0 to $N_L - 1$. For the typical case of eight lags and a sample rate of 4 MHz, each of the eight bins has a nominal width of $4\,\mathrm{MHz}/N_L = 0.5$ MHz. Because the channels are single-sideband, four of the eight bins contain noise and are ignored by Fit. After expanding the real and imaginary parts of [2.1], the variance of $\vec{\rho}_b(t)$ can be written

$$\mathrm{Var}[\mathrm{Re}\,\vec{\rho}_b(t)] = \frac{1}{{N_L}^2} \sum_{l=0}^{N_L-1} \left[\mathrm{Var}[\mathrm{Re}\,\vec{\rho}_l(t)] \cos^2\left(\frac{2\pi bl}{N_L}\right) + \mathrm{Var}[\mathrm{Im}\,\vec{\rho}_l(t)] \sin^2\left(\frac{2\pi bl}{N_L}\right) \right] \qquad [2.2]$$

$$\mathrm{Var}[\mathrm{Im}\,\vec{\rho}_b(t)] = \frac{1}{{N_L}^2} \sum_{l=0}^{N_L-1} \left[\mathrm{Var}[\mathrm{Im}\,\vec{\rho}_l(t)] \cos^2\left(\frac{2\pi bl}{N_L}\right) + \mathrm{Var}[\mathrm{Re}\,\vec{\rho}_l(t)] \sin^2\left(\frac{2\pi bl}{N_L}\right) \right].$$

This step assumes each real and imaginary component is statistically independent of every other component, real or imaginary, as derived in Reference 4 (this has been tested by measuring the autocorrelation of the Block II bitstreams[5]). The lag domain correlation coefficient after counterrotation (also called lobe rotation), $\vec{\rho}_l(t)$, can be expressed in terms of the correlation coefficient before counterrotation as

$$\vec{\rho}_l(t) = \sum_{j=1}^{V} \beta_l(t_j^b) e^{-i\phi_j^{fm}} \qquad [2.3]$$

where $\beta_l(t_j^b)$ is lag l's single-bit correlation coefficient before lobe rotation, ϕ_j^{fm} is the model fringe phase, t_j^b is the time tag of the jth bit in the sum and V is the total number of bits in the sum, typically around 8×10^6 for two-second integrations. Assuming the observed bandwidth is not oversampled and no DC bias exists (so that each bit is statistically independent and each component of the correlation coefficients has zero mean), the variance of the real and imaginary parts of $\vec{\rho}_l(t)$ can be written

$$\mathrm{Var}[\mathrm{Re}\,\vec{\rho}_l(t)] = \sum_{j=1}^{V} \mathrm{Var}[\beta_l(t_j^b)] \cos^2 \phi_j^{fm} \qquad [2.4]$$

$$\mathrm{Var}[\mathrm{Im}\,\vec{\rho}_l(t)] = \sum_{j=1}^{V} \mathrm{Var}[\beta_l(t_j^b)] \sin^2 \phi_j^{fm}.$$

Equations [2.4] can be evaluated from the variance of the like and unlike-sign counts which are binomially distributed. For the digital three-level lobe rotator used in the Block II correlator, the $\cos^2 \phi_j^{fm}$ and $\sin^2 \phi_j^{fm}$ terms will be $+1$ when not blanked and zero when blanked (see references 2 and 6 for more detail on lobe rotation). For an interval of V bits, the real and imaginary components of equation [2.3] become

$$\mathrm{Re}\,\vec{\rho}_l(t) = \frac{(L_x - U_x)}{V} = \frac{(2L_x + B_x - V)}{V} \qquad [2.5]$$

$$\mathrm{Im}\,\vec{\rho}_l(t) = \frac{(L_y - U_y)}{V} = \frac{(2L_y + B_y - V)}{V},$$

where $V = L_x + U_x + B_x = L_y + U_y + B_y$ and $L_{x(y)}$ and $U_{x(y)}$ are the number of like and unlike-sign counts of the real (imaginary) component of $\vec{\rho}_l$ (commonly referred to as the cosine (sine) accumulation) and $B_{x(y)}$ is the number of blanked bits in the interval. From [2.5], the variance of the $x(y)$ component of $\vec{\rho}_l$ is $4/V^2$ times the variance of $L_{x(y)}$. Using the binomial distribution's expression for the unbiased variance estimate of the number of successes in $V - B_x$ trials, given the actual number of successes is L_x, gives

$$\mathrm{Var}[\mathrm{Re}\,\vec{\rho}_l(t)] = \frac{4}{V^2}\Big(\frac{V - B_x}{V - B_x - 1}\Big)(V - B_x)\Big(\frac{L_x}{V - B_x}\Big)\Big(1 - \frac{L_x}{V - B_x}\Big), \qquad [2.6]$$

with a similar expression for the variance of the imaginary component of $\vec{\rho}_l$. Solving the first equation in [2.5] for L_x and substituting leads to

$$\mathrm{Var}[\mathrm{Re}\,\vec{\rho}_l(t)] = \frac{V - B_x}{V^2}\Big(\frac{V - B_x}{V - B_x - 1}\Big)\Big[1 - \Big(\frac{V}{V - B_x}\Big)^2[\mathrm{Re}\,\vec{\rho}_l(t)]^2\Big]. \qquad [2.7]$$

Using $V - B_{x(y)} \gg 1$, $|\vec{\rho}_l| \ll 1$ and the imaginary component analog to [2.7] gives, to very good approximation

$$\mathrm{Var}[\mathrm{Re}\,\vec{\rho}_l(t)] \simeq \mathrm{Var}[\mathrm{Im}\,\vec{\rho}_l(t)] \simeq \frac{V - B}{V^2}, \qquad [2.8]$$

where B is the average of the blanking counts for the sine and cosine accumulations; for typical 2-second integration intervals and several KHz fringe rates, the two blanking counts are nearly identical. Finally, substituting this into equations [2.2] leads to

$$\sigma^2 \equiv \mathrm{Var}[\mathrm{Re}\,\vec{\rho}_b(t)] \simeq \mathrm{Var}[\mathrm{Im}\,\vec{\rho}_b(t)] \simeq \frac{V - B}{N_L V^2}, \qquad [2.9]$$

where σ^2 is the variance of either component of $\vec{\rho}_b$. This shows the system noise associated with a given fringe phasor depends only on the number of processed bits and number of lags (given the above approximations). For the Block II lobe rotator, $B \approx V/4$ so

$$\sigma^2 \simeq \frac{3}{4N_L V}. \qquad [2.10]$$

Expressing the Correlation Coefficients and their Variances in terms of Correlator Output

For each dump interval, the Block II correlator passes the user the like-sign and blanking counts for the sine and cosine accumulations along with the invalid counts. The invalid counts were ignored in the above analysis but can be included by interpreting V as the number of valid counts: the total number of bits, N, minus the invalid count, I. The real component of the correlation coefficient can be written as (see [2.5])

$$\begin{aligned} \mathrm{Re}\,\vec{\rho}_l &= \frac{L_x - U_x}{N - I} \\ &= \frac{2L_x - N + I + B_x}{N - I}, \end{aligned} \qquad [2.11]$$

with a similar expression for the imaginary component. The Block II correlator hardware has a flip-flop circuit before each accumulator which results in the counts sent to the user being only half the expected value. Therefore, $\hat{L}_{x(y)} = L_{x(y)}/2$, $\hat{B}_{x(y)} = B_{x(y)}/2$ and $\hat{I} = I/2$ where the hat ($\hat{}$) represents quantities passed to the user by the correlator (the correlator accumulator flip-flop circuits alternately begin with 0 or 1 to avoid inducing a bias, on average). Thus,

$$\begin{aligned} \mathrm{Re}\,\vec{\rho}_l &= \frac{\hat{L}_x - N/4 + \hat{I}/2 + \hat{B}_x/2}{N/4 - \hat{I}/2} \\ &= \frac{\hat{L}_x - Z_x}{M}, \end{aligned} \qquad [2.12]$$

where $Z_x = N/4 - \hat{B}_x/2 - \hat{I}/2$ is a DC bias and $M = N/4 - \hat{I}/2$ is a normalization factor (Z_x is a DC bias in the sense that the Block II hardware accumulators can only increment, and must therefore be offset by Z_x, so the cosine accumulator contains $\hat{L}_x - Z_x$, for example). The expression for the imaginary component of $\vec{\rho}_l$ is similar. After the lag FT, given by [2.1], the fringe phasor is

$$\vec{\rho}_b \equiv (\rho_x, \rho_y) = \left(\frac{\hat{C}}{N/4 - \hat{I}/2}, \frac{\hat{S}}{N/4 - \hat{I}/2}\right) = \left(\frac{\hat{C}}{M}, \frac{\hat{S}}{M}\right), \qquad [2.13]$$

where $\hat{S}$ and $\hat{C}$ are the like-sign sine and cosine counts from the correlator (the Block II can process data in either "lag" or "bin" mode; the sine and cosine counts passed to the user are given by $\hat{L}_x$ and $\hat{L}_y$ in equation [2.12] when in lag mode, and $\hat{C}$ and $\hat{S}$ in [2.13] when in bin mode, which is the mode assumed in this report; in both cases, $\hat{C}$ and $\hat{S}$ are integers, because, when in bin mode, [2.1] is calculated using integer arithmetic). The error on each component, obtained from [2.9] above, is

$$\sigma^2 = \frac{N - I - B}{N_L(N-I)^2} = \frac{V - 2\hat{B}}{N_L V^2} = \frac{M - \hat{B}/2}{4N_L M^2} \qquad [2.14]$$

where $V \equiv N - 2\hat{I} = 4M$. The software program Fit uses [2.13] to calculate the correlation coefficients and [2.14] to calculate the distribution variance, with $\hat{B}$ equal to the numerical average of the sine and cosine blanking accumulations, as noted above.

Because of the large number of bits processed by the Block II for each phasor in a typical two-second dump, usually about 8×10^6, and the inherently small correlation coefficient, the central limit theorem implies the probability distribution of either component of $\vec{\rho}_b$ is normal to very high accuracy. The real and imaginary components of $\vec{\rho}_b(t)$ are therefore independent, as proved in Reference 4, and have a Gaussian probability distribution. The means of the real and imaginary components, ρ_x and ρ_y, are the components of $\vec{\rho}_b$ given in equation [2.13] and σ^2 is the variance of either component as defined in [2.14].

Phase and Amplitude Distributions and Variances

Given the Gaussian probability distributions for the real and imaginary part of the fringe phasor, with means and variances given by [2.13] and [2.14] above, it is possible to change variables to derive the distribution for the phase and amplitude. Appendix A contains a complete derivation of the phase and amplitude probability distributions which are summarized below. Defining $\phi \equiv \arctan(\rho_y, \rho_x)$ and $A^2 \equiv \rho_x^2 + \rho_y^2$ for a given bin, the

phase distribution, $P(\phi)$, mean phase, $\langle\phi\rangle$, and phase variance, σ_ϕ^2, are given by

$$P(\phi) = \frac{1}{2\pi} e^{\frac{-R^2}{2\sigma^2}} \left[1 + \sqrt{\frac{\pi}{2}} \frac{R}{\sigma} \cos(\phi - \phi^R) e^{\frac{R^2 \cos^2(\phi-\phi^R)}{2\sigma^2}} \left(1 + \text{erf} \frac{R\cos(\phi - \phi^R)}{\sqrt{2}\sigma} \right) \right] \quad [2.15a]$$

$$\langle\phi\rangle = \phi^R \quad [2.15b]$$

$$\sigma_\phi^2 = \frac{\pi^2}{3} e^{\frac{-R^2}{2\sigma^2}} + \frac{R}{\sqrt{2\pi}\sigma} \int_0^\pi d\theta\, \theta^2 \cos\theta\, e^{\frac{-R^2 \sin^2\theta}{2\sigma^2}} \left(1 + \text{erf} \frac{R\cos\theta}{\sqrt{2}\sigma} \right) \quad [2.15c]$$

where ϕ^R and R are the polar coordinates of the parent probability distribution's center (see below). The amplitude distribution, mean, and variance are given by

$$P(A) = \frac{A}{\sigma^2} e^{\frac{-(R^2+A^2)}{2\sigma^2}} I_0\left(\frac{AR}{\sigma^2}\right) \quad [2.16a]$$

$$\langle A\rangle = \sqrt{\frac{\pi}{2}}\sigma e^{\frac{-R^2}{4\sigma^2}} \left[\left(1 + \frac{R^2}{2\sigma^2}\right) I_0\left(\frac{R^2}{4\sigma^2}\right) + \frac{R^2}{2\sigma^2} I_1\left(\frac{R^2}{4\sigma^2}\right) \right] \quad [2.16b]$$

$$\sigma_A^2 = R^2 + 2\sigma^2 - \frac{\pi}{2}\sigma^2 e^{\frac{-R^2}{2\sigma^2}} \left[\left(1 + \frac{R^2}{2\sigma^2}\right) I_0\left(\frac{R^2}{4\sigma^2}\right) + \frac{R^2}{2\sigma^2} I_1\left(\frac{R^2}{4\sigma^2}\right) \right]^2 \quad [2.16c]$$

where I_0 and I_1 are modified Bessel functions of zero and first order. Table 2.1 shows some of these expressions for the no signal, weak signal and strong signal limits. Figure 2.1 shows σ_ϕ plotted as a function of R/σ along with the weak and strong signal limits. Note that R/σ is defined to be the signal to noise ratio (SNR) for a given phasor.

In the above expressions, a careful distinction between R and A should be made. The parent probability distribution for $\vec{\rho}_b$ is a two-dimensional Gaussian centered at polar coordinates (R, ϕ^R). In the no-signal case, R is zero. The amplitude of a given phasor, A, drawn from the parent distribution will always be non-negative, even in the no-signal case. Thus A is a biased estimate of R as seen in [2.16b] or the first row of Table 2.1. Figure 2.2 shows $\langle A\rangle/\sigma$ as a function of R/σ.

EXPRESSIONS FOR $\langle A \rangle$, σ_A AND σ_ϕ IN LIMITING CASES			
Statistic	White Noise	Weak Signal	Strong Signal
$\langle A \rangle$	$\sigma\sqrt{\frac{\pi}{2}}$	$\sigma\sqrt{\frac{\pi}{2}}(1+\frac{R^2}{4\sigma^2})$	$R(1+\frac{\sigma^2}{2R^2})$
σ_A	$\sigma\sqrt{2-\frac{\pi}{2}}$	$\sigma\sqrt{2-\frac{\pi}{2}}(1+\frac{R^2}{4\sigma^2})$	$\sigma(1-\frac{\sigma^2}{4R^2})$
σ_ϕ	$\frac{\pi}{\sqrt{3}}$	$\frac{\pi}{\sqrt{3}}(1-\sqrt{\frac{9}{2\pi^3}}\frac{R}{\sigma})$	σ/R

Table 2.1 Expressions for the mean amplitude, amplitude sigma and phase sigma in the no signal, weak signal and strong signal cases. R is defined in the text and σ is given by [2.14].

Error Analysis of Instrumental Phase Calibration Data

Instrumental phase calibration tones are injected near the front of the station electronics. These tones traverse the same instrumentation as the actual data so phase or delay instabilities induced by the electronics at each station can be analyzed (see section 4 of this report, and references 2, 5 and 7 for more detail). The Block II lobe rotates the bitstream from each station in quadrature by a model of the tone phase, for each tone. The counterrotated bitstreams are summed over many bits, typically 8×10^6, to raise the SNR. This process is similar to the cross-correlation counterrotation except instead of a 3-level digital lobe rotator, the tone lobe rotator uses 128 levels. Following similar arguments as above (equations [2.3] through [2.10]), the variance of station i's tone phasor is

$$\sigma^2_{t_i} \equiv \mathrm{Var}[\mathrm{Re}\,\vec{\rho}_{t_i}(t)] \simeq \mathrm{Var}[\mathrm{Im}\,\vec{\rho}_{t_i}(t)] \simeq \frac{1}{2V_{t_i}}, \qquad [2.17]$$

where $\vec{\rho}_{t_i}$ is station i's tone phasor and V_{t_i} is the number of valid tone counts. This result is analogous to [2.10] above; N_L is 1 because there is only one "lag" for tone processing and the $\frac{1}{2}$ compared to $\frac{3}{4}$ is the result of better modeling of the sine and cosine functions

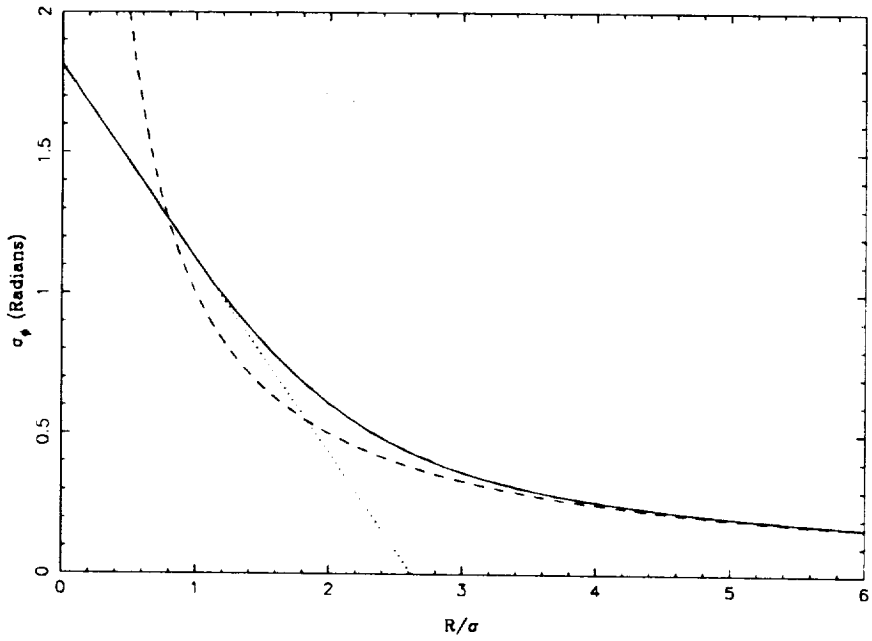

Fig. 2.1 Plot of σ_ϕ as a function of R/σ (solid). The strong signal limit (dashed) and weak signal limit (dotted) are also shown.

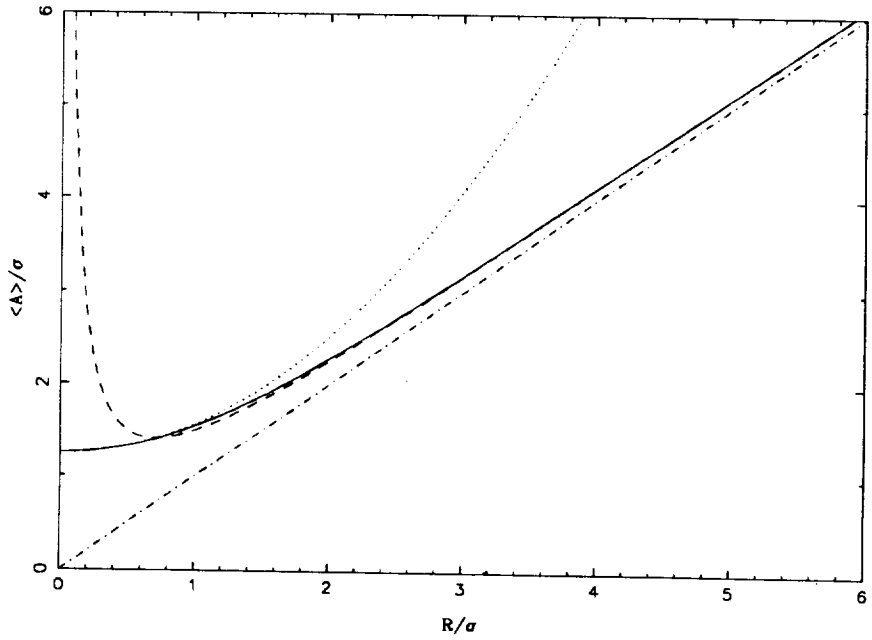

Fig. 2.2 Plot of $\langle A \rangle / \sigma$ as a function of R/σ (solid). The strong signal limit (dashed), weak signal limit (dotted) and $\langle A \rangle = R$ (dot-dashed) lines are also shown.

for tone lobe rotation (these factors come from averaging $\sin^2\phi_j^{fm}$ and $\cos^2\phi_j^{fm}$ for the lobe rotation model in the cross-correlation data and similar factors for the tone models).

When calculating [2.17] from the correlator output, multiplexing of the tone lobe rotator must be considered. The tone lobe rotator is time multiplexed over 4 tones (no multiplexing is done for the cross-correlation lags), resulting in hardware counts from the correlator being a factor of 4 smaller than otherwise expected. The analogous expression to [2.14] for each station is

$$\sigma_{t_i}^2 = \frac{1}{2(N - 8\hat{I}_{t_i})}, \qquad [2.18]$$

where $\sigma_{t_i}^2$ is the variance of either tone phasor component, $\hat{I}_{t_i}$ is the station tone invalid count and the 8 results from a factor of 2 for the flip-flop circuit and 4 from multiplexing.

One option in Fit is to have each cross-correlation phasor counterrotated by the appropriate tone phasor from either one or both stations (section 4 covers this procedure in more detail). After calibrating the cross-correlation phasor by counterrotation, the resulting phasor has variance given by (see [4.3])

$$\sigma^2 \leftarrow \sigma^2 + \left(\frac{A}{A_{t_1}}\right)^2 \sigma_{t_1}^2 + \left(\frac{A}{A_{t_2}}\right)^2 \sigma_{t_2}^2, \qquad [2.19]$$

where the 1 and 2 refer to the two stations, A is the cross-correlation amplitude, A_{t_i} is the station i tone amplitude, and σ^2 and $\sigma_{t_i}^2$ are given by [2.14] and [2.18]. If the tone data are used for calibration, the replacement indicated by equation [2.19] should be assumed implicitly in place of [2.14].

Section 3

Band Reference Time and Frequency

A reference frequency for each observation band and an overall scan reference time are necessary at many stages of the analysis. The expressions for these references are summarized here because they are needed immediately for the a priori calculation; derivations are postponed to later sections where necessary supporting material is given (see sections 14 and 17). Additional reference frequencies are required for each band and each observable (BWS delay, phase delay rate and phase delay) for the charged particle calibration described in section 17; expressions and derivations for these frequencies can be found there.

The scan reference time, t_0, is the only time reference necessary in the analysis and is given by (see [14.11] and Appendix C)

$$t_0 = \frac{\sum_{ij}^{(X)} \frac{\omega_i t_j}{\sigma^2_{\phi_{ij}}}}{\sum_{ij}^{(X)} \frac{\omega_i}{\sigma^2_{\phi_{ij}}}} \equiv \frac{X_5}{X_1}, \qquad [3.1]$$

where i runs over all frequency bins in the highest frequency band (assumed to be X band), j runs over all time points, t_i, ω_i is bin i's observation frequency, $\sigma^2_{\phi_{ij}}$ is the phase variance given by equation [2.15c], and X_5 and X_1 are the X-band counterparts to the expressions given by [C.1]. Missing or bad data points are implicitly excluded from the sums.

The X-band reference frequency is given by (see [14.12] and Appendix C)

$$\omega_{0X} = \frac{X_{19} - t_0 X_{16}}{X_{09} - 2t_0 X_{06} + t_0^2 X_{02}} \equiv \frac{X_{t3}}{X_{t0}}, \qquad [3.2]$$

with a similar expression for other observation bands (ω_{0S} is the S-band reference frequency and ω_0 is a generic band's reference frequency, for example), and the undefined quantities

are given by [C.3] and [C.10]. If t_0 is defined as in [3.1], this expression for the highest frequency band simplifies to

$$\omega_{0X} = \frac{\sum_{ij}^{(X)} \frac{\omega_i}{\sigma^2_{\phi_{ij}}}}{\sum_{ij}^{(X)} \frac{1}{\sigma^2_{\phi_{ij}}}} = \frac{X_1}{X_0}. \qquad [3.3]$$

The above expressions are evaluated early in the analysis to give a preliminary t_0 and ω_0 used in the a priori calculation. After the phasor time integration, described in section 12, these expressions are reevaluated because some phasors may have been combined or eliminated, changing the summations. The new t_0 and ω_0's calculated there are the final values for these references. The change in these references caused by their reevaluation induces implicit shifts in the a priori delay, phase delay rate and phase which must be accounted for, as described in the last subsection of section 12.

Section 4

Instrumental Phase Calibration

The instrumental phase calibration tones injected near the front-end of the station electronics are processed by the Block II correlator by counterrotating the bitstreams from each station by a tone phase model[7]. Residual phases about this model are passed to the user as like-sign sine and cosine sums. The counterrotated tone phasors for station i are calculated similarly to [2.12] since there is no lag FT:

$$\vec{\rho}_{t_i} = \frac{64}{63}\left(\frac{\hat{C}_{t_i} - M_{t_i}}{M_{t_i}}, \frac{\hat{S}_{t_i} - M_{t_i}}{M_{t_i}}\right), \qquad [4.1]$$

where $M_{t_i} = N/16 - \hat{I}_{t_i}/2$ is the tone normalization, $\hat{C}_{t_i}$, $\hat{S}_{t_i}$ and $\hat{I}_{t_i}$ are the sine, cosine and invalid tone counts directly from the Block II, and N is the total number of bits processed. The factor of 64/63 is the result of hardware accumulator offsets.[5] The variance of each phasor component is given by [2.18].

The cross-correlation phases are corrected by counterrotating by the phase of the counterrotated tone phasors, for each bin and integration interval. The Block II is capable of performing this correction automatically every 25 milliseconds. The disadvantage of this operation is that the user cannot reconstruct the counterrotation on that time scale for post-correlation analysis; the Block II only passes the tone counts each dump interval, typically every two seconds. To have more complete control over the analysis, Fit allows the user to apply the two-second tone phasors to the cross-correlation data in software rather than during correlation. Actually, Fit allows the processing of any combination of the three available data types for each baseline: the cross-correlation data and the tone data from each of the two stations. This also allows detailed study of the tone data alone before its application to the cross-correlation data. The equations expressing the combined phasors' components and variances in terms of the cross-correlation and tone data are

$$\phi \leftarrow \phi - \phi_{t_1} + \phi_{t_2} \qquad [4.2a]$$

$$A \leftarrow A \qquad [4.2b]$$

$$\sigma \leftarrow A\nu \qquad [4.2c]$$

where

$$\nu^2 \equiv \left(\frac{\sigma}{A}\right)^2 + \left(\frac{\sigma_{t_1}}{A_{t_1}}\right)^2 + \left(\frac{\sigma_{t_2}}{A_{t_2}}\right)^2, \qquad [4.3]$$

(A, ϕ) and (A_{t_i}, ϕ_{t_i}) are the polar coordinates of the cross-correlation and station i tone phasors, and σ^2 and $\sigma_{t_i}^2$ are the cross-correlation and tone variances. If the tone data are used for calibration, the replacements indicated by equations [4.2] should be assumed implicitly in place of the uncalibrated variables. Equations [4.2a], [4.2c] and [4.3] are applicable for any combination of cross-correlation and tone data if one sets $\phi = \sigma = 0$ when cross correlation data is not desired in the combination, and $\phi_{t_i} = \sigma_{t_i} = 0$ when station i tone data is not wanted. Equation [4.2b] is applicable only when cross-correlation data are in the combination; otherwise $A \leftarrow \sqrt{A_{t_1} A_{t_2}}$ when tone data from both stations is selected or $A \leftarrow A_{t_i}$ when just station i is used. These calibrated phasors are now processed without regard to the data type(s) in the combination except for the phasor time integration, explained in section 12, which involves summing the cross-correlation and station data before combining them as described here.

Section 5

Manual (Self) Phase Calibration

Each of the Mark III video converters introduces an arbitrary phase in the channel it records. In addition, instrumental phase non-linearities across the 2 MHz bandpass induce phase offsets for each bin in a given channel. These phase offsets can be calibrated with instrumental phase calibration discussed in the previous section or they can be calibrated by the method presented here, or both methods may be used. If these phase offsets were constant in time and data drop-out effects were negligible, there would be no need for this calibration; it will be shown below that drop-out effects are large, making this calibration almost always required.

Figure 5.1 shows a sample time-averaged phase (shown with error bars) as a function of observation frequency. For simplicity, phase non-linearities across the 2 MHz bandpass are not included here. Three S-band channels with four bins each are shown in this simplified example. Because the phase is determined only modulo a cycle, several possible cycle assignments are also shown. The residual (about the correlator model) BWS delay is the slope of the line connecting these phase points. The dashed line shows the best fit to these data, without channel phase corrections, giving a residual BWS delay that is different than the slope obtained from the four bins in any single channel, shown by the dotted lines (the slope of the dotted lines is referred to as the bit-stream alignment (BSA) delay for the given channel). The large bias between the BWS and average BSA delays is caused by the channel phase offsets, which can be seen in Figure 5.1 as vertical offsets between the dotted lines.

The residual phases about the dashed line in Figure 5.1 show systematic upward trends for the four bins in each channel. If these trends are constant in time, the residual delays for all scans will have a constant, clock-like term added to them. In practice, the trends are *not* constant in time due to data drop-outs, resulting in significant delay estimate errors. This can be seen dramatically by assuming the data in the first channel were lost. The best fit line in this case is shown by the dot-dashed line, and results in a 250 nanosecond

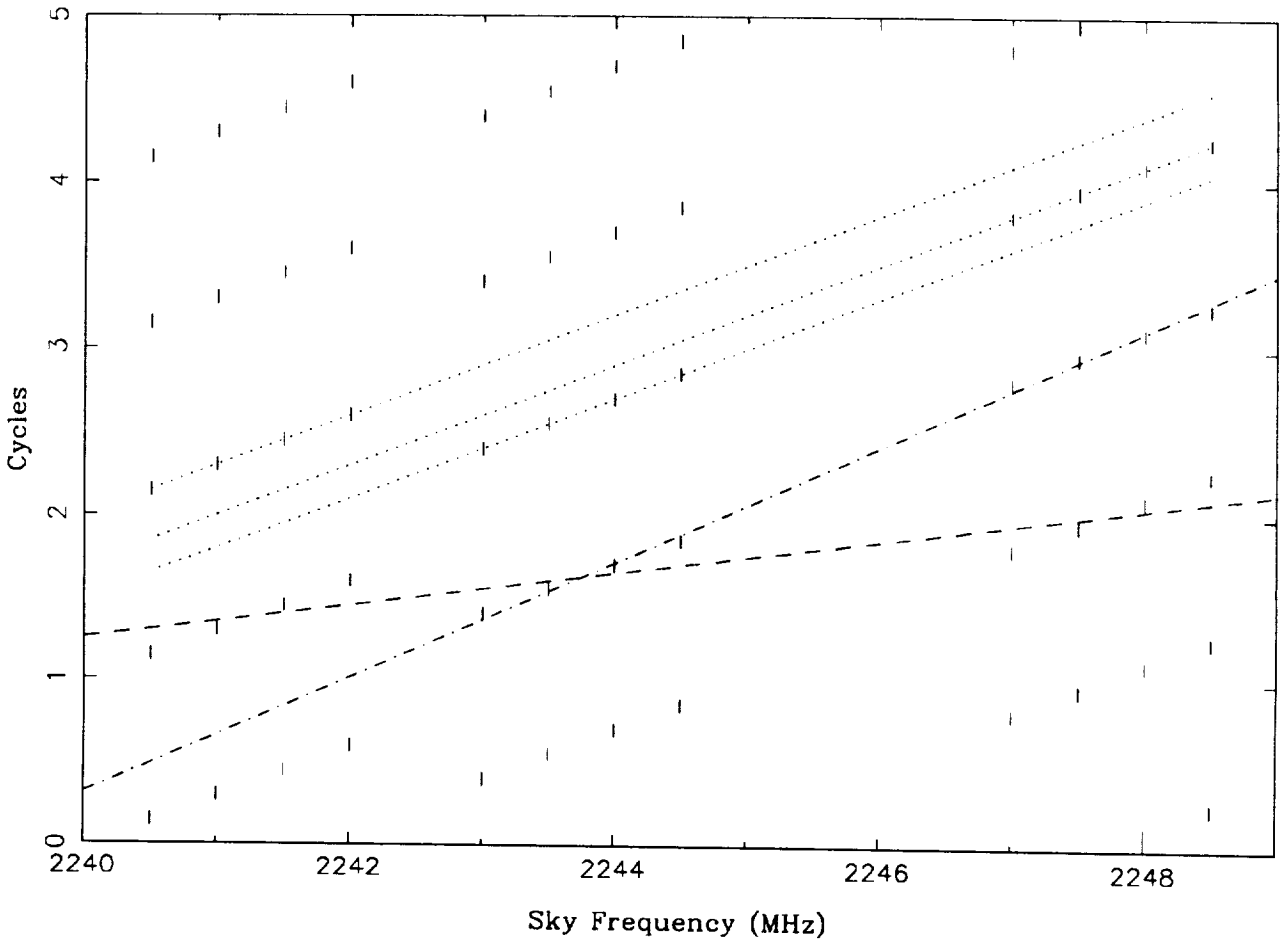

Fig. 5.1 Plot of phase, shown with error bars, as a function of bin frequency for several cycles. In this simplified example, the dashed line shows the best fit line (BWS delay) for all three channels, while the dot-dashed line shows the best fit line for the two highest frequency channels. The dotted lines show the BSA delays for the three channels; the differences in vertical offset between these lines correspond to the channel phase offsets.

change in residual delay from the slope of the dashed line. Even the small fraction of data drop-outs caused by tape playback at the correlator can cause changes in the phase variances which translate into significant biases in residual delay; a drop-out error causing the fit BWS delay slope across 100 MHz to shift one degree at one end of the band leads to a 28 picosecond error. The sensitivity to data drop-outs can be minimized if the residual

phases are all as close to zero as possible.

The program Fit minimizes the phase residuals by solving for a constant phase offset for each bin in a specified scan. This removes the bandpass phase non-linearity in the bins of a single channel as well as the channel phase offsets. A straight line with arbitrary slope can be drawn on Figure 5.1 and the phase differences between the data points and this line can be taken as the set of bin phase offsets; subtracting these offsets from the data will cause the phase points to lie on the line. Because the slope of the line is arbitrary, this method introduces an arbitrary clock-like term in the final delay estimate for each observation band. By using the specified scan to determine the bin phase offsets, and using these offsets for all scans in the experiment, the arbitrary clock for each band is equal for all scans. If a high SNR scan is used to obtain the bin phase offsets and the instrumentation is stable, the phase residuals for all scans (after subtracting the bin phase offsets) will be near zero, and changes in the phase variances caused by data drop-outs will have a minimal effect. The arbitrary line Fit chooses is one with slope equal to the average BSA delay for the band and has zero phase at the band reference frequency, ω_0. As discussed below, this choice minimizes an error source in the final, charged particle calibrated delay.

Obtaining Bin Reference Phases

Before Fit can determine the bin phase offsets described above, it must first obtain the time-averaged phase points shown in Figure 5.1. This is done by fitting the phases for each bin in the band to the model phase $\phi_{ij}^{\rm mpc}$, given by

$$\phi_{ij}^{\rm mpc} = \dot{\tau}^{\rm mpc}\omega_i(t_j - t_0) + \phi_{0i}^{\rm mpc}, \qquad [5.1]$$

where bin i has frequency ω_i, time point j has time t_j, $\dot{\tau}^{\rm mpc}$ is the model phase delay rate for the band, and $\phi_{0k}^{\rm mpc}$ is a reference phase for bin k (the points shown in Figure 5.1). The reference phases and the phase delay rate can be obtained by minimizing the chi-square

$$\chi^2 = \sum_{ij} \frac{\left(\phi_{ij} - \dot{\tau}^{\rm mpc}\omega_i(t_j - t_0) - \phi_{0k}^{\rm mpc}\right)^2}{\sigma_{\phi_{ij}}^2}, \qquad [5.2]$$

as a function of these parameters, where ϕ_{ij} is the phase of the data phasors and $\sigma^2_{\phi_{ij}}$ is given by [2.15c]. Setting the partial derivatives of [5.2] to zero leads to the following equations, valid for all k:

$$\sum_i \omega_i E_i = \dot{\tau}^{\rm mpc} \sum_i \omega_i^2 U_i + \sum_i \phi_{0k}^{\rm mpc} \omega_i T_i \qquad [5.3]$$
$$D_k = \dot{\tau}^{\rm mpc} \omega_k T_k + \phi_{0k}^{\rm mpc} S_k,$$

where the summations

$$S_i \equiv \sum_j \frac{1}{\sigma^2_{\phi_{ij}}} \qquad D_i \equiv \sum_j \frac{\phi_{ij}}{\sigma^2_{\phi_{ij}}} \qquad [5.4]$$
$$T_i \equiv \sum_j \frac{(t_j - t_0)}{\sigma^2_{\phi_{ij}}} \qquad E_i \equiv \sum_j \frac{\phi_{ij}(t_j - t_0)}{\sigma^2_{\phi_{ij}}}$$
$$U_i \equiv \sum_j \frac{(t_j - t_0)^2}{\sigma^2_{\phi_{ij}}}$$

have been used. Solving equations [5.3] for $\phi_{0k}^{\rm mpc}$ and $\dot{\tau}^{\rm mpc}$ leads to

$$\dot{\tau}^{\rm mpc} = \frac{\sum_i \omega_i \left(E_i - \frac{T_i D_i}{S_i} \right)}{\sum_i \omega_i^2 \left(U_i - \frac{T_i^2}{S_i} \right)} \qquad [5.5]$$
$$\phi_{0k}^{\rm mpc} = \frac{D_k - \dot{\tau}^{\rm mpc} \omega_k T_k}{S_k}.$$

The expressions for D_i and E_i in [5.4] involve using the phase of the data phasors. If the phase traverses cycles in time, as shown in Figure 7.1, D_i and E_i will have erroneous values because relative cycle ambiguities are not assigned (the phase traversing several cycles during the scan is typical behaviour because the correlator model is usually not accurate enough to approximately stop the phase over a several minute scan). This problem is discussed and solved in detail in section 7. The solution there as here is to obtain accurate parameter estimates using Fourier transforms over time for each bin and counterrotating

these effects from the data. In this case, the fringe frequency, ω_i^b, and phase, ϕ_i^b, at time t_0 are found from Fourier transforms for each bin. The data phasors are then counterrotated so that

$$\bar{\phi}_{ij} = \phi_{ij} - \omega_i^b(t_j - t_0) - \phi_i^b, \qquad [5.6]$$

where ϕ_{ij} is the phase of the original data phasor and $\bar{\phi}_{ij}$ is the counterrotated phase. If ω_i^b and ϕ_i^b are determined with sufficient accuracy, the new average phase and phase delay rate will be about zero. If the system noise and unmodeled phase fluctuations are small, phase tracking (discussed in sections 12 and 13) is not necessary, and the following summations will be free of cycle ambiguity effects:

$$\bar{D}_i = \sum_j \frac{\bar{\phi}_{ij}}{\sigma^2_{\phi_{ij}}} \qquad \bar{E}_i = \sum_j \frac{\bar{\phi}_{ij}(t_j - t_0)}{\sigma^2_{\phi_{ij}}}. \qquad [5.7]$$

Substituting these expressions and [5.6] into [5.4] gives the following relations

$$\begin{aligned} D_i &= \bar{D}_i + \omega_i^b T_i + \phi_i^b S_i \qquad [5.8] \\ E_i &= \bar{E}_i + \omega_i^b U_i + \phi_i^b T_i. \end{aligned}$$

Finally, these are substituted into equations [5.5] to give

$$\dot{\tau}^{\rm mpc} = \frac{\sum_i \omega_i(\bar{E}_i - T_i\bar{D}_i/S_i + \omega_i^b Z_i)}{\sum_i \omega_i^2 Z_i} \qquad [5.9]$$

$$\phi_{0k}^{\rm mpc} = \frac{\bar{D}_k + (\omega_k^b - \dot{\tau}^{\rm mpc}\omega_k)T_k}{S_k} + \phi_k^b, \qquad [5.10]$$

where

$$Z_i \equiv U_i - T_i^2/S_i. \qquad [5.11]$$

This result depends on the two assumptions noted above: 1) the manual phase calibration (MPC) scan should have a high SNR relative to other scans in the experiment, and 2)

the phase residuals should not show deviations large enough to require phase tracking (this requirement could be eliminated if phase tracking were used to assign relative cycle ambiguities so the sums in [5.7] use the correct phase; Fit does not do this at present as this option has not been needed). The bin reference phases given by [5.10] correspond to those shown in Figure 5.1. The differences between these reference phases and a line with slope equal to the average BSA delay, $\tau_{\rm BSA}$, and with zero phase at ω_0 are the bin phase offsets for bin k, ϕ_k^*:

$$\phi_k^* \equiv \phi_{0k}^{\rm mpc} - \tau_{\rm BSA}(\omega_k - \omega_0). \qquad [5.12]$$

The BSA delay for each channel is calculated by performing a Fourier transform on all bin reference phases in that channel. This method gives the best estimate of BSA delay regardless of cycle ambiguities which are difficult to determine otherwise because of the large instrumental phase non-linearities across the 2 MHz bandpass. These channel BSA delays are then averaged over all channels in each band.

When requested, Fit writes the bin phase offsets to an external file. These offset phases can be read in later and applied during the analysis of each scan in the experiment. This results in all phasors in a given bin being counterrotated by the same offset, for all scans. A possible improvement to the procedure given above would be to average the phase offsets from a number of scans; this would further minimize residual phases over the duration of the experiment.

Note that since each observation band is processed separately, each has a separate arbitrary clock offset. This would pass through the charged particle calibration (section 17) as a constant clock-like term if the delay reference band frequencies, given by [17.29], were constant for all scans; this is not the case in practice. The delay error from this effect is equal to the change in the delay weights, given by [17.6], over the scans in the experiment, times the difference in the S and X-band clock errors. The delay weights for a several hundred scan experiment are usually all within about 5×10^{-4}. As long as the difference in S and X-band clock errors is less than 20 nanoseconds, the delay error caused by this effect will be below about 10 picoseconds. In choosing the average BSA

delay as the line used to obtain the bin phase offsets, Fit attempts to minimize this error by minimizing the clock error. It should be noted, however, at this time, neither the instrumentally induced clock differences nor the clock differences induced by using the average BSA delay as discussed in this section have been measured. Thus, the size of this effect has not yet been adequately determined (this error term is shown explicitly in equation [17.32a]).

Manual Phase Calibration Consider Analysis: No Media Effects

This subsection is devoted to obtaining expressions for the data phases after subtracting the bin phase offsets discussed above. The analysis presented here omits media effects but is expanded to include charged particle and tropospheric effects in the next subsection. The model phase, ϕ_{ij}^{Im}, is assumed to be given by

$$\phi_{ij}^{Im} = \phi_0 + \tau(\omega_i - \omega_0) + \dot{\tau}\omega_i(t_j - t_0) + \phi_i^I, \qquad [5.13]$$

where ϕ_0 is the residual (about the correlator model) phase, τ is the residual delay, $\dot{\tau}$ is the residual phase delay rate, ϕ_i^I is an instrumental phase offset for each bin, assumed constant with time, j runs over all time points, t_j, and i runs over all bin frequencies, ω_i. The first three terms represent the phase without instrumental effects (see [6.2] and [14.1]). Substituting this phase into the expressions for D_i and E_i in [5.4] gives

$$\begin{aligned} D_i &= [\phi_0 + \tau(\omega_i - \omega_0) + \phi_i^I]S_i + \dot{\tau}\omega_i T_i \\ E_i &= [\phi_0 + \tau(\omega_i - \omega_0) + \phi_i^I]T_i + \dot{\tau}\omega_i U_i. \end{aligned} \qquad [5.14]$$

Substituting these expressions into [5.5] gives

$$\dot{\tau}^{\mathrm{mpc}} = \dot{\tau} \qquad [5.15]$$

$$\phi_{0k}^{\mathrm{mpc}} = \phi_0 + \tau(\omega_k - \omega_0) + \phi_k^I. \qquad [5.16]$$

Equation [5.15] indicates this method of obtaining the phase delay rate estimate is unbiased, again, assuming no media effects. Equation [5.16] is the expression for the kth bin reference frequency. The bin phase offset for bin k, ϕ_k^*, is obtained by subtracting $\tau_{\rm BSA}(\omega_k - \omega_0)$ from the reference phase (substitute [5.16] into [5.12]). Thus, the bin phase offset for bin k is given by

$$\phi_k^* = \phi_0 + (\tau - \tau_{\rm BSA})(\omega_k - \omega_0) + \phi_k^I. \qquad [5.17]$$

These are the phases which are subtracted from each time point in a given bin, for all scans in an experiment. If these MPC phases were applied to the same scan they were obtained from, the form of the resulting phases would be

$$\begin{aligned} \phi'_{ij} &= \phi_{ij} - \phi_i^* \qquad [5.18] \\ &= \tau_{\rm BSA}(\omega_i - \omega_0) + \dot{\tau}\omega_i(t_j - t_0), \end{aligned}$$

where the prime here denotes phases after MPC. This shows that applying MPC on the same scan from which the phase offsets were obtained leads to phases where the instrumental phase offsets, ϕ_i^I, are removed, the band residual phase, ϕ_0, is set to zero, the delay is changed to the average BSA delay and the phase delay rate is unaffected (see the consider analysis at the end of section 14 for a proof of this statement). For other scans in the experiment, the calibrated phases are

$$\begin{aligned} \phi'_{ij} &= \phi_{ij} - \phi_0^* - (\tau^* - \tau_{\rm BSA}^*)(\omega_i - \omega_0) - \phi_k^I \qquad [5.19] \\ &= (\phi_0 - \phi_0^*) + (\tau - \tau^* + \tau_{\rm BSA}^*)(\omega_i - \omega_0) + \dot{\tau}\omega_i(t_j - t_0), \end{aligned}$$

where the * superscript denotes quantities from the MPC scan. This shows the resulting band residual phase will be offset by ϕ_0^*, the delay will be offset by the constant clock-like term equal to $\tau^* - \tau_{\rm BSA}^*$, and the resulting phase delay rate will be unaffected. In summary, if media effects are neglected, manual phase calibration eliminates the instrumental phase offsets and induces a constant clock-like term and phase offset for all scans in the experiment.

Manual Phase Calibration Consider Analysis: Dispersive and Tropospheric Effects

The following subsection expands the consider analysis to include dispersive and tropospheric effects. This material can be skipped on first reading; much of it is related to material found in section 17 on charged particle calibration. To avoid repetition, a discussion of dispersive effects on phase, the meaning of k_j below, the sign convention and other supporting material can be found in section 17.

To include dispersive and tropospheric media effects into the consider analysis, equation [5.13] must expanded:

$$\phi_{ij}^m = \phi_0 + \tau(\omega_i - \omega_0) + \dot{\tau}\omega_i(t_j - t_0) + \phi_i^I - k_j/\omega_i + \tau_j^t\omega_i, \qquad [5.20]$$

where k_j is proportional to the differential total electron content in the Block II sign convention and τ_j^t is the differential tropospheric delay at time t_j. Expanding k_j and τ_j^t about a linear model gives

$$\begin{aligned} k_j &\equiv \bar{k} + (t_j - t_0)\dot{\bar{k}} + k_j^r \qquad [5.21] \\ \tau_j^t &\equiv \bar{\tau}^t + (t_j - t_0)\dot{\bar{\tau}}^t + \tau_j^{tr}, \end{aligned}$$

where all quantities are in the Block II sign convention. Substituting these back into [5.20] gives the model phase including dispersive, tropospheric and instrumental effects:

$$\begin{aligned} \phi_{ij}^m = (\phi_0 + \bar{\tau}^t\omega_0) + (\tau + \bar{\tau}^t)(\omega_i - \omega_0) + (\dot{\tau} + \dot{\bar{\tau}}^t)\omega_i(t_j - t_0) \qquad [5.22] \\ + \phi_i^I - \frac{\bar{k}}{\omega_i} - \frac{\dot{\bar{k}}(t_j - t_0)}{\omega_i} - \frac{k_j^r}{\omega_i} + \omega_i\tau_j^{tr}. \end{aligned}$$

Note the linear component of the tropospheric delay enters the first three groups of terms as expected; the phase and group delays have an additional $\bar{\tau}^t$ and the phase delay rate has an additional $\dot{\bar{\tau}}^t$ (see the consider analysis at the end of section 14). This equation can

be substituted into the expressions for D_i and E_i in [5.4] to give analogous expressions to [5.14]:

$$\begin{aligned} D_i &= [(\phi_0 + \bar{\tau}^t\omega_0) + (\tau + \bar{\tau}^t)(\omega_i - \omega_0) + \phi_i^I]S_i + (\dot{\tau} + \bar{\dot{\tau}}^t)\omega_i T_i \\ &\quad - \bar{k}S_i/\omega_i - \bar{\dot{k}}T_i/\omega_i - F_i/\omega_i + \omega_i M_i \\ E_i &= [(\phi_0 + \bar{\tau}^t\omega_0) + (\tau + \bar{\tau}^t)(\omega_i - \omega_0) + \phi_i^I]T_i + (\dot{\tau} + \bar{\dot{\tau}}^t)\omega_i U_i \\ &\quad - \bar{k}T_i/\omega_i - \bar{\dot{k}}U_i/\omega_i - G_i/\omega_i + \omega_i N_i, \end{aligned} \qquad [5.23]$$

where

$$\begin{aligned} F_i &\equiv \sum_j \frac{k_j^r}{\sigma^2_{\phi_{ij}}} & M_i &\equiv \sum_j \frac{\tau_j^{tr}}{\sigma^2_{\phi_{ij}}} \\ G_i &\equiv \sum_j \frac{k_j^r(t_j - t_0)}{\sigma^2_{\phi_{ij}}} & N_i &\equiv \sum_j \frac{\tau_j^{tr}(t_j - t_0)}{\sigma^2_{\phi_{ij}}}. \end{aligned} \qquad [5.24]$$

Substituting equations [5.23] into [5.5] gives expressions analogous to [5.15] and [5.16]:

$$\dot{\tau}^{\mathrm{mpc}} = \dot{\tau} + \bar{\dot{\tau}}^t - \bar{\dot{k}}\frac{\sum_l Z_l}{\sum_l \omega_l^2 Z_l} - \frac{\sum_l (G_l - F_l T_l/S_l)}{\sum_l \omega_l^2 Z_l} + \frac{\sum_l \omega_l^2 (N_l - M_l T_l/S_l)}{\sum_l \omega_l^2 Z_l} \qquad [5.25]$$

$$\begin{aligned} \phi_{0k}^{\mathrm{mpc}} &= \phi_0 + \bar{\tau}^t\omega_0 + (\tau + \bar{\tau}^t)(\omega_k - \omega_0) + \phi_k^I - \frac{\bar{k}}{\omega_k} - \bar{\dot{k}}\frac{T_k}{\omega_k S_k}\left[1 - \frac{\omega_k^2 \sum_l Z_l}{\sum_l w_l^2 Z_l}\right] \\ &\quad - \frac{F_k}{\omega_k S_k} + \frac{\omega_k T_k}{S_k}\frac{\sum_l (G_l - F_l T_l/S_l)}{\sum_l \omega_l^2 Z_l} \\ &\quad + \omega_k \frac{M_k}{S_k} - \frac{\omega_k T_k}{S_k}\frac{\sum_l \omega_l^2 (N_l - M_l T_l/S_l)}{\sum_l \omega_l^2 Z_l}. \end{aligned}$$

The bin phase offsets can be found as above to give

$$\begin{aligned} \phi_k^* &= (\phi_0^* + \bar{\tau}^{t*}\omega_0^*) + (\tau^* + \bar{\tau}^{t*} - \tau_{\mathrm{BSA}}^*)(\omega_k - \omega_0^*) + \phi_k^I - \frac{\bar{k}^*}{\omega_k} \\ &\quad - \bar{\dot{k}}^* \frac{t_{1k}^*}{\omega_k} - \frac{\omega_0^{*2} t_{2k}^*}{\omega_k} + \omega_k(t_{3k}^* + t_{5k}^* - t_{6k}^*), \end{aligned} \qquad [5.26]$$

where ω_0^* is the MPC scan's reference frequency, the following time definitions,

$$t_{1k}^* \equiv \frac{T_k}{S_k}\left[1 - \frac{\omega_k^2 \sum_i Z_i}{\sum_i w_i^2 Z_i}\right] \qquad t_{4k}^* = 0 \qquad [5.27]$$

$$t_{2k}^* \equiv \frac{F_k}{\omega_0^{*2} S_k} \qquad t_{5k}^* \equiv \frac{M_k}{S_k}$$

$$t_{3k}^* \equiv \frac{T_k}{S_k} \frac{\sum_i (G_i - F_i T_i / S_i)}{\sum_i \omega_i^2 Z_i} \qquad t_{6k}^* \equiv \frac{T_k}{S_k} \frac{\sum_i \omega_i^2 (N_i - M_i T_i / S_i)}{\sum_i \omega_i^2 Z_i},$$

are used, and the superscript * has been inserted to explicitly show quantities from the MPC scan (t_{4k}^*, the analogous expression to t_{1k} for the tropospheric delay, is zero and will not be used elsewhere in this report).

Note that $\tau_{\rm BSA}^*$ is corrupted by dispersive effects in the MPC scan. Dispersive effects corrupt the BSA delays for each channel, which are averaged to obtain $\tau_{\rm BSA}^*$. Introducing a small, constant correction delay, $\tau_{\rm cor}^*$, the BSA delay can be written

$$\tau_{\rm BSA}^* = \bar{\tau}_{\rm BSA}^* + \bar{k}^* / \omega_\tau^{*2} + \tau_{\rm cor}^*, \qquad [5.28]$$

where ω_τ^* (including the band subscript) is given by [17.29] for the MPC scan and $\bar{\tau}_{\rm BSA}^*$ is the band averaged BSA delay if no dispersive effects were present. The $\bar{k}^*/\omega_\tau^{*2}$ term accounts for almost all of the dispersive effect; $\tau_{\rm cor}^*$ is only introduced to make [5.28] a strict equality. The bin phase offsets can now be written

$$\phi_k^* = (\phi_0^* + \bar{\tau}^{t*}\omega_0^*) + (\tau_{\rm cl}^* + \bar{\tau}^{t*} - \frac{\bar{k}^*}{\omega_\tau^{*2}})(\omega_k - \omega_0^*) + \phi_k^I - \frac{\bar{k}^*}{\omega_k} \qquad [5.29]$$
$$- \bar{k}^* \frac{t_{1k}^*}{\omega_k} - \frac{\omega_0^{*2} t_{2k}^*}{\omega_k} + \omega_k (t_{3k}^* + t_{5k}^* - t_{6k}^*),$$

where

$$\tau_{\rm cl}^* \equiv \tau^* - \bar{\tau}_{\rm BSA}^* - \tau_{\rm cor}^* \qquad [5.30]$$

both represents the constant clock-like error discussed above and is used to absorb the small correction term in [5.28].

If MPC is applied to any scan in general, the phase after calibration can be written (see [5.19] for comparison):

$$\phi'_{ij} = \left[\phi_0 - \phi_0^* + \omega_0(\bar{\tau}^t - \bar{\tau}^{t*}) - \Delta\omega_0\left(\tau_{cl}^* - \frac{\bar{k}^*}{\omega_\tau^{*2}}\right)\right] \qquad [5.31]$$

$$+ (\tau - \tau_{cl}^* + \bar{\tau}^t - \bar{\tau}^{t*} + \frac{\bar{k}^*}{\omega_\tau^{*2}})(\omega_i - \omega_0) + (\dot{\tau} + \dot{\bar{\tau}}^t)\omega_i(t_j - t_0)$$

$$- \frac{\bar{k} - \bar{k}^*}{\omega_i} - \dot{\bar{k}}\frac{(t_j - t_0)}{\omega_i} + \dot{\bar{k}}^*\frac{t_{1i}^*}{\omega_i} + \omega_0^{*2}\frac{t_{2i}^*}{\omega_i} - \omega_i(t_{3i}^* + t_{5i}^* - t_{6i}^*) - \frac{k_j^r}{\omega_i} + \omega_i\tau_j^{tr},$$

where

$$\Delta\omega_0 \equiv \omega_0 - \omega_0^*. \qquad [5.32]$$

The first two lines of terms show the effects on the phase, group delay and phase delay rate, the next six terms describe dispersive effects and the last term describes the effect from the non-linear component of the tropospheric delay. Note the mixture of effects from both the scan in question and the MPC scan. A consider analysis in section 17 will show the effect each term has on the phase fit observables, the group delay, phase delay rate and phase delay, for each band.

Section 6

A Priori Parameter Estimation

This section, along with sections 7 through 11, is concerned with source detection, defined in section 10, and obtaining an a priori estimate of the residual BWS delay, phase delay rate and phase for each observation band (the band phase observable is usually not important except when phase connection is used to derive the phase delay, as given in [18.1]). These a priori estimates are obtained to effectively improve the correlator model; the model phase derived from the a priori observables is removed from the data to simplify further processing. The model phasor used for source detection, $\vec{P}_{ij}^{m}$, is given by

$$\vec{P}_{ij}^{m} = A_b e^{i\phi_{ij}^{a}} \qquad [6.1]$$

where i runs over all bin frequencies ω_i in the band, j runs over time points t_j, A_b is the band amplitude, ϕ_{ij}^{a} is the model phase given by

$$\phi_{ij}^{a} = \phi_0^{a} + \tau^{a}(\omega_i - \omega_0) + \dot{\tau}^{a}\omega_i(t_j - t_0), \qquad [6.2]$$

τ^{a} is the a priori residual BWS delay, $\dot{\tau}^{a}$ is the a priori residual phase delay rate and ϕ_0^{a} is the a priori residual phase. The term "residual" here is relative to the correlator model which has already been subtracted from the data phasors by the Block II correlator. The parameters A_b, ϕ_0^{a}, τ^{a} and $\dot{\tau}^{a}$ are to be estimated by coherently integrating the data as described in the next several sections. After determining these preliminary values, the phase of each data phasor is counterrotated by the model given by [6.2]. If the signal strength is great enough, the resulting counterrotated phases can be tracked as discussed in sections 12 and 13 and fit using the linear least-squares analysis described in section 14. If the signal strength is too low, the counterrotated phasors are fit using the linear least-squares analysis discussed in section 15.

The band amplitude, given by A_b in [6.1], is obtained from the a priori estimation procedure but is not the final amplitude Fit passes to Modest. Equation [14.17] gives the estimated band amplitude sent to Modest (see reference 9 for more details).

It is important to note that although the model given by equation [6.1] is useful for source detection and obtaining the a priori estimate discussed in the next few sections, it is insensitive to phase changes of an integral number of cycles. A loss of coherence will result if the residual phase about this model fluctuates over several cycles. In practice, the coherent integration implemented with [6.1] will detect moderately weak signals even if cycle fluctuations on the order of several cycles are present but will result in inaccurate a priori parameter estimates, especially for the phase delay rate. This is a common problem at S-band (and even worse at lower frequencies) where ionospheric charged particle fluctuations commonly induce phase changes on the order of a cycle per minute. Larger fluctuations are seen in observations less than about 15 degrees from the sun due to solar plasma fluctuations. If the detection SNR is high enough, phase tracking with a sufficiently high sampling rate can improve the parameter estimation. This is equivalent to an improved model because phase tracking, defined in section 13, *is* sensitive to phase changes of an integral number of cycles. If the SNR is high enough for detection but too low to allow phase tracking, no verification that the phase has not traversed cycles can be made, making the delay and phase delay rate estimation more inaccurate than the formal error would indicate.

In summary, the model given by equations [6.1] and [6.2] is used for the a priori estimate because of its ability to detect weak sources and because it allows the fast Fourier transforms discussed in the following sections. If the SNR is high enough, phase tracking can be used to improve the model and thus the parameter estimates. If the SNR is not high enough to allow phase tracking and there is some possibility of phase fluctuations from any source being on the order of one cycle or more, the formal errors on the final observables will be underestimated.

Section 7

Time Fourier Transform to Obtain Residual Fringe Frequency

The Block II correlator passes to the user the complex correlation coefficient, given by [2.13], at each dump interval and each data bin, typically every two seconds and four per 2 MHz channel, respectively. These data are fit to the model given by [6.1] and [6.2] to extract the a priori BWS delay (τ^a), the phase delay rate ($\dot{\tau}^a$) and phase (ϕ_0^a). This would be a simple least-squares fit in the absence of cycle discontinuities in the phase. Figure 7.1 shows the phase of the complex correlation coefficient as a function of time for a single data bin. The phase can be seen to traverse several cycles over the scan, where the slope of the line passing through these points is the residual fringe rate. This behavior is expected because the correlator model is generally not accurate enough to stop such a small fringe rate: about 0.025 Hz in this case. A naive linear least-squares fit to the phases would not produce the solid line shown in figure 7.1, but rather a line with approximately zero slope along zero phase. Thus, cycle ambiguities must be resolved before least-squares fitting.

There are simple algorithms which allow cycle ambiguity resolution. For example, moving each point in the time series to within a half cycle of the previous point would line up the phases as shown in Figure 7.2. This algorithm has the disadvantage that the signal must have a sufficiently high SNR and low residual fringe rate that there is little chance of a time point being truly more than half a cycle away from the previous point; otherwise the algorithm will erroneously move the next point and thus all later points in the time series. When the SNR is moderate to low, or the residual fringe rate is large, a search algorithm is the only robust approach to finding the residual fringe rate and phase. One could search for the best solution by fitting the phase time series to a large range of slopes (residual fringe rates) and intercepts (phases), while handling the cycle changes explicitly. This is essentially the approach taken here except, without the refinements given below, it is computationally too expensive.

Imagine subtracting a linear phase model of the form $\phi^{lm}(t) = \Omega\, t$ from the residual

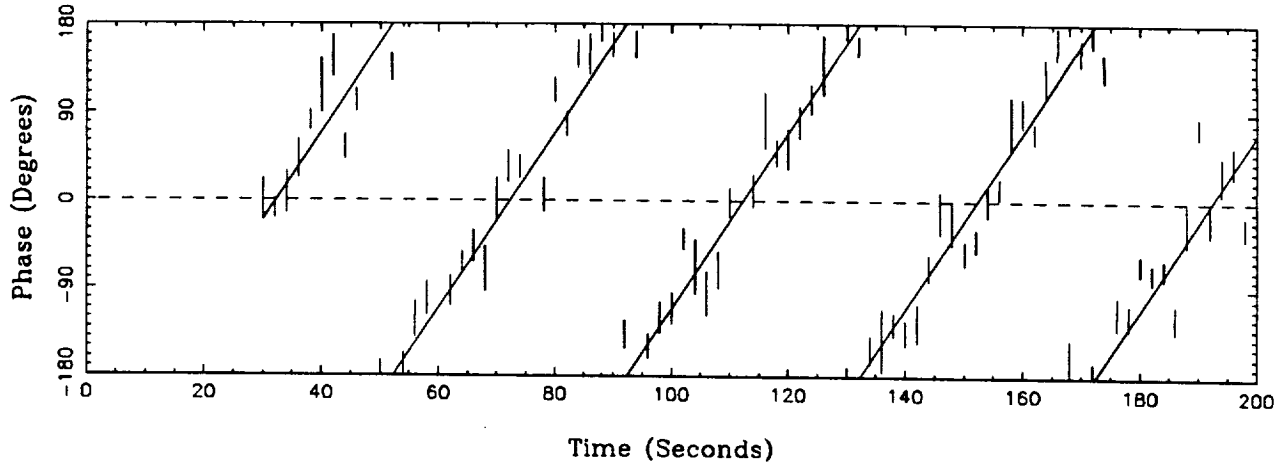

Fig. 7.1 Residual phase as a function of time for one bin. Because the phase traverses several cycles, a simple linear least-squares fit to these data cannot be performed. The solid line shows the best fit if cycle changes are handled correctly.

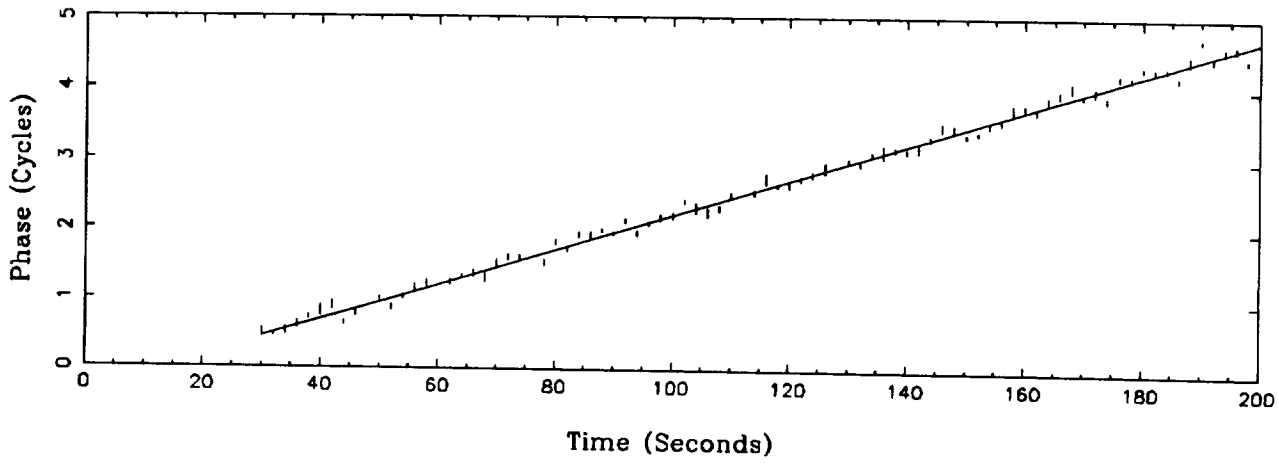

Fig. 7.2 Residual phase as a function of time after cycle ambiguities have been resolved. The solid line shows the linear least-squares fit to the data.

phase shown in figure 7.1, where Ω is a trial fringe rate. If Ω were close to the true residual fringe rate, the phases would line up almost horizontally, as shown in figure 7.3. A search for the Ω which results in the best horizontal alignment is equivalent to searching for the best residual fringe rate. The concept of subtracting a trial phase model and looking for

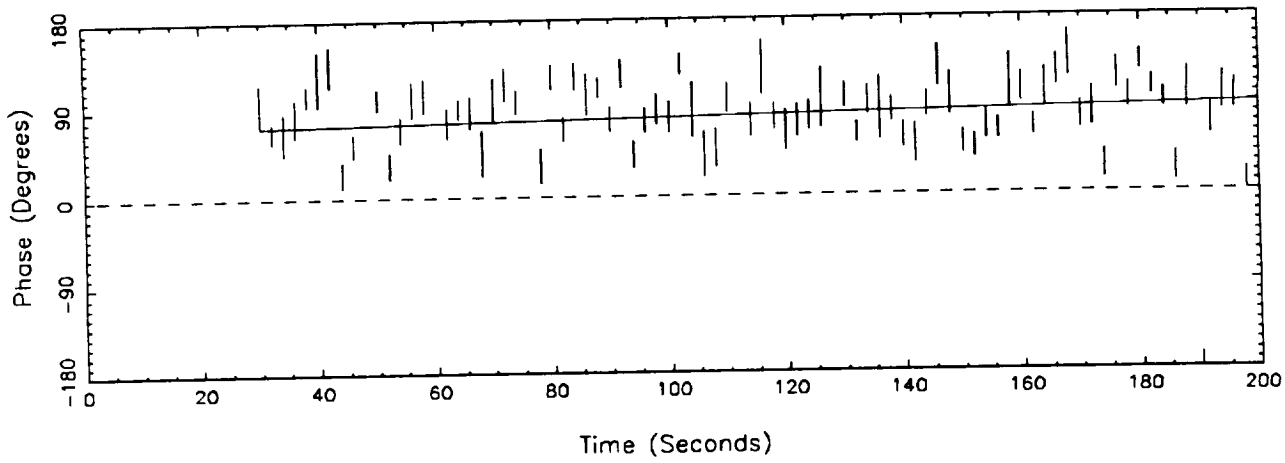

Fig. 7.3 Residual phase after subtracting a trial linear model. The solid line shows the linear least-squares fit to the residual phases.

a constant phase can be extended to the complex correlation phasors. Here, the phasors are counterrotated by multiplying by $e^{-i\Omega t}$. If Ω is close to the residual fringe rate, the phasors will, on average, line up with the same phase. One can test for this condition by calculating the amplitude of the phasor sum, which can be expressed as

$$A^t = \left| \sum_{j=1}^{n} \vec{\rho}_b(t_j)\, e^{-i\Omega t_j} \right|, \qquad [7.1]$$

where $\vec{\rho}_b(t_j)$ is the phasor at the jth time point, given by [2.13]. Only when the phasors are lined up will they sum coherently, resulting in a large relative amplitude. This phasor test has the advantage that it does not fail when the phase is very close to ± 180 degrees, where the average phase can be calculated to be near zero (if about half the phases are around $+180$ and half around -180 degrees). The amplitude can be calculated for a number of trial frequencies, Ω_k, as

$$A^t_k = \left| \sum_{j=1}^{n} \vec{\rho}_b(t_j)\, e^{-i\Omega_k t_j} \right|, \qquad [7.2]$$

so that the maximum amplitude as a function of k corresponds to the best trial residual fringe frequency.

Equation [7.2] is quite similar to that of the discrete Fourier Transform

$$A_k^{ft} = \left| \sum_{j=0}^{n-1} \vec{\rho}_b(t_{j+1}) e^{2\pi i(\frac{kj}{n})} \right| = \left| \sum_{j=1}^{n} \vec{\rho}_b(t_j) e^{2\pi i(\frac{k(j-1)}{n})} \right|, \qquad [7.3]$$

where $k = 0, 1, \ldots, n-1$ (see [B.1] and [B.2] for FFT definitions). Equating the exponents in [7.2] and [7.3] gives the effective frequency tested as a function of k. Performing this sum explicitly is still computationally expensive; the number of computations grows as n^2. If n is a power of two or can be factored into powers of small primes, a fast Fourier Transform algorithm (FFT) can be used to greatly cut the computation time. If n is a power of two, the number of computations grows approximately as $n \log n$. The FFT can be improved for this application by defining additional phasors with zero amplitude beyond the actual number of data phasors. This padding of the FFT algorithm with zero-amplitude phasors results in a finer resolution in the transform space (residual fringe frequency), but does not change in any way the result for a given value of residual fringe frequency; it only decreases the spacing between trial values (see appendix B for details).

Fit performs an FFT on each data bin using n chosen to be a power of two between two and four times the number of data phasors. Such an n is greater than necessary to uniquely determine the maximum-amplitude phasor and obtain the residual fringe frequency, but this higher density of points improves the rescaling and interpolation discussed in the next section.

Section 8

Rescaling Residual Fringe Frequency to Residual Phase Rate

Transforming each bin with an FFT over time results in a new set of phasors. The new phasor with the greatest amplitude corresponds to the best estimate of the residual fringe frequency for that bin, given the discrete sampling of the FFT; the true maximum may lie between two transformed phasors. Coherently summing the data across all bins in a frequency band both increases the SNR (necessary for weak sources) and allows the determination of the a priori residual BWS delay, τ^a. Such a sum involves a second FFT across frequency, discussed in the next section, but should not be performed at this stage of the analysis due to the residual fringe frequency dependence on bin frequency. The physical observable desired is the residual phase delay rate, $\dot{\tau}$, and is equal to the residual fringe frequency, ω_i^f, divided by bin frequency; $\dot{\tau} = \omega_i^f/\omega_i$, where ω_i is the observation frequency of the ith bin. Because $\dot{\tau}$ is constant over bins, the maximum phasor for each bin will occur at a slightly different fringe frequency. Thus, a coherent sum over bins should not be done until the peak amplitudes are aligned to avoid amplitude smearing. This effect is shown in the upper plot in figure 8.1.

If ω_0 is the band reference frequency, a scale factor $\psi_i \equiv \omega_i/\omega_0$ can be defined so that

$$\omega_i^f = \dot{\tau}\omega_i = \dot{\tau}\omega_0\psi_i = \dot{\phi}\psi_i, \qquad [8.1]$$

where $\dot{\phi} \equiv \omega_0\dot{\tau}$ is the phase rate. The bin frequency dependence of the transformed phasors can be removed by contracting the scale of residual fringe frequency by ψ_i for each bin, resulting in a new phase rate scale. Computationally, nothing is done except to reinterpret the residual fringe frequency associated with each transformed phasor. The middle plot in figure 8.1 shows the effect of rescaling; it has changed the spacing between points in different bins. The final step before the coherent frequency sum is to calculate phasors corresponding to a common set of phase rates for all bins in the band. This is done by interpolating the phasors already in hand to these common phase rates.

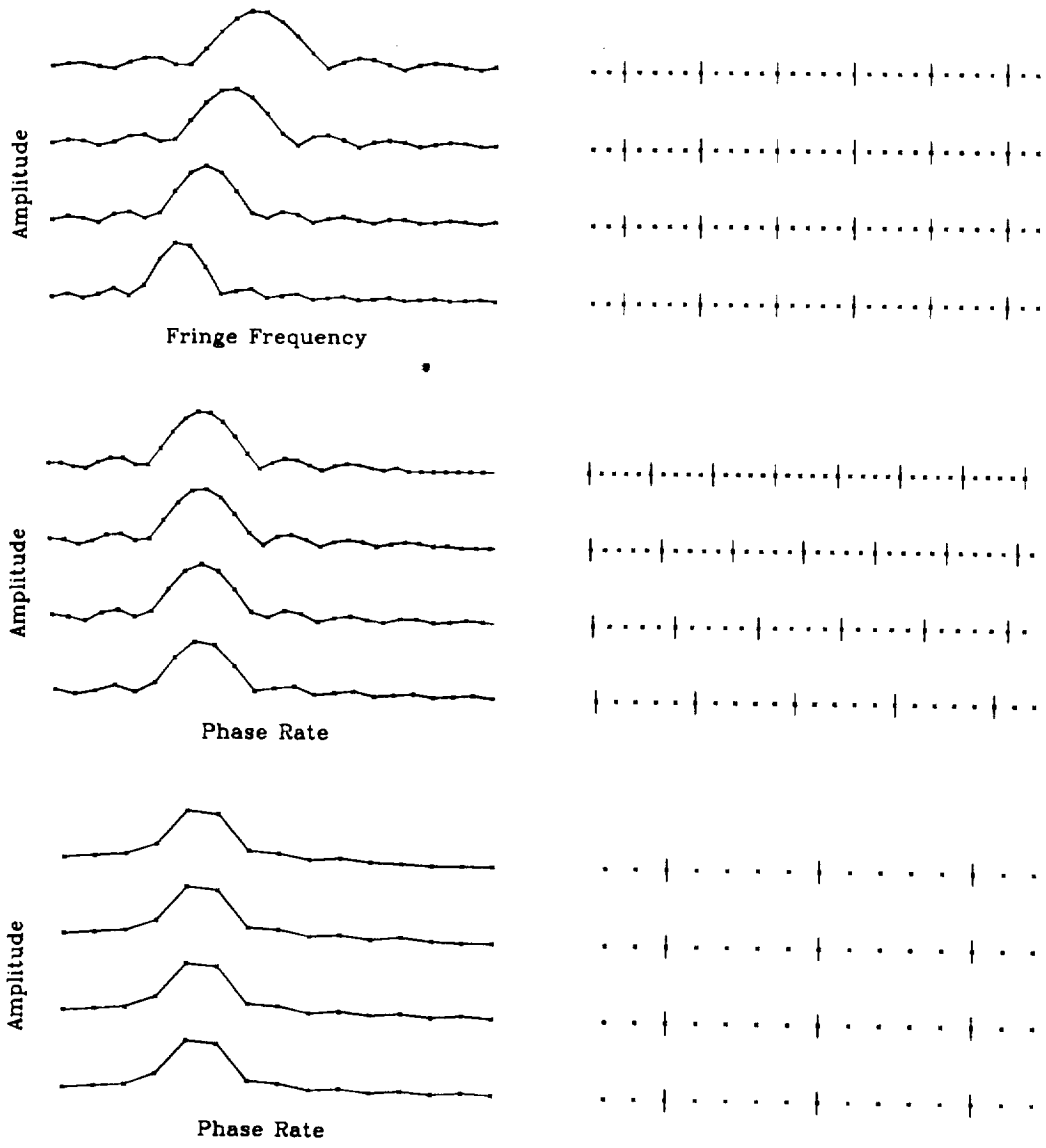

Fig. 8.1 Schematic representation of fringe frequency rescaling. The upper plot shows an exaggerated example of the phasor amplitude after the time FFT for four bins. The fringe frequency dependence on bin frequency causes a shift in the maximum amplitude. The middle plot shows the effect of rescaling the horizontal axis to phase rate. The lower plot shows the interpolated values along a regular grid so that an FFT over frequency is possible. The density of points reflects that used by Fit; the top and middle plots have a higher density to allow a better phasor interpolation, but the density is reduced in the lower plot to satisfy computer memory constraints. The plots on the right show more clearly the relative spacing of points in the plots on the left.

The phasor interpolation results in a phasor with amplitude equal to the weighted geometric average and with a phase equal to the weighted arithmetic average of the two interpolating phasors. This can be calculated quickly using the following

$$\vec{\rho} = (\vec{\rho}_1)^h (\vec{\rho}_2)^{1-h}, \qquad [8.2]$$

where $\vec{\rho}$ is the interpolated phasor, $\vec{\rho}_1$ and $\vec{\rho}_2$ are the interpolating phasors and h is the difference in phase rate between $\vec{\rho}$ and $\vec{\rho}_1$ divided by the phase rate difference between $\vec{\rho}_2$ and $\vec{\rho}_1$. The actual calculation counterrotates both phasors by the phase of the nearest interpolating phasor before the multiplication, and rotates the result back the same amount to avoid the branch cut along the negative real axis when doing the complex exponentiation.

As noted in the previous section, to improve the phasor interpolation accuracy, the density of fringe frequency points across each bin is about twice that needed to find the maximum. The program Fit chooses the common set of phase rate points to have a density half that found in a hypothetical bin having the band reference frequency, ω_0. This reduction in the density of points is necessary to satisfy computer memory constraints, but is dense enough to locate the maximum unambiguously. The final plot in figure 8.1 schematically shows the interpolation and density reduction. The interpolated phasors are now ready to be coherently summed over frequency.

Section 9

Frequency FFT to Obtain Residual BWS Delay

The cross correlation phasors, after having each bin's time series transformed to residual fringe frequency and rescaled to residual phase rate, are ready to be combined to increase the SNR and derive the a priori residual BWS delay. This combination is done with an FFT over frequency.

A possible procedure at this point, though not the one used by Fit (the first, private version of Fit *did* do this), is given to motivate the overall procedure. After the time FFT and rescaling are performed on a high SNR observation, the maximum-amplitude phasor in each bin can be used to give the best estimate of the residual phase rate, and thus phase delay rate, for that bin; a fit to interpolate between the discrete FFT phasors is used to obtain the best estimate. A weighted average of these rate estimates from all bins can give an overall estimate of the residual phase delay rate for the band. This can then be multiplied by each bin's observation frequency to give the best estimate of the residual fringe frequency for each bin. The phase of the original time series of phasors (before the time FFT) for each bin can be fit to a line with slope equal to this calculated residual fringe frequency, with the fit determining the phase intercept at the scan reference time, t_0 (this assumes the SNR is great enough that phase tracking in time can be done easily). Figure 9.1 shows an example of these phase intercepts plotted as a function of bin frequency (this procedure is very similar to that discussed in section 5 on manual phase calibration). The slope of the line connecting the points is the residual BWS delay, τ^a, and the phase intercept at the reference frequency is the residual phase, ϕ_0^a, in equation [6.2]. The slope of the line connecting the bins for a single channel is the BSA delay for that channel. In analogy with the time sequence of points shown in figure 7.1, the cycle changes in figure 9.1 make fitting a line difficult. The only robust method of determining the slope is by fitting with trial slopes and searching for the best fit. Just as in the time series case, an FFT is needed to perform the search in an efficient manner.

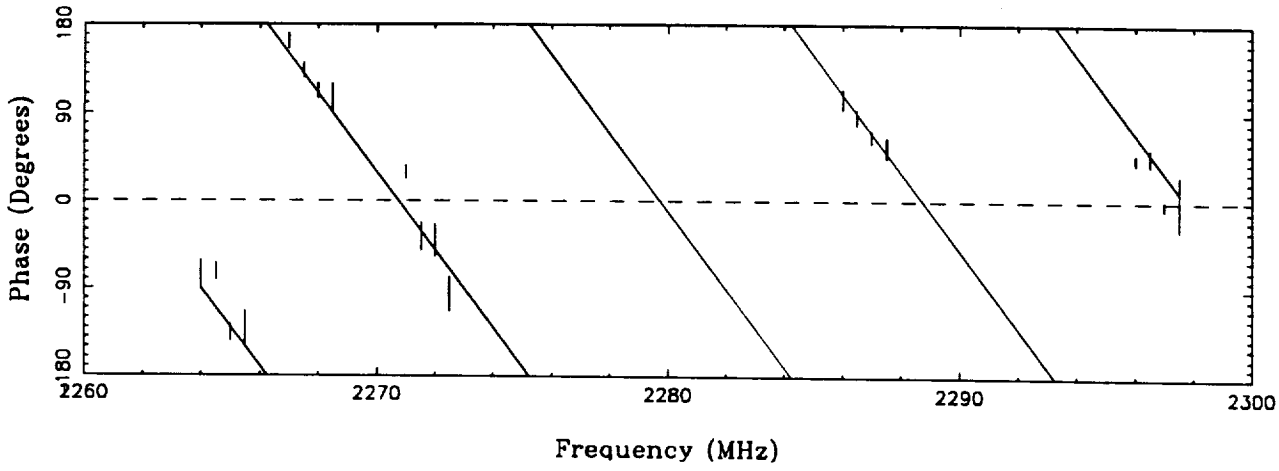

Fig. 9.1 The fit phase at the reference time as a function of bin frequency. Because the phase traverses several cycles, a simple linear least-squares fit to these data cannot be performed. The solid line shows the best fit if cycle changes are handled correctly.

The analysis presented in the last paragraph has the disadvantage that low SNR observations will preclude the time series fit to the original data. Performing the frequency FFT directly on the time-transformed phasors avoids this problem. The resulting two-dimensional (2-D) FFT is equivalent to a 2-D search for best residual BWS delay and phase delay rate estimates; the amplitude of a phasor in the 2-D transformed space indicates how well that trial delay and rate fit the data.

The FFT over frequency has one complication not found in the time series FFT: the points to be transformed using the fast algorithm must occur at integer intervals but the bin frequencies are often selected by the experimenter to avoid even frequency gaps. This problem can be approximately solved by noting that the lowest frequency channel in the band has n bins which can be assigned to the first n integers. This sets the slope and offset needed to calculate the integers corresponding to the other bins in the band. If other bins do not lie exactly on an integer, the nearest one is chosen. This is usually a good approximation because the channel LO frequencies are typically separated by multiples of 0.5 MHz with small offsets on the order of 0.01 MHz. This approximation is later dropped by calculating the Fourier Transform explicitly as discussed in the next section. Integers

not associated with actual data points use zero-amplitude phasors, and additional zero-amplitude phasors are added to the end of the sequence to at least double its length and to make the total number of points a power of two.

After the phasors are Fourier transformed over frequency, the original two-dimensional time/bin frequency data will be transformed to a residual phase delay rate/residual BWS delay plane. A search for the maximum-amplitude phasor will correspond approximately to the best estimate of residual phase delay rate and residual BWS delay; the best estimate corresponds to a point near the maximum phasor due to the discrete sampling of the FFTs. The phase of the maximum-amplitude phasor corresponds to the residual phase, ϕ_0^a. The two-dimensional grid of points is usually dense enough to unambiguously find the nearest phasor to the true peak amplitude among the discrete transformed phasors, but is not dense enough to obtain sufficiently accurate estimates of the residual observables. A higher density of points could be obtained by padding the FFTs with more zero-amplitude phasors, but this option is eventually restricted by memory limitations. The solution used by Fit is to perform the two-dimensional Fourier sums explicitly to obtain the transformed phasor at any point; an iterative search is used to locate the true maximum-amplitude phasor (see Appendix B). The next section covers this technique in detail.

Section 10

Exact Fourier Transform to Obtain Residual Phase Delay Rate and BWS Delay

After applying the time FFT, rescaling, and frequency FFT, the bin/time phasors are transformed to residual phase delay rate/BWS delay phasors. The phasor in this latter space having the maximum amplitude corresponds approximately to the best estimate of the residual phase delay rate and BWS delay. The phase of this phasor corresponds approximately to the best estimate of the residual phase. Because memory and computation constraints limit the size of the residual phase delay rate/BWS delay grid, an interpolation is needed to find the true maximum-amplitude phasor. One approach is to use the phasors already calculated to fit the data with the expected functional form near the peak. This function is approximately $\sin x/x$ in the rate direction and the delay resolution function in the delay direction. This approach is rejected because 1) the complicated functional form makes the fit difficult and 2) when large temporal phase fluctuations are present, this is not an accurate model anyway. The method used by Fit is to calculate the transformed phasors explicitly using a slow Fourier transform. This allows the calculation of the transformed phasor at any point in the residual phase delay rate/BWS delay plane. An iterative search for the maximum amplitude is then performed. This approach has the added advantage that the approximations made to obtain the phasors in hand, namely the phasor interpolation used in the rescaling operation and the rounding of the bin frequencies needed for the frequency FFT, can be dropped in the explicit calculation. In addition, the iterative search utilizes a fairly straightforward and robust algorithm. The primary disadvantage of this method is the calculational cost of performing an explicit FT.

The explicit FT is designed to reproduce exactly those phasors already calculated with the FFTs, assuming the two approximations mentioned above have a negligible effect. The detailed steps needed to derive the form of the explicit FT can be found in appendix B,

but the final equation can be written as (see [B.9])

$$\vec{T}_{ij} = \sum_{l=1}^{n_b} \sum_{k=1}^{n_r} \vec{\rho}_{kl} \exp 2\pi \mathrm{i} \Big[\frac{(k-1)(2i - n_t/2 - 1)}{n_t} \frac{\omega_l}{\omega_0} + \frac{(\omega_l - \omega_1)(j - n_f/2 - 1)}{\omega_b \, n_f} \Big], \tag{10.1}$$

where $\vec{\rho}_{kl}$ is the data phasor for the kth time point and lth bin, $\vec{T}_{ij}$ is the transformed phasor for the ith phase delay rate and jth BWS delay point, n_b and n_r are the number of bins and data time points respectively, n_f and n_t are the number of BWS delay and phase delay rate points in the respective FFT and are each a power of two, and ω_0, ω_1 and ω_k are the band reference frequency, the first bin's frequency and kth bin's frequency, respectively. Comparing the exponent phase in equation [10.1] with the model phase in equation [6.2] leads to the following identifications (see the last subsection in appendix B where these equations are derived in more detail):

$$\begin{aligned} \tau^a &= -\frac{2\pi \bar{x}_i}{\omega_0 t_c}(t_0 - t_1) - \frac{2\pi \bar{x}_j}{\omega_b} \\ \dot{\tau}^a &= -\frac{2\pi}{\omega_0 t_c} \bar{x}_i \\ \phi_0^a &= \phi_{\max} - \frac{2\pi}{t_c}(t_0 - t_1)\bar{x}_i - \frac{2\pi}{\omega_b}(\omega_0 - \omega_1)\bar{x}_j, \end{aligned} \tag{10.2}$$

where t_c is the interval between time points, usually two seconds, $\phi_{\max}$ is the phase of the maximum-amplitude phasor, t_0 is the scan reference time, t_1 is the time tag of the first point in the time series, ω_b is the bandwidth of a single bin and

$$\begin{aligned} \bar{x}_i &\equiv \frac{2x_i - n_t/2 - 1}{n_t} \\ \bar{x}_j &\equiv \frac{x_j - n_f/2 - 1}{n_f}. \end{aligned} \tag{10.3}$$

The variables x_i and x_j correspond to i and j in equation [10.1] but can take real values as opposed to integers (necessary for the interpolation).

The first step in the search for the maximum-amplitude phasor is to recalculate the transformed phasors with the exact FT for a three by three grid centered on the maximum phasor found with the FFTs. This is done to ensure that the maximum does not change location when dropping the two approximations noted above. In some rare cases the peak will move, usually by just one point (if it does, a new three by three grid is calculated). After locating the maximum amplitude in the three by three grid, the center phasor and the nearest four adjacent phasors are used to perform a two-dimensional parabolic fit. The amplitude of the five phasors is fit to the function

$$A^m = a_1 x_i^2 + a_2 x_j^2 + a_3 x_i + a_4 x_j + a_5 \qquad [10.4]$$

where the coefficients a_1 through a_5 can be determined from the center and nearest four phasor amplitudes. This paraboloid has a maximum at the point

$$\left(x_i^c - \frac{\Delta x_i}{2}\left(\frac{A^m_{+0} - A^m_{-0}}{A^m_{+0} - 2A^m_{00} + A^m_{-0}}\right), x_j^c - \frac{\Delta x_j}{2}\left(\frac{A^m_{0+} - A^m_{0-}}{A^m_{0+} - 2A^m_{00} + A^m_{0-}}\right)\right)$$

where the superscript c refers to the location of the central phasor, Δx_i and Δx_j are the spacings between the phasors in the x_i and x_j directions, and the A^m_{**} terms are the five phasor amplitudes arranged in the two-dimensional x_i and x_j plane as follows

$$\begin{array}{ccc} & A^m_{0+} & \\ A^m_{-0} & A^m_{00} & A^m_{+0} \\ & A^m_{0-} & \end{array}.$$

The center of the paraboloid is taken to be the new maximum amplitude location and five new phasors are calculated: one centered on this point and four surrounding it as shown above. Typically, the center phasor has the greatest amplitude of these five. If this turns out not to be true, the phasor having the greatest amplitude is chosen to be the center and the four phasors adjacent to it are calculated. The spacing between the phasors in the grid is also reduced to converge on the maximum more quickly. This process is repeated a

number of times until the last iteration gives the final location of the maximum-amplitude phasor.

If the amplitude of the final, maximum-amplitude phasor is significantly greater than the amplitude of phasors away from the peak region, the peak is assumed to be a result of the source signal; this defines source detection. If no source is present, or the source is too weak to detect, a maximum amplitude phasor will still be found but it will usually have an amplitude only about 3 times greater than the average amplitude of phasors away from the peak region; this ratio is usually at least 10 for well detected sources.

The maximum-amplitude search just described is very CPU intensive. To reduce computation time, the number of iterations and the grid spacing reduction rate have been empirically optimized. At present, Fit reduces the grid spacing by a factor of four on each of four iterations. A larger reduction in grid spacing results in a greater probability that the center of the five new phasors does not have the greatest amplitude. This essentially adds at least one iteration to the nominal four. Even with this optimization, about 25% of Fit's total processing time is used here. Shifting some of this computational load back to the FFTs by padding the time and frequency arrays with more zeros is less efficient. For example, doubling the number of points in the time and frequency FFTs will increase the computation there by about a factor of four, which at present, accounts for about 30% of Fit's total computation time.

Once the maximum-amplitude phasor is found as a function of x_i and x_j, and its phase $\phi_{\max}$ calculated, equations [10.2] are used to obtain the best a priori estimates of residual BWS delay, τ^a, residual phase delay rate, $\dot{\tau}^a$, and residual phase, ϕ_0^a. No approximations have been made in deriving these quantities, and they are exact if the iterative search for the maximum phasor is done with sufficient accuracy and the model shown in [6.1] is appropriate. Typically, equation [6.1] is *not* the best model as discussed in section 6 and further analysis is necessary as described in sections 12–15.

Section 11

Phase Counterrotation by the A Priori Model

After deriving a priori estimates for the residual BWS delay, phase delay rate and phase, the phase of the data phasors is counterrotated by the model given in equation [6.2]. This is done to allow more robust phase tracking algorithms, discussed in the next section, and to permit an initial view of the phase residuals with Fit's plotting software. If $\vec{\rho}_{ij}$ is the original data phasor for frequency ω_i, at time t_j, the counterrotated phasor, $\vec{\rho}^{\,c}_{ij}$, can be written

$$\vec{\rho}^{\,c}_{ij} = \vec{\rho}_{ij} e^{-i\phi^a_{ij}} \qquad [11.1]$$

and ϕ^a_{ij} is identical to [6.2]:

$$\phi^a_{ij} = \phi^a_0 + \tau^a(\omega_i - \omega_0) + \dot{\tau}^a \omega_i (t_j - t_0). \qquad [11.2]$$

Parameter estimates based on these counterrotated data are now residuals of the a priori estimates, which are themselves residuals of the correlator model. The term residual should now refer implicitly to the estimated parameters which are added to the a priori estimates and the correlator model to obtain total observables.

Section 12

Phasor Time Integration

This section and the following three are concerned with obtaining the final estimates of residual BWS delay, phase delay rate and phase using least-squares analysis. Accurate estimates of these parameters have been determined and removed (counterrotated using [11.1] and [11.2]) from the data using the phasor model given by [6.1] and [6.2]. If the SNR is great enough, as defined below, the phasor model can be improved by tracking the phasor's phase as a function of time (discussed in the next section) and fitting it to the model given by [6.2] alone (section 14). If the detection SNR is too low, a linear least-squares fit using the phasor model is performed to obtain the residual parameter means and covariance matrix, as discussed in section 15. The parameter means for this latter fit are small, and would be zero in the limit that the iterative search described in section 10 were done perfectly, because the model is identical in both cases. This section is concerned with determining which analysis path, phase tracking with the phase fit or the phasor fit alone, should be used.

Phase tracking involves assigning an integer number of cycles to the phase of each data phasor in the observation band so that the relative phase difference in each bin's time series and each time's frequency series is handled correctly; an overall cycle ambiguity for the entire band is left unresolved (phase connection, discussed in section 18, involves determining the overall band cycle ambiguity). Some assumptions about the phase time variation must be made to correctly assign the integer cycles to each data phasor. The first assumption is that over a correlator integration interval the phase residuals fluctuate less than about one radian. Unmodeled fluctuations in the phase delay rate greater than about a radian per integration interval cause coherence loss, leave the relative phase ambiguity between time points difficult to assign and create a phase delay rate error greater than that predicted by the formal error. Tracking the phase with more frequent correlator integrations can help solve these problems but at the cost of lowering the SNR per integration. If the source SNR is too low, sampling the phase often enough to track the fluctuations will fail because the phase error on each phasor will be so large that the cycle ambiguity is

again arbitrary. The strategy used by Fit is for the user to obtain correlator integrations as often as possible: usually every two seconds with the present Block II configuration (with a much greater effort, the standard Block II sampling bandwidth of 0.5 Hz can be raised to 40 Hz). If the phase errors for these highest bandwidth phasors are too large, Fit time integrates the phasors in software until a sufficient fraction of them meet an SNR threshold; the small fraction of data points not making the SNR cutoff is deleted. This results in a phasor time series with the greatest sampling bandwidth, with each phasor having at least the threshold SNR. If the phase fluctuates by more than about a radian over one of these software integration intervals, the phase tracking may still give erroneous results; either the data are not sensitive enough to reliably track the phase or the SNR threshold is too high.

The phasor SNR is defined to be R/σ, where R is the center of the phasor's amplitude probability distribution. This is estimated using A/σ (since R is an unknown) where A is the measured phasor amplitude and σ is given by [2.9] or [2.19]. Figure 12.1 shows the phase probability density, given by [2.15a], as a function of phase for different SNR levels. As the SNR level drops, the tails of the distribution from different cycles begin to merge. This results in a much higher probability for an outlying phasor to have its cycle ambiguity resolved incorrectly, even when the surrounding phasors in the time series have small unmodeled phase fluctuations. The plot indicates the SNR threshold should be about two; a higher level lowers Fit's software sampling bandwidth, while a lower level increases the probability of resolving the relative cycle ambiguities incorrectly. Empirically, the most efficient value of the SNR threshold changes from scan to scan but is often between 1.5 and 2.0.

Phasor Integration

The phasors are integrated in software using a variation of equations [2.13] and [2.14]:

$$\vec{\rho}_I = \left(\frac{\hat{C}_I}{N_I/4 - \hat{I}_I/2}, \frac{\hat{S}_I}{N_I/4 - \hat{I}_I/2} \right), \qquad [12.1]$$

where $\vec{\rho}_I$ is the resulting integrated phasor, $\hat{S}_I$, $\hat{C}_I$, and $\hat{I}_I$ are the like-sign sine, like-sign cosine, and invalid counts and N_I is the total number of bits, summed over all phasors in

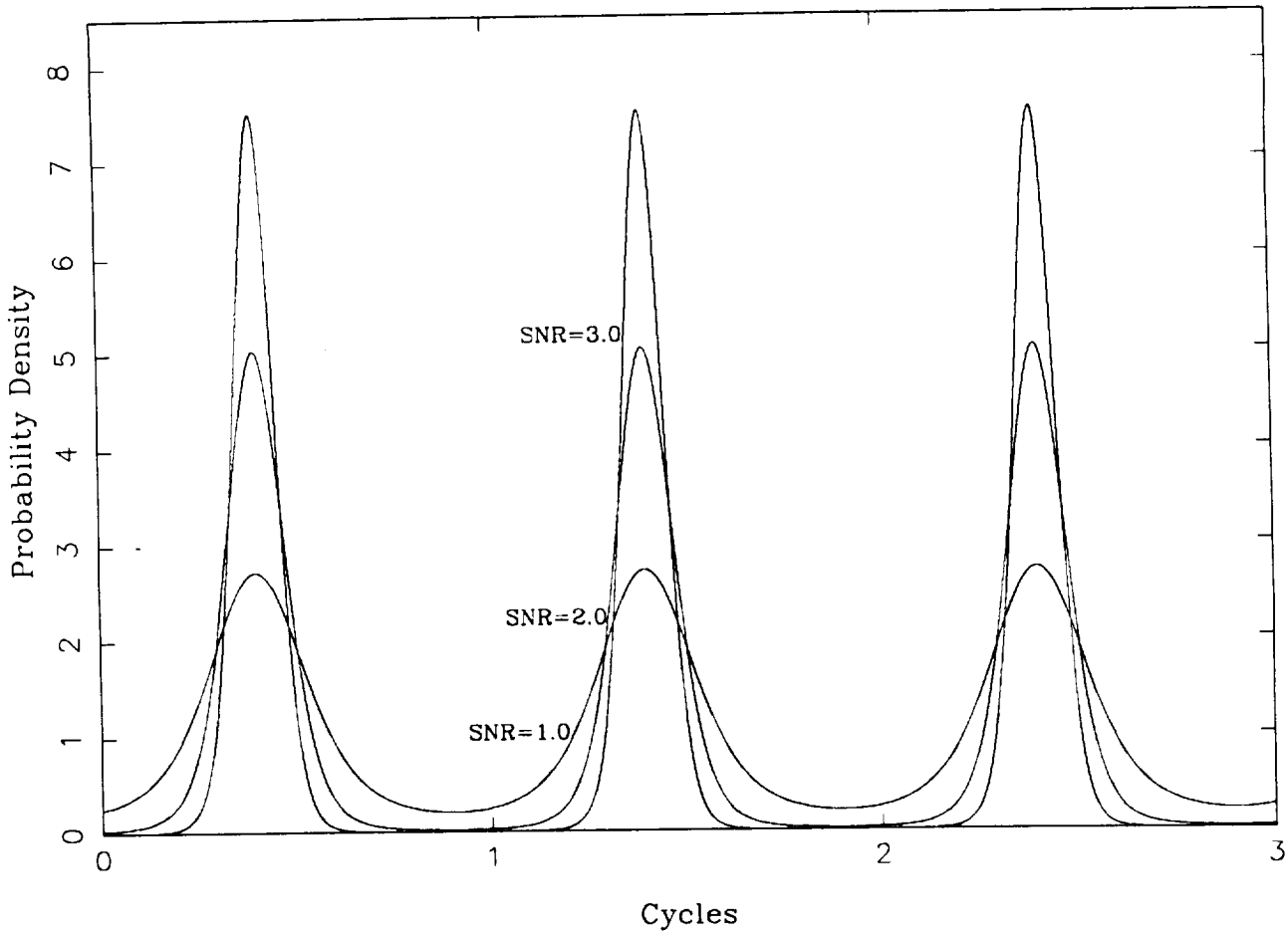

Fig. 12.1 Phase probability distribution for various SNR values; see equation [2.15a] and [A.14]. The probability distribution for high SNR levels is nearly Gaussian and remains clearly separated between cycles. For SNR levels below about 2.0, the distribution flattens and the contributions from adjacent cycles become merged.

the integration interval. Similarly, the error on each phasor component is given by

$$\sigma_I^2 = \frac{V_I - 2\hat{B}_I}{N_L {V_I}^2} \qquad [12.2]$$

where V_I is the integrated valid counts, $V_I = N_I - 2\hat{I}_I$, and $\hat{B}_I$ is the integrated blanking counts.

Fit incrementally increases the integration interval and calculates the fraction of data phasors having the threshold SNR. The smallest integration interval in which a specified fraction (usually about 0.90–0.95) of integrated phasors exceeds the SNR threshold is used. If the integration interval exceeds $\frac{1}{4}$ of the scan's duration or a user-specified time interval (usually 1 minute), whichever is smaller, without the specified fraction of phasors having the SNR threshold, Fit does no phase tracking and fits with the phasor fit. Otherwise, the sequence of integrated phasors is phase tracked as discussed in the next section and fit with the phase model. For long scans, the upper limit on the time integration should be less than $\frac{1}{4}$ the scan duration because the chance of integrating over cycle slips increases with the integration interval.

If tone data are used to calibrate the cross-correlation phasors, as described in section 4, the tone accumulator counts must also be summed. The summed tone counts are used to calculate the tone phasors using an expression analogous to [4.1]. The summed cross-correlation phasors are then calibrated using equations [4.2] and [4.3].

Shift in A Priori Estimates

Before further analysis, the final values of t_0 and ω_0 are computed. The phasor sums and the elimination of summed phasors not having the SNR threshold have changed both the phasor time tags, which are always centered in the integration interval, and the phase variances, $\sigma^2_{\phi_{ij}}$. Equations [3.1] and [3.2] are re-evaluated at this point in the analysis to give the final t_0 and ω_0 values. This re-evaluation induces an implicit change in the a priori estimates; to keep the counterrotation phase ϕ^a_{ij}, given by [11.2], unchanged, shifts in the a priori estimates are necessary to compensate for changes in t_0 and ω_0. If primes denote new values, the counterrotation equations become

$$\begin{aligned} \phi^a_{ij} &= \phi^a_0 \ + \tau^a(\omega_i - \omega_0) \ + \dot{\tau}^a\omega_i(t_j - t_0) \\ \phi^{a\,\prime}_{ij} &= \phi^{a\prime}_0 + \tau^{a\prime}(\omega_i - \omega'_0) + \dot{\tau}^{a\prime}\omega_i(t_j - t'_0). \end{aligned} \qquad [12.3]$$

Setting ϕ_{ij}^a equal to $\phi_{ij}^{a\prime}$ and equating terms with the same i and j dependence leads to

$$\begin{aligned}
\phi_0^{a\prime} &= \phi_0^a + (\omega_0' - \omega_0)\tau^a + (t_0' - t_0)\omega_0'\dot{\tau}^a \qquad [12.4]\\
\tau^{a\prime} &= \tau^a + (t_0' - t_0)\dot{\tau}^a\\
\dot{\tau}^{a\prime} &= \dot{\tau}^a.
\end{aligned}$$

Fit uses these expressions to adjust the a priori estimates; further references to a priori estimates imply these modified (primed) values implicitly.

Section 13

Phase Tracking to Improve the Model

After integrating the phasors in software so that each resulting phasor has at least the threshold SNR at the highest sampling bandwidth, the cycle ambiguities for each phasor are assigned. Figure 13.1 shows the residual phase as a function of time for one of several S-band channels after removing the a priori phase estimate. The phase clearly traverses two full cycles near the center of the scan. Because the a priori model is insensitive to integer cycles, this solution was presumably obtained for its linear regions near the beginning and end of the scan. If the phasor model, [6.1], were used to fit the residuals, this would be very close to the best fit solution because the models are identical. This solution results in an incorrect phase delay rate; the true slope after the phase ambiguities have been resolved can be seen by eye to be about 0.014 Hz (2 cycles over 140 seconds), corresponding to a bias in the phase delay rate of about 6.1×10^{-12}. The error in the delay direction is more difficult to calculate; the phases of the other channels in the band are necessary to completely analyze the BWS slope (Monte Carlo simulations using a random walk for the phase fluctuations indicate that fluctuations on the order of a cycle per minute result in a delay error on the order of 10 picoseconds). If the SNR had been too low to observe the cycle changes, or if the phase changed too fast for the correlator sampling to track (two seconds per point in this case), the large bias in the rate and perhaps a small delay bias would go unseen, leading to an underestimate of the formal errors. A phase fit at this point (with no phase tracking) will definitely result in a biased delay and rate; the resulting rate would have the same problem as the phasor fit and the delay near a cycle crossing, for example at $t = 95$ seconds, is large and biased because the phase in the first three bins is near $+180$ degrees while the last bin's phase is near -180 degrees.

Resolving the phase ambiguities in figure 13.1 can be easily accomplished by eye, but is much more difficult to implement in software. Several empirical algorithms have been tried and rejected. The algorithm presently used by Fit performs reasonably well in most cases. The algorithm makes the assumption that the unmodeled phase fluctuations are

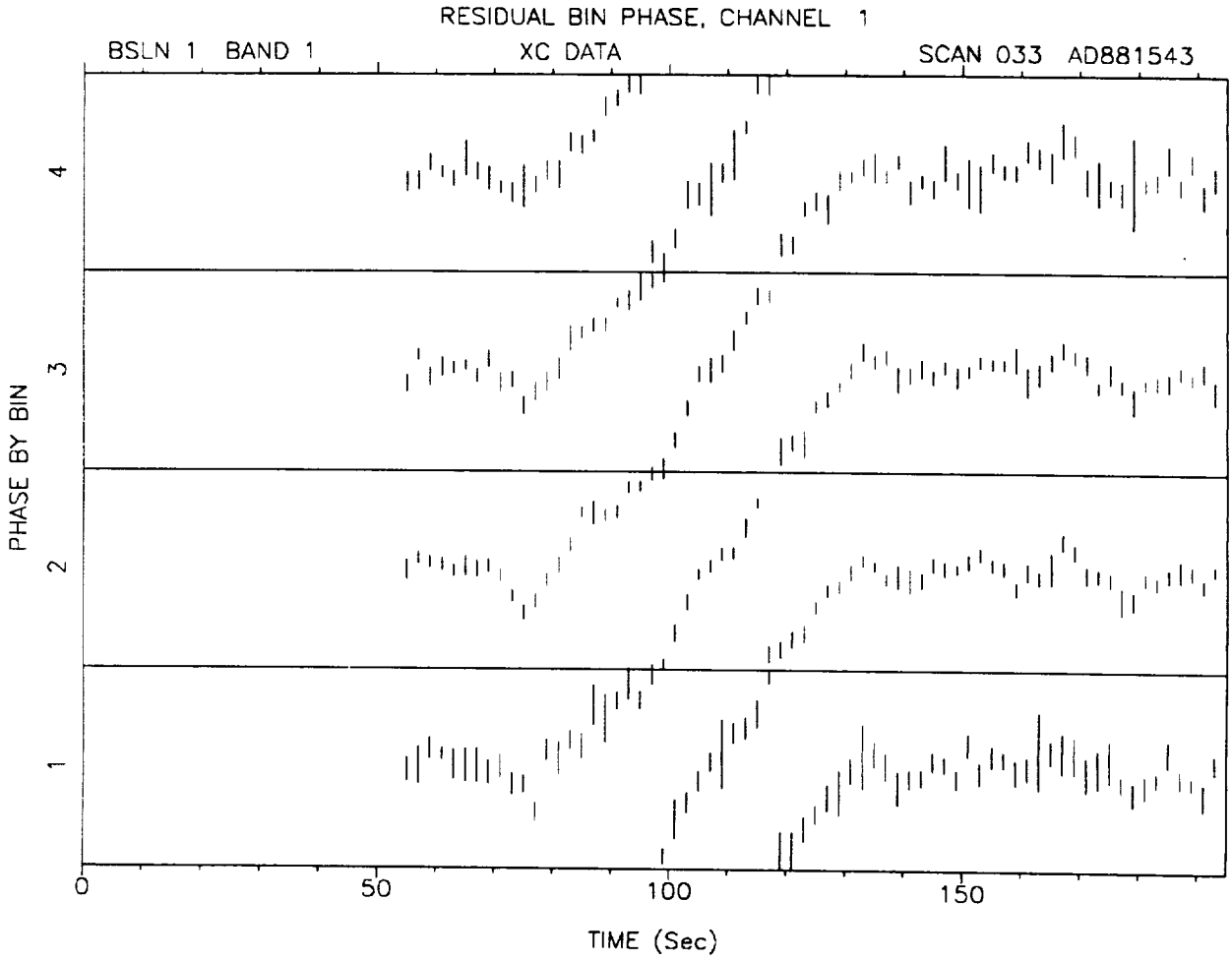

Fig. 13.1 Residual phase as a function of time for the four bins of a single channel. The scale for each bin is ±180 degrees. The phase traverses two cycles near the scan center.

approximately equal for each channel in a band. This is not strictly true for dispersive effects where the phase change is proportional to the inverse observation frequency or for tropospheric delays where the phase fluctuation is directly proportional to the observation frequency, but for the spanned bandwidths and observation frequencies typical of most VLBI experiments, this is a good approximation. The assumption is also made that, at a given time, the phases of all bins in the band are approximately equal. This implies the instrumental channel-to-channel phase offsets must be calibrated with either instrumental phase calibration discussed in section 4, and/or a manual phase calibration explained in

section 5, for this phase tracking algorithm to work properly (note that manual phase calibration will remove linear trends caused by the above media effects; see [5.28], for example).

The first step in the phase tracking algorithm is to form a frequency averaged phase, φ_j, defined as

$$\varphi_j \equiv \arg\Big(\sum_i \vec{\rho}_{ij}\Big), \qquad [13.1]$$

where the sum runs over all frequency bins in the band and $\vec{\rho}_{ij}$ is the complex data phasor. This phasor sum avoids problems near a cycle crossing because it is insensitive to integer cycles, and results in a more accurate phase from averaging many frequency bins. The problem is now reduced to phase tracking the φ_j to obtain an average cycle ambiguity at each time point.

The phase ambiguity of φ_j at time t_j is resolved by fitting the previous three points, φ_{j-3}, φ_{j-2} and φ_{j-1}, to a line and calculating the expected phase at t_j. The integer number of cycles needed to move φ_j to within $\pm\frac{1}{2}$ cycle of this predicted phase is taken to be the cycle ambiguity. This integer ambiguity is then applied to each frequency bin in the band being analyzed. Finally, each bin's cycle at t_j is adjusted to be within $\pm\frac{1}{2}$ cycle of the average phasor's phase, the phase tracked φ_j. This process is repeated for each time point in the scan resulting in a cycle ambiguity assignment for every integrated phasor. Figure 13.2 shows the result of phase tracking for the same channel shown in figure 13.1. These phases are now fit with the phase model discussed in the next section.

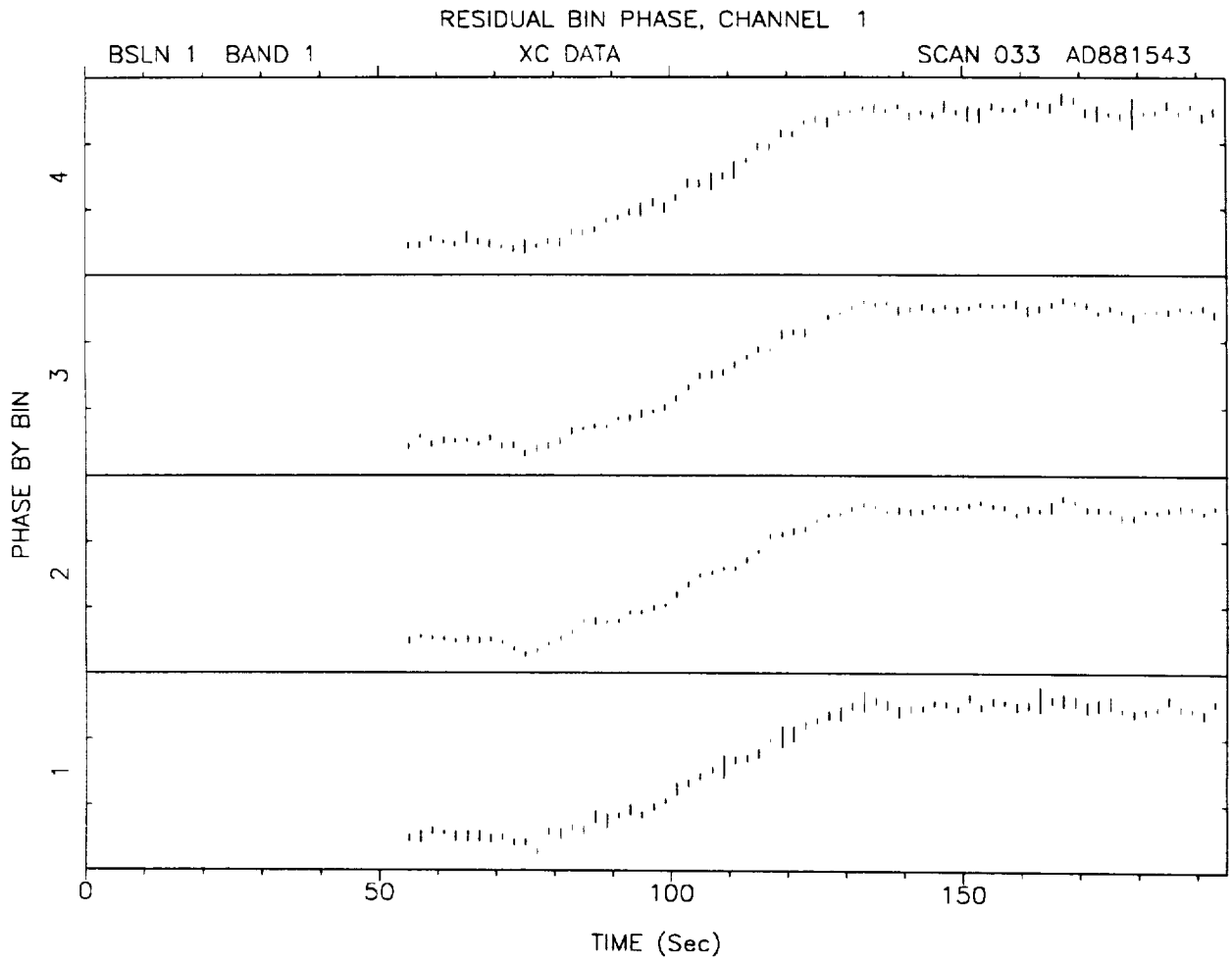

Fig. 13.2 Residual phase as a function of time for the four bins of a single channel after resolving cycle ambiguities. The tick marks on the vertical axis are full cycles. These tracked phases are next fit with least-squares analysis.

Section 14

Least-Squares Fit of Residuals: The Phase Model

Two different models can be used to obtain the final parameter estimates. This section describes a fit to the phase model given by [6.2], while the phasor model fit, given by [6.1] and [6.2], and identical to the a priori model, is described in the next section. Fitting to this model requires the phasor cycle ambiguities to be correctly assigned as described in the previous two sections.

The final parameter estimates are obtained using a linear least-squares fit to the phase of the data phasors using the model

$$\phi^r_{ij} = \phi^r_0 + \tau^r(\omega_i - \omega_0) + \dot{\tau}^r\omega_i(t_j - t_0), \qquad [14.1]$$

for the ith bin and jth time point. The parameters to be estimated, ϕ^r_0, τ^r and $\dot{\tau}^r$, are the residual phase, BWS delay and phase delay rate, and the superscript r denotes the residual values after removing the a priori estimates with the phasor counterrotation. Note that no media or instrumental terms are included here; only the three parameters indicated above are estimated in this analysis. The effects on these parameters from a linear troposphere model are given at the end of this section; the effects from a more general dispersive and tropospheric model are calculated in the consider analysis presented at the end of section 17. Using a least-squares analysis[8], the following matrices can be defined:

$$\mathcal{X} = \begin{pmatrix} \phi^r_0 \\ \tau^r \\ \dot{\tau}^r \end{pmatrix} \qquad [14.2]$$

is the matrix of parameters, and

$$\mathcal{F} = \begin{pmatrix} \phi_1 \\ \phi_2 \\ \vdots \\ \phi_n \end{pmatrix} \qquad [14.3]$$

is the matrix of observations (the phase of the integrated phasors) where n implicitly includes all time points in all bins. The design matrix, which is the matrix of partial derivatives of the model, [14.1], with respect to the parameters, [14.2], is given by

$$\mathcal{A} = \begin{pmatrix} 1 & \omega_1 - \omega_0 & \omega_1(t_1 - t_0) \\ 1 & \omega_2 - \omega_0 & \omega_2(t_2 - t_0) \\ \vdots & \vdots & \vdots \\ 1 & \omega_n - \omega_0 & \omega_n(t_n - t_0) \end{pmatrix}. \qquad [14.4]$$

The weight matrix, $\mathcal{W}$, is the inverse of the observation covariance matrix and is assumed to be diagonal for now:

$$\mathcal{W} = \begin{pmatrix} 1/\sigma^2_{\phi_1} & 0 & \dots & 0 \\ 0 & 1/\sigma^2_{\phi_2} & \dots & 0 \\ \vdots & \vdots & \ddots & \vdots \\ 0 & 0 & \dots & 1/\sigma^2_{\phi_n} \end{pmatrix} \qquad [14.5]$$

where $\sigma^2_{\phi_i}$ is given by equation [2.15c] (off-diagonal elements could be included, for example, to model temporal phase correlations due to tropospheric fluctuations). The $\mathcal{A}^T\mathcal{W}\mathcal{A}$ matrix is given by

$$\mathcal{A}^T\mathcal{W}\mathcal{A} = \begin{pmatrix} \sum \frac{1}{\sigma^2_{\phi_i}} & \sum \frac{(\omega_i - \omega_0)}{\sigma^2_{\phi_i}} & \sum \frac{\omega_i(t_i - t_0)}{\sigma^2_{\phi_i}} \\ \sum \frac{(\omega_i - \omega_0)}{\sigma^2_{\phi_i}} & \sum \frac{(\omega_i - \omega_0)^2}{\sigma^2_{\phi_i}} & \sum \frac{\omega_i(\omega_i - \omega_0)(t_i - t_0)}{\sigma^2_{\phi_i}} \\ \sum \frac{\omega_i(t_i - t_0)}{\sigma^2_{\phi_i}} & \sum \frac{\omega_i(\omega_i - \omega_0)(t_i - t_0)}{\sigma^2_{\phi_i}} & \sum \frac{\omega_i^2(t_i - t_0)^2}{\sigma^2_{\phi_i}} \end{pmatrix} \qquad [14.6]$$

where the sums run over all time and frequency points in the band. The S-band $\mathcal{A}^T\mathcal{W}\mathcal{A}$, for example, can be written in terms of the symbols defined in Appendix C (refer there for variables not defined in this text)

$$\mathcal{A}^T\mathcal{W}\mathcal{A} = \begin{pmatrix} S_0 & S_1 - \omega_0 S_0 & S_5 - t_0 S_1 \\ S_1 - \omega_0 S_0 & S_2 - 2\omega_0 S_1 + \omega_0^2 S_0 & S_6 - t_0 S_2 - \omega_0 S_5 + \omega_0 t_0 S_1 \\ S_5 - t_0 S_1 & S_6 - t_0 S_2 - \omega_0 S_5 + \omega_0 t_0 S_1 & S_9 - 2t_0 S_6 + t_0^2 S_2 \end{pmatrix}; \qquad [14.7]$$

a similar expression is used for other frequency bands. The inverse of this matrix is the covariance matrix for the parameters in the $\mathcal{X}$ matrix, [14.2].

Calculating $(\mathcal{A}^T \mathcal{W} \mathcal{A})^{-1}$ explicitly allows the minimization of the parameter variances by appropriate definition of t_0 and ω_0:

$$(\mathcal{A}^T \mathcal{W} \mathcal{A})^{-1} = \frac{1}{S_{d0}} \begin{pmatrix} S_{29} - 2\omega_0 S_{t3} + \omega_0^2 S_{t0} & -S_{t3} + \omega_0 S_{t0} & S_{16} - \omega_0 S_{t1} \\ -S_{t3} + \omega_0 S_{t0} & S_{t0} & -S_{t1} \\ S_{16} - \omega_0 S_{t1} & -S_{t1} & S_{02} \end{pmatrix}, \qquad [14.8]$$

where all ω_0 dependence is shown explicitly and all t_0 dependence is contained implicitly in the S_{t*} variables defined in [C.10]. Comparing this with the definition of the covariance matrix

$$(\mathcal{A}^T \mathcal{W} \mathcal{A})^{-1} = \begin{pmatrix} \sigma_{\phi_0}^2 & \rho_{\phi\tau}\sigma_{\phi_0}\sigma_\tau & \rho_{\phi\dot{\tau}}\sigma_{\phi_0}\sigma_{\dot{\tau}} \\ \rho_{\phi\tau}\sigma_\tau\sigma_{\phi_0} & \sigma_\tau^2 & \rho_{\tau\dot{\tau}}\sigma_\tau\sigma_{\dot{\tau}} \\ \rho_{\phi\dot{\tau}}\sigma_{\dot{\tau}}\sigma_{\phi_0} & \rho_{\tau\dot{\tau}}\sigma_{\dot{\tau}}\sigma_\tau & \sigma_{\dot{\tau}}^2 \end{pmatrix} \qquad [14.9]$$

leads to the following:

$$\sigma_{\phi_0}^2 = \frac{S_{29} - 2\omega_0 S_{t3} + \omega_0^2 S_{t0}}{S_{d0}} \qquad [14.10a]$$

$$\sigma_\tau^2 = \frac{S_{09} - 2t_0 S_{06} + t_0^2 S_{02}}{S_{d0}} \qquad [14.10b]$$

$$\sigma_{\dot{\tau}}^2 = \frac{S_{02}}{S_{d0}} \qquad [14.10c]$$

$$\rho_{\phi\tau} = \frac{-S_{t3} + \omega_0 S_{t0}}{S_{d0}\,\sigma_\phi^2\,\sigma_\tau^2} \qquad [14.10d]$$

$$\rho_{\phi\dot{\tau}} = \frac{S_{16} - \omega_0 S_{t1}}{S_{d0}\,\sigma_\phi^2\,\sigma_{\dot{\tau}}^2} \qquad [14.10e]$$

$$\rho_{\tau\dot{\tau}} = \frac{-S_{t1}}{S_{d0}\,\sigma_\tau^2\,\sigma_{\dot{\tau}}^2}. \qquad [14.10f]$$

These equations lead to the following conclusions:

- The phase variance is minimized if $t_0 = S_5/S_1$ and $\omega_0 = S_{t3}/S_{t0}$. This definition of ω_0 simplifies to $\omega_0 = S_1/S_0$ for the t_0 definition given. The phase variance is $1/S_0$ at the minimum.
- The delay variance is minimized by $t_0 = S_{06}/S_{02}$ and is equal to S_0/S_{02} at its minimum.
- The rate variance does not depend on t_0 or ω_0; it is always equal to S_{02}/S_{d0}.
- The phase-delay correlation coefficient is zero for $\omega_0 = S_{t3}/S_{t0}$. This simplifies to $\omega_0 = S_1/S_0$ for either $t_0 = S_5/S_1$ or $t_0 = S_{06}/S_{02}$.
- The phase-rate correlation coefficient is zero for $\omega_0 = S_{16}/S_{t1}$. This also simplifies to $\omega_0 = S_1/S_0$ for $t_0 = S_5/S_1$, but ω_0 is undefined for $t_0 = S_{06}/S_{02}$.
- The delay-rate correlation coefficient is zero for $t_0 = S_{06}/S_{02}$.

From these facts, there are only two viable candidates for the definition of t_0: $t_0 = S_5/S_1$ or $t_0 = S_{06}/S_{02}$. The latter appears to be the better choice because it both minimizes the delay variance and makes the delay-rate correlation vanish. This definition must be rejected, however, because this t_0 is often numerically far from the center of the scan; sometimes it even appears before the scan start or after the scan's end. For this reason, Fit uses $t_0 = S_5/S_1$ as the reference time definition. Because there is only one time reference for the scan, t_0 is calculated from the highest frequency band data. Thus, if X band is the highest frequency band,

$$t_0 = X_5/X_1 \qquad [14.11]$$

(see equation [3.1] and [C.1]). For the band frequency reference, Fit uses

$$\omega_{0X} = X_{t3}/X_{t0} \qquad [14.12]$$

(see [3.2] and [C.10]), and a similar expression for other bands, because this is the best definition in all cases above except for the phase-rate correlation. Even that case simplifies

to the optimal value with the t_0 defined in [14.11] for the highest frequency band, and is close to optimal for other bands. Fit uses [14.12] to compute ω_0 in case the user overrides the default t_0 value given by [14.11] or when the band in question is not the highest in frequency. For reference, when t_0 and ω_0 are given by [14.11] and [14.12] (as is the case for the highest frequency band), $(\mathcal{A}^T\mathcal{W}\mathcal{A})^{-1}$ becomes

$$(\mathcal{A}^T\mathcal{W}\mathcal{A})^{-1} = \begin{pmatrix} \frac{1}{X_0} & 0 & 0 \\ 0 & \frac{X_0(X_1X_{19} - X_5X_{16})}{X_1^2X_{d0}} & \frac{-X_0X_{16}}{X_1X_{d0}} \\ 0 & \frac{-X_0X_{16}}{X_1X_{d0}} & \frac{X_{02}}{X_{d0}} \end{pmatrix}. \qquad [14.13]$$

The matrix $(\mathcal{A}^T\mathcal{W}\mathcal{A})^{-1}(\mathcal{A}^T\mathcal{W}\mathcal{F})$ gives minimum variance, unbiased estimates of the parameters in $\mathcal{X}$. $\mathcal{A}^T\mathcal{W}\mathcal{F}$ is (see [C.2])

$$\mathcal{A}^T\mathcal{W}\mathcal{F} = \begin{pmatrix} \sum \frac{\phi_i}{\sigma_{\phi_i}^2} \\ \sum \frac{\phi_i(\omega_i - \omega_0)}{\sigma_{\phi_i}^2} \\ \sum \frac{\phi_i\omega_i(t_i - t_0)}{\sigma_{\phi_i}^2} \end{pmatrix} = \begin{pmatrix} S_a \\ S_b - \omega_0 S_a \\ S_c - t_0 S_b \end{pmatrix}. \qquad [14.14]$$

Multiplying this by [14.8] gives (see [C.7], [C.8] and [C.10])

$$\begin{pmatrix} \phi_0^r \\ \tau^r \\ \dot{\tau}^r \end{pmatrix} = \frac{1}{S_{d0}} \begin{pmatrix} \vec{S}_\phi \cdot [\vec{S}_{s1} + \omega_0\vec{S}_{s2} + \omega_0 t_0 \vec{S}_{s3}] \\ \vec{S}_\phi \cdot [\vec{S}_{s2} + t_0\vec{S}_{s3}] \\ \vec{S}_\phi \cdot \vec{S}_{s3} \end{pmatrix}, \qquad [14.15]$$

so that

$$\phi_0^r = \frac{1}{S_{d0}}(\vec{S}_\phi \cdot \vec{S}_{s1}) + \omega_0\tau^r \qquad [14.16a]$$

$$\tau^r = \frac{1}{S_{d0}}(\vec{S}_\phi \cdot \vec{S}_{s2}) + t_0\dot{\tau}^r \qquad [14.16b]$$

$$\dot{\tau}^r = \frac{1}{S_{d0}}(\vec{S}_\phi \cdot \vec{S}_{s3}). \qquad [14.16c]$$

This explicitly shows the delay dependence on the phase delay rate and the phase dependence on the delay (and thus rate) are as expected. Once the fit values are obtained using $(\mathcal{A}^T \mathcal{W} \mathcal{A})^{-1} \mathcal{A}^T \mathcal{W} \mathcal{F}$, they can be added to the a priori values to give the final estimates for the residual BWS delay, phase delay rate and phase. Summing these residual values with the correlator model values, discussed in section 16, gives the final total observables for each band.

The band amplitude is not determined from the phase fit given in this section, but it can be determined separately from a weighted average of all phasor amplitudes in the band given by

$$A_b = N_L \sum_{ij} \frac{A'_{ij}}{\sigma^2_{A'_{ij}}} \Big/ \sum_{ij} \frac{1}{\sigma^2_{A'_{ij}}}, \qquad [14.17]$$

$$\sigma^2_{A_b} = N_L^2 \Big/ \sum_{ij} \frac{1}{\sigma^2_{A'_{ij}}},$$

where N_L is the number of lags used during the Block II correlation, A'_{ij} is the bandpass-corrected phasor amplitude, $\sigma^2_{A'_{ij}}$ is the amplitude variance, and i and j run over all frequency bins and time points respectively. The primes denote the amplitude and its variance after a bandpass correction; $A'_{ij} = A_{ij} B_i$ and $\sigma_{A'_{ij}} = \sigma_{A_{ij}} B_i$, where A_{ij} is the phasor amplitude, $\sigma_{A_{ij}}$ is given by [2.16c] and B_i depends only on the bin number within each 2 MHz channel, and accounts for one source of instrumental amplitude loss[9].

After fitting, the data are counterrotated by [14.1] using the estimated residual parameters. The counterrotation is done in the exact manner discussed in section 11 using

$$\vec{\rho}^{\,cc}_{ij} = \vec{\rho}^{\,c}_{ij} e^{-i\phi^r_{ij}} \qquad [14.18]$$

and ϕ^r_{ij} as the counterrotation phase, instead of ϕ^a_{ij} in [11.1]. This final counterrotation is done to place the data phasors in their final residual form, making residual plots easy to generate by Fit. Figure 14.1 shows the final residual plot corresponding to those shown in the previous section.

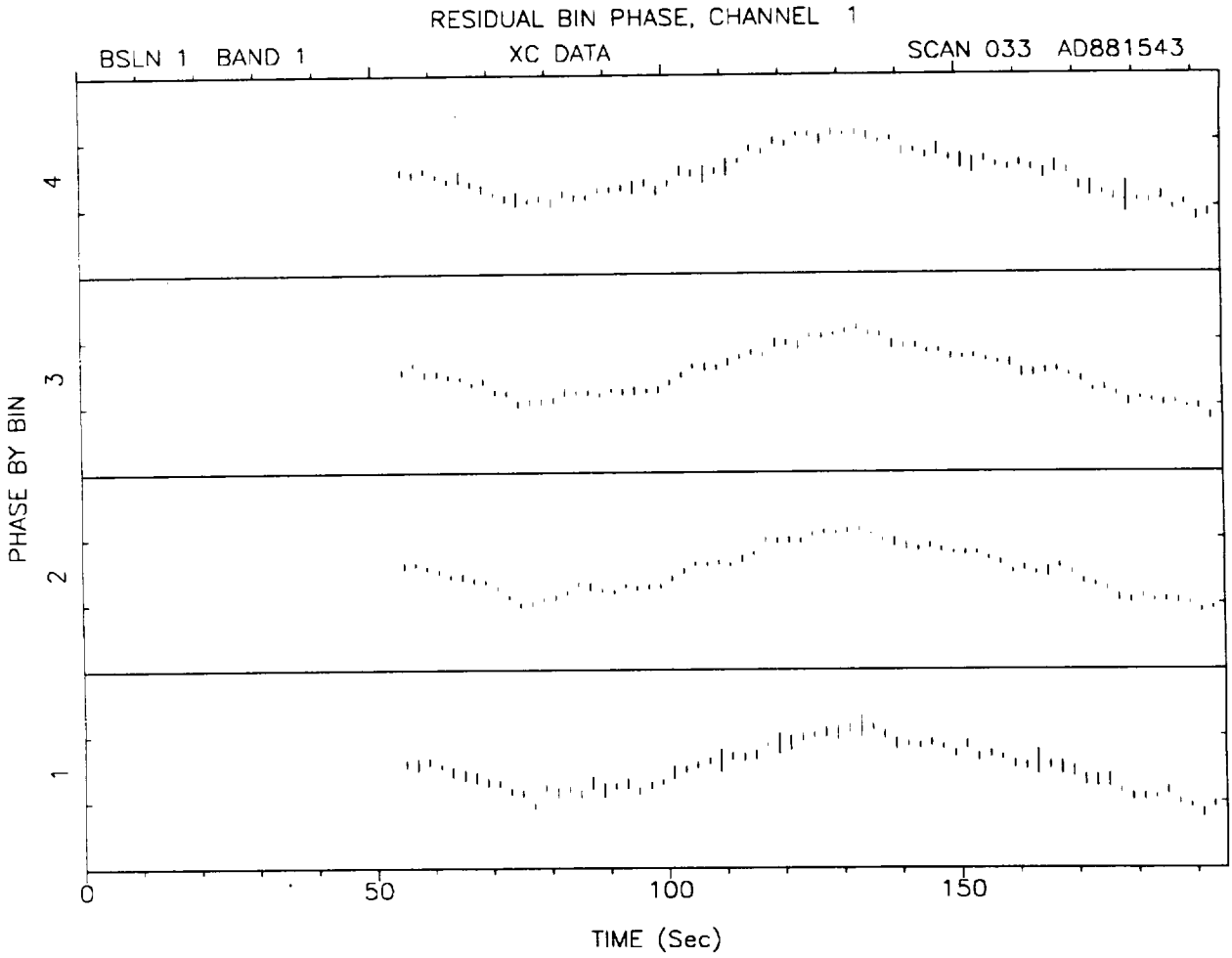

Fig. 14.1 Residual phase as a function of time for the four bins of a single channel after the final fit. The tick marks on the vertical axis are full cycles. This final residual plot corresponds to those shown in the previous section.

Consider Analysis: Linear Troposphere Model

This subsection calculates the effects of a temporally linear troposphere model on the parameter estimates; a more thorough treatment of media effects on parameter estimates is given in the last subsection of section 17. This simple example illustrates that consider errors having the same form as an estimated parameter affect the estimated parameter directly. Assume the model phase, ϕ_{ij}^{tm}, is given by

$$\phi_{ij}^{tm} = \phi_0 + \tau(\omega_i - \omega_0) + \dot{\tau}\omega_i(t_j - t_0) + \omega_i\tau^{lt}, \qquad [14.19]$$

where

$$\tau^{lt} \equiv \bar{\tau}^t + \dot{\bar{\tau}}^t (t_j - t_0) \qquad [14.20]$$

is the tropospheric delay, and $\bar{\tau}^t$ and $\dot{\bar{\tau}}^t$ are parameters modeling the constant and linear trend of the troposphere. This expression for ϕ_{ij} can be substituted into [14.3] to calculate

$$\hat{\mathcal{X}} = (\mathcal{A}^T \mathcal{W} \mathcal{A})^{-1} \mathcal{A}^T \mathcal{W} \mathcal{F}, \qquad [14.21]$$

where $\hat{\mathcal{X}}$ is the matrix of estimated parameters corresponding to $\mathcal{X}$. A shortcut to this computation is to notice that the model phase can be rewritten as

$$\phi_{ij}^{tm} = (\phi_0 + \bar{\tau}^t \omega_0) + (\tau + \bar{\tau}^t)(\omega_i - \omega_0) + (\dot{\tau} + \dot{\bar{\tau}}^t)\omega_i (t_j - t_0). \qquad [14.22]$$

Written in this form, it can be seen that [14.3] becomes $\mathcal{F} = \mathcal{A}\mathcal{Y}$ where the matrix $\mathcal{Y}$ is

$$\mathcal{Y} = \begin{pmatrix} \phi_0 + \bar{\tau}^t \omega_0 \\ \tau + \bar{\tau}^t \\ \dot{\tau} + \dot{\bar{\tau}}^t \end{pmatrix}. \qquad [14.23]$$

Substituting $\mathcal{A}\mathcal{Y}$ for $\mathcal{F}$ in [14.21] leads immediately to $\hat{\mathcal{X}} = \mathcal{Y}$. In other words, all constant terms in the model phase pass through the least-squares formalism into the residual phase parameter, all terms (independent of i and j) multiplying $\omega_i - \omega_0$ pass into the delay, and all terms multiplying $\omega_i(t_j - t_0)$ pass into the phase delay rate. Any additional terms in the model phase which cannot be put into one of the three categories above (for example, terms in the last line of [5.31]) will impact the parameter estimates in a more complicated manner. The consider analysis of section 17 will examine such additional terms. In summary, once [14.19] is put into the form [14.22], the observable effects can be seen immediately:

$$\begin{aligned} \phi_0 &\rightarrow \phi_0 + \bar{\tau}^t \omega_0 \\ \tau &\rightarrow \tau + \bar{\tau}^t \\ \dot{\tau} &\rightarrow \dot{\tau} + \dot{\bar{\tau}}^t. \end{aligned} \qquad [14.24]$$

From this specific example, it can be seen that the troposphere delay and rate enter the observables as expected.

Section 15

Least-Squares Fit of Residuals: The Phasor Model

This section describes a fit to the data using the phasor model given by [6.1] and [6.2], and is typically used when the SNR is too low to accurately track the phase. The primary results of this fit are the parameter variances. Because the model used here is identical to that used for the a priori estimate, the estimated parameter means are usually very small, usually on the order of 10 femtoseconds for the delay, 10 attoseconds/second for the phase delay rate, and 1 millidegree for the phase (for detected sources); the fit would give zero means in the limit that the a priori estimation were done perfectly. The numbers above indicate the a priori estimate is usually sufficiently accurate, and improving the search for the maximum amplitude phasor, described in section 10, is computationally inefficient. The final parameter estimates are obtained with a least-squares fit using the model

$$\vec{M}_i = A_b \exp \mathrm{i}\Big(\phi_0^r + \tau^r(\omega_i - \omega_0) + \dot{\tau}^r \omega_i\,(t_j - t_0)\Big), \qquad [15.1]$$

where $\vec{M}_i$ is the model phasor and A_b, ϕ_0^r, τ^r and $\dot{\tau}^r$ are to be estimated (see [14.1]). This model must be linearized by expanding it about trial estimates which are assumed to be close to the final, best estimates. Call the trial parameters $\check{A}_b$, $\check{\phi}_0$, $\check{\tau}$ and $\check{\dot{\tau}}$ and expand the model about them to obtain

$$\vec{M}_i \simeq \check{\vec{M}}_i + e^{\mathrm{i}\check{\phi}_i}[(A_b - \check{A}_b) + \mathrm{i}\check{A}_b\,(\phi_0^r - \check{\phi}_0) + \mathrm{i}(\omega_i - \omega_0)(\tau^r - \check{\tau})\check{A}_b \qquad [15.2]$$
$$+ \mathrm{i}\,\omega_i\,(t_i - t_0)(\dot{\tau}^r - \check{\dot{\tau}})\check{A}_b]$$

where

$$\check{\vec{M}}_i \equiv \check{A}_b\, e^{\mathrm{i}\check{\phi}_i} = \check{A}_b\, e^{\mathrm{i}[\check{\phi}_0 + \check{\tau}(\omega_i - \omega_0) + \omega_i \check{\dot{\tau}}\,(t_i - t_0)]}. \qquad [15.3]$$

This can be rewritten as

$$\Big(\frac{\vec{M}_i}{\check{\vec{M}}_i} - 1\Big) \simeq \frac{1}{\check{A}_b}(A_b - \check{A}_b) + \mathrm{i}(t\phi_0^r - \check{\phi}_0) + \mathrm{i}(\omega_i - \omega_0)(\tau^r - \check{\tau}) + \mathrm{i}\,\omega_i\,(t_1 - t_0)(\dot{\tau}^r - \check{\dot{\tau}}). \qquad [15.4]$$

Changing to matrix notation, and using the same formalism as in the previous section, we can define the following:

$$\mathcal{X} = \begin{pmatrix} A_b - \check{A}_b \\ \phi_0^r - \check{\phi}_0 \\ \tau^r - \check{\tau} \\ \dot{\tau}^r - \check{\dot{\tau}} \end{pmatrix} \qquad [15.5]$$

$$\mathcal{F} = \begin{pmatrix} \frac{\vec{\rho}_1}{\check{M}_1} - 1 \\ \frac{\vec{\rho}_2}{\check{M}_2} - 1 \\ \vdots \\ \frac{\vec{\rho}_n}{\check{M}_n} - 1 \end{pmatrix} = \begin{pmatrix} \frac{A_1}{\check{A}_b} e^{\mathrm{i}(\phi_1 - \check{\phi}_1)} - 1 \\ \frac{A_2}{\check{A}_b} e^{\mathrm{i}(\phi_2 - \check{\phi}_2)} - 1 \\ \vdots \\ \frac{A_n}{\check{A}_b} e^{\mathrm{i}(\phi_n - \check{\phi}_n)} - 1 \end{pmatrix} \qquad [15.6]$$

$$\mathcal{A} = \begin{pmatrix} \frac{1}{\check{A}_b} & \mathrm{i} & \mathrm{i}(\omega_1 - \omega_0) & \mathrm{i}\omega_1(t_1 - t_0) \\ \frac{1}{\check{A}_b} & \mathrm{i} & \mathrm{i}(\omega_2 - \omega_0) & \mathrm{i}\omega_2(t_2 - t_0) \\ \vdots & \vdots & \vdots & \vdots \\ \frac{1}{\check{A}_b} & \mathrm{i} & \mathrm{i}(\omega_n - \omega_0) & \mathrm{i}\omega_n(t_n - t_0) \end{pmatrix} \qquad [15.7]$$

$$\mathcal{W} = \begin{pmatrix} 1/\sigma_{A_1}^2 & 0 & \dots & 0 \\ 0 & 1/\sigma_{A_2}^2 & \dots & 0 \\ \vdots & \vdots & \ddots & \vdots \\ 0 & 0 & \dots & 1/\sigma_{A_n}^2 \end{pmatrix} \qquad [15.8]$$

where A_i and ϕ_i are the amplitude and phase of the ith data phasor, $\vec{\rho}_i$, $\sigma_{A_i}^2$ is given by equation [2.16c] and i implicitly includes all time-bins points. For complex design and observation matrices with real parameters, the covariance matrix is $(\mathcal{A}_R^T \mathcal{W} \mathcal{A}_R + \mathcal{A}_I^T \mathcal{W} \mathcal{A}_I)^{-1}$ and the minimum variance, unbiased estimate of the parameters is

$$\hat{\mathcal{X}} = (\mathcal{A}_R^T \mathcal{W} \mathcal{A}_R + \mathcal{A}_I^T \mathcal{W} \mathcal{A}_I)^{-1} (\mathcal{A}_R^T \mathcal{W} \mathcal{F}_R + \mathcal{A}_I^T \mathcal{W} \mathcal{F}_I) \qquad [15.9]$$

where the R and I subscripts refer to the real and imaginary parts. The following matrices

are given for reference:

$$(\mathcal{A}_R^T \mathcal{W} \mathcal{A}_R + \mathcal{A}_I^T \mathcal{W} \mathcal{A}_I) = \begin{pmatrix} \frac{1}{\check{A}_b^2} \sum \frac{1}{\sigma_{A_i}^2} & 0 & 0 & 0 \\ 0 & \sum \frac{1}{\sigma_{A_i}^2} & \sum \frac{(\omega_i - \omega_0)}{\sigma_{A_i}^2} & \sum \frac{\omega_i (t_i - t_0)}{\sigma_{A_i}^2} \\ 0 & \sum \frac{(\omega_i - \omega_0)}{\sigma_{A_i}^2} & \sum \frac{(\omega_i - \omega_0)^2}{\sigma_{A_i}^2} & \sum \frac{\omega_i (\omega_i - \omega_0)(t_i - t_0)}{\sigma_{A_i}^2} \\ 0 & \sum \frac{\omega_i (t_i - t_0)}{\sigma_{A_i}^2} & \sum \frac{\omega_i (\omega_i - \omega_0)(t_i - t_0)}{\sigma_{A_i}^2} & \sum \frac{\omega_i^2 (t_i - t_0)^2}{\sigma_{A_i}^2} \end{pmatrix}$$

$$(\mathcal{A}_R^T \mathcal{W} \mathcal{F}_R + \mathcal{A}_I^T \mathcal{W} \mathcal{F}_I) = \begin{pmatrix} \frac{1}{\check{A}_b^2} \sum \frac{A_i \cos(\phi_i - \check{\phi}_i)}{\sigma_{A_i}^2} - \frac{1}{\check{A}_b} \sum \frac{1}{\sigma_{A_i}^2} \\ \frac{1}{\check{A}_b} \sum \frac{A_i \sin(\phi_i - \check{\phi}_i)}{\sigma_{A_i}^2} \\ \frac{1}{\check{A}_b} \sum \frac{A_i (\omega_i - \omega_0) \sin(\phi_i - \check{\phi}_i)}{\sigma_{A_i}^2} \\ \frac{1}{\check{A}_b} \sum \frac{A_i \omega_i (t_i - t_0) \sin(\phi_i - \check{\phi}_i)}{\sigma_{A_i}^2} \end{pmatrix} . \qquad [15.10]$$

Because the model is nonlinear, the fit must be done iteratively; the estimates obtained for $\hat{\mathcal{X}}$, which are the differences between the final values and the trial values, must be added to the trial values to become the new trial estimates. The process is repeated until the elements of $\hat{\mathcal{X}}$ are sufficiently close to zero. Fit iterates this process 10 times; this is more than enough for the parameter estimates to converge, while the computational cost of performing too many iterations is small.

Although the amplitude is obtained here as an estimated parameter, it is not passed to Modest. The amplitude sent to Modest is given by [14.17] (see reference 9 for more details).

Once the final fit values are obtained, they can be summed with the a priori estimates to give the final estimates for the residual BWS delay, phase delay rate and phase. Summing these residual values with the correlator model values, discussed in the next section,

gives the final total observables for each band. After fitting, the data are counterrotated by the phase model using the values obtained here. The counterrotation is done in the same manner given in sections 11 and 14 using equations [11.1] and [14.18]. This final counterrotation is done to place the data phasors in their final residual form, making it easy for Fit to generate residual plots.

Section 16

Correlator Model Restoration to Obtain Total Observables

The quantity of interest for the fitting package Modest is the retarded baseline delay, given by

$$\tau_b^r(t) = \frac{\hat{k}}{c} \cdot [\vec{r}_2(t + \tau_b^r(t)) - \vec{r}_1(t)], \qquad [16.1]$$

and its time derivative, where $\vec{r}_i(t)$ is the location of station i at time t, $\hat{k}$ is the unit wave vector in the direction of propagation, and c is the speed of light; media effects are not considered here but are included in the actual correlator models. The retarded baseline delay is obtained by first calculating station i's model delay, $\tau_{s_i}^m \equiv \hat{k} \cdot \vec{r}_i/c$, and its time derivative, for each station i. The difference between these quantities for the two stations gives the model symmetric baseline delay, $\tau_b^m(t)$, and its derivatives. These are combined with the a priori and least-squares residuals to give the measured symmetric baseline delay, τ_b, and rate, $\dot{\tau}_b$. Finally, corrections for the retarded baseline are applied giving the total retarded quantities, τ_b^r and $\dot{\tau}_b^r$, appropriate for Modest. The rest of this section is devoted to the details of this calculation.

The Block II correlator passes to the user the model delays actually applied to the station bitstreams at specific reference times. These reference times are at the start, finish and at two intermediate times of a user supplied dump interval, where a typical interval might be about 20 seconds. The model delays at these four time points (from the appropriate dump) are fit with a cubic polynomial to derive the model delay and its first three time derivatives at the scan reference time, t_0. Note that, at present, Fit uses only the four points from a single dump interval in the cubic polynomial fit so that t_0 will be randomly distributed across the interval; no attempt is made to use points from adjacent dumps which may be closer to t_0 than those used (if this were done, t_0 would always lie in the center third of the 4-point interval).

The maximum error introduced in the delay and its derivatives by this method of interpolation can be estimated by calculating the exact geometric delay and its derivatives

MAXIMUM ERROR FROM MODEL INTERPOLATION				
Quantity	10 Sec Dump	20 Sec Dump	30 Sec Dump	60 Sec Dump
$\tau_{s_i}^m$	4.8×10^{-18} sec	5.1×10^{-17} sec	2.5×10^{-16} sec	4.0×10^{-15} sec
$\dot{\tau}_{s_i}^m$	8.9×10^{-17}	1.1×10^{-16}	2.0×10^{-16}	1.2×10^{-15}
$\ddot{\tau}_{s_i}^m$	6.4×10^{-18} sec^{-1}	2.4×10^{-17} sec^{-1}	5.5×10^{-17} sec^{-1}	2.2×10^{-16} sec^{-1}
$\dddot{\tau}_{s_i}^m$	3.0×10^{-18} sec^{-2}	6.0×10^{-18} sec^{-2}	9.0×10^{-18} sec^{-2}	1.8×10^{-17} sec^{-2}

Table 16.1 The maximum error in the retarded station delay and its derivatives due to model interpolation for example dump intervals.

at the scan reference time and differencing these values with the fit values. This calculation can be done as a function of baseline orientation to the source position and as a function of the scan reference time within the four time points in the dump interval. Table 16.1 shows the maximum error found for the delay and its derivatives for several example dump intervals. It will be shown below that these model interpolation errors dominate other systematic effects in the model restoration procedure. Note that these are the maximum interpolation errors expected when calculating the correlator model at a specific reference time; they do not account for errors, if any, which are caused by the application of this model at the correlator.

The station model delay (for station i), $\tau_{s_i}^{mr}(t)$, applied to the bitstreams by the Block II correlator is a *retarded* delay designed to cancel significant effects in the fringe phase caused by offsetting the bitstreams by the quantized model delay (see equation (7.11) in reference 2). It is defined in terms of the unretarded station delay, $\tau_{s_i}^m(t)$, as

$$\tau_{s_i}^{mr}(t) = \tau_{s_i}^m(t)\,(1 - \dot{\tau}_{s_i}^m(t)) \qquad [16.2]$$

(see equation (6.2) in reference 2; the equation given here is different, but is the actual expression used by the Block II correlator). This retarded station delay should not be confused with the retarded baseline correction discussed below.

The retarded station delay and its derivatives are given by

$$\begin{aligned}
\tau^{mr}_{s_i}(t) &= \tau^{m}_{s_i}(t) - \tau^{m}_{s_i}(t)\,\dot{\tau}^{m}_{s_i}(t) \\
\dot{\tau}^{mr}_{s_i}(t) &= \dot{\tau}^{m}_{s_i}(t) - \tau^{m}_{s_i}(t)\,\ddot{\tau}^{m}_{s_i}(t) - \dot{\tau}^{m\,2}_{s_i}(t) \\
\ddot{\tau}^{mr}_{s_i}(t) &= \ddot{\tau}^{m}_{s_i}(t) - \tau^{m}_{s_i}(t)\,\dddot{\tau}^{m}_{s_i}(t) - 3\dot{\tau}^{m}_{s_i}(t)\,\ddot{\tau}^{m}_{s_i}(t) \\
\dddot{\tau}^{mr}_{s_i}(t) &= \dddot{\tau}^{m}_{s_i}(t) + O(4).
\end{aligned} \qquad [16.3]$$

Terms having four or more time derivatives (lumped into $O(4)$) have been dropped. To calculate the unretarded delay and its derivatives requires that these equations be inverted so that $\tau^{m}_{s_i}(t)$ and its derivatives are functions of $\tau^{mr}_{s_i}(t)$ and its derivatives. After some algebra, the inverse equations are found to be

$$\begin{aligned}
\tau^{m}_{s_i}(t) &= \tau^{mr}_{s_i}(t) + \tau^{mr}_{s_i}(t)\,\dot{\tau}^{mr}_{s_i}(t) + 2\tau^{mr}_{s_i}(t)\,\dot{\tau}^{mr\,2}_{s_i}(t) + \tau^{mr\,2}_{s_i}(t)\,\ddot{\tau}^{mr}_{s_i}(t) + 5\tau^{mr}_{s_i}(t)\,\dot{\tau}^{mr\,3}_{s_i}(t) + \\
&\qquad \tau^{mr\,3}_{s_i}(t)\,\dddot{\tau}^{mr}_{s_i}(t) + 8\tau^{mr\,2}_{s_i}(t)\,\dot{\tau}^{mr}_{s_i}(t)\,\ddot{\tau}^{mr}_{s_i}(t) + O(4) \qquad [16.4] \\
\dot{\tau}^{m}_{s_i}(t) &= \dot{\tau}^{mr}_{s_i}(t) + \tau^{mr}_{s_i}(t)\,\ddot{\tau}^{mr}_{s_i}(t) + \dot{\tau}^{mr\,2}_{s_i}(t) + 2\dot{\tau}^{mr\,3}_{s_i}(t) + 6\tau^{mr}_{s_i}(t)\,\dot{\tau}^{mr}_{s_i}(t)\,\ddot{\tau}^{mr}_{s_i}(t) + \\
&\qquad \tau^{mr\,2}_{s_i}(t)\,\dddot{\tau}^{mr}_{s_i}(t) + O(4) \\
\ddot{\tau}^{m}_{s_i}(t) &= \ddot{\tau}^{mr}_{s_i}(t) + \tau^{mr}_{s_i}(t)\,\dddot{\tau}^{mr}_{s_i}(t) + 3\dot{\tau}^{mr}_{s_i}(t)\,\ddot{\tau}^{mr}_{s_i}(t) + O(4) \\
\dddot{\tau}^{m}_{s_i}(t) &= \dddot{\tau}^{mr}_{s_i}(t) + O(4)
\end{aligned}$$

These expressions, neglecting the fourth-order terms, are used by Fit to obtain the unretarded station delays and their derivatives.

To estimate the errors made by using [16.4], equations [16.3] were calculated to fourth order in time derivatives and inverted exactly to that order. The contributions from the additional fourth-order terms were estimated by substituting the maximum values of delay and its derivatives for earth-bound stations, neglecting correlations between these maximum values. There are five forth-order unretarded delay terms, the largest of which are $48\tau^{mr\,2}_{s_i}(t)\,\dot{\tau}^{mr\,2}_{s_i}(t)\,\ddot{\tau}^{mr}_{s_i}(t)$ and $14\tau^{mr}_{s_i}(t)\,\dot{\tau}^{mr\,4}_{s_i}(t)$. The sum of the five terms is always less

than about 6.4×10^{-23} seconds. There are also five additional fourth-order rate terms with the largest being $31\tau_{s_i}^{mr}(t)\,\dot{\tau}_{s_i}^{mr\,2}(t)\,\ddot{\tau}_{s_i}^{mr}(t)$. The sum of the five rate terms is always less than about 1.6×10^{-21}. The additional fourth order terms for $\ddot{\tau}_{s_i}^{m}(t)$ and $\dddot{\tau}_{s_i}^{m}(t)$ contribute less than 2.6×10^{-20} sec^{-1} and 2.7×10^{-19} sec^{-2}, respectively. These numbers are all well below the interpolation errors shown above in Table 16.1 (and higher order terms should be much smaller), indicating that they can be safely ignored.

The unretarded station model delays are differenced to form the model symmetric baseline delay and rate:

$$\begin{aligned} \tau_b^m(t) &= \tau_{s_2}^m(t) - \tau_{s_1}^m(t) \\ \dot{\tau}_b^m(t) &= \dot{\tau}_{s_2}^m(t) - \dot{\tau}_{s_1}^m(t), \end{aligned} \qquad [16.5]$$

where the station indices are shown explicitly. This is combined with the a priori and least-squares residual estimates to obtain the measured symmetric baseline delay:

$$\begin{aligned} \tau_b(t) &= \tau_b^m(t) - \tau^a(t) - \tau^r(t), \\ \dot{\tau}_b(t) &= \dot{\tau}_b^m(t) - \dot{\tau}^a(t) - \dot{\tau}^r(t), \end{aligned} \qquad [16.6]$$

where τ^a and $\dot{\tau}^a$ are the a priori estimates and τ^r and $\dot{\tau}^r$ are the least-squares fit residuals. The minus signs are necessary to change τ^a and τ^r (in the correlator sign convention) into the Modest sign convention. Modest requires delays to be in the retarded form shown by equation [16.1].

Expanding [16.1] and taking derivatives give expressions for the retarded baseline delay and its derivatives:

$$\begin{aligned} \tau_b^r(t) &= \tau_b(t) + \tau_b^r(t)\,\dot{\tau}_{s_2}(t) + \frac{1}{2}\tau_b^{r\,2}(t)\,\ddot{\tau}_{s_2}(t) + \frac{1}{6}\tau_b^{r\,3}(t)\,\dddot{\tau}_{s_2}(t) + O(4) \\ \dot{\tau}_b^r(t) &= \dot{\tau}_b(t) + \tau_b^r(t)\,\ddot{\tau}_{s_2}(t) + \dot{\tau}_b^r(t)\,\dot{\tau}_{s_2}(t) + \frac{1}{2}\tau_b^{r\,2}(t)\,\dddot{\tau}_{s_2}(t) + \tau_b^r(t)\,\dot{\tau}_b^r(t)\,\ddot{\tau}_{s_2}(t) + O(4) \\ \ddot{\tau}_b^r(t) &= \ddot{\tau}_b(t) + \tau_b^r(t)\,\dddot{\tau}_{s_2}(t) + 2\dot{\tau}_b^r(t)\,\ddot{\tau}_{s_2}(t) + \ddot{\tau}_b^r(t)\,\dot{\tau}_{s_2}(t) + O(4) \\ \dddot{\tau}_b^r(t) &= \dddot{\tau}_b(t) + O(4), \end{aligned} \qquad [16.7]$$

where $\tau_{s_2}(t)$ is station two's delay. These expressions can be substituted into themselves while dropping fourth-order terms to eliminate the retarded terms on the right. This is done iteratively to give

$$\tau_b^r(t) = \tau_b(t) + \tau_b(t)\,\dot{\tau}_{s_2}(t) + \tau_b(t)\,\dot{\tau}_{s_2}{}^2(t) + \tau_b(t)\,\dot{\tau}_{s_2}{}^3(t) + \frac{1}{2}\tau_b{}^2(t)\,\ddot{\tau}_{s_2}(t) + \qquad [16.8]$$
$$\frac{3}{2}\tau_b{}^2(t)\,\dot{\tau}_{s_2}(t)\,\ddot{\tau}_{s_2}(t) + \frac{1}{6}\tau_b{}^3(t)\,\dddot{\tau}_{s_2}(t) + O(4)$$
$$\dot{\tau}_b^r(t) = \dot{\tau}_b(t) + \dot{\tau}_b(t)\,\dot{\tau}_{s_2}(t) + \dot{\tau}_b(t)\,\dot{\tau}_{s_2}{}^2(t) + \tau_b(t)\,\ddot{\tau}_{s_2}(t) + \tau_b(t)\,\dot{\tau}_b(t)\,\ddot{\tau}_{s_2}(t) +$$
$$2\tau_b(t)\,\dot{\tau}_{s_2}(t)\,\ddot{\tau}_{s_2}(t) + \frac{1}{2}\tau_b{}^2(t)\,\dddot{\tau}_{s_2}(t) + O(4)$$
$$\ddot{\tau}_b^r(t) = \ddot{\tau}_b(t) + \ddot{\tau}_b(t)\,\dot{\tau}_{s_2}(t) + \tau_b(t)\,\dddot{\tau}_{s_2}(t) + 2\dot{\tau}_b(t)\,\ddot{\tau}_{s_2}(t) + O(4)$$
$$\dddot{\tau}_b^r(t) = \dddot{\tau}_b(t) + O(4).$$

Equations [16.6] can be substituted into the first term right of the equal sign in the delay and rate equations of [16.8] to give

$$\tau_b^r(t) = \tau_b^{mr}(t) - \tau^a(t) - \tau^r(t), \qquad [16.9]$$
$$\dot{\tau}_b^r(t) = \dot{\tau}_b^{mr}(t) - \dot{\tau}^a(t) - \dot{\tau}^r(t),$$

where

$$\tau_b^{mr}(t) \equiv \tau_b^m(t) + \tau_b(t)\,\dot{\tau}_{s_2}^m(t) + \tau_b(t)\,\dot{\tau}_{s_2}^{m\,2}(t) + \tau_b(t)\,\dot{\tau}_{s_2}^{m\,3}(t) + \frac{1}{2}\tau_b{}^2(t)\,\ddot{\tau}_{s_2}^m(t) + \qquad [16.10]$$
$$\frac{3}{2}\tau_b{}^2(t)\,\dot{\tau}_{s_2}^m(t)\,\ddot{\tau}_{s_2}^m(t) + \frac{1}{6}\tau_b{}^3(t)\,\dddot{\tau}_{s_2}^m(t) + O(4)$$
$$\dot{\tau}_b^{mr}(t) = \dot{\tau}_b^m(t) + \dot{\tau}_b(t)\,\dot{\tau}_{s_2}^m(t) + \dot{\tau}_b(t)\,\dot{\tau}_{s_2}^{m\,2}(t) + \tau_b(t)\,\ddot{\tau}_{s_2}^m(t) + \tau_b(t)\,\dot{\tau}_b(t)\,\ddot{\tau}_{s_2}^m(t) +$$
$$2\tau_b(t)\,\dot{\tau}_{s_2}^m(t)\,\ddot{\tau}_{s_2}^m(t) + \frac{1}{2}\tau_b{}^2(t)\,\dddot{\tau}_{s_2}^m(t) + O(4)$$

and $\dot{\tau}_{s_2}^m(t)$, $\ddot{\tau}_{s_2}^m(t)$ and $\dddot{\tau}_{s_2}^m(t)$ model $\dot{\tau}_{s_2}(t)$, $\ddot{\tau}_{s_2}(t)$ and $\dddot{\tau}_{s_2}(t)$. Equations [16.9] give the retarded delay and rate for each band in the final form acceptable to Modest. Note that the a priori and residual quantities are applied to the symmetric delay before retardation in equations

[16.6]; this is formally correct to avoid small retardation errors when the measured residuals are large, but the difference is usually negligible in practice.

The total delays and rates obtained here for different frequency bands can be combined to eliminate dispersive effects caused by the presence of charged particles along the observing raypaths. This combination is described in the next section.

Section 17

Charged Particle Calibration

The radio signal received at the two VLBI stations is corrupted by the presence of charged particles along the observed raypaths. These charged particles retard the observed single station phase by k_s/ω, where k_s is proportional to the total electron content (TEC) along the single raypath and ω is the observation frequency (a conversion factor between TEC and k_s is $cr_e/2\pi = 1.3445 \times 10^{-7}\,\mathrm{m^2 cyc^2/sec}$, where $r_e = 2.8179 \times 10^{-15}\,\mathrm{m}$ is the classical electron radius). The two-station interferometric phase is *advanced* by

$$\phi^{cp} = -k(t)/\omega, \qquad [17.1]$$

where $k(t)$ is proportional to the difference in TEC along the two raypaths in the same sign convention (either Block II or Modest) as ϕ^{cp}. Higher order terms proportional to ω^{-2} and ω^{-3} have been dropped from this equation. These terms can be important at lower frequencies, but are usually negligible for observations at S and X-band frequencies (2285 MHz and 8440 MHz, respectively) assumed here. The development given below will therefore be valid for higher frequency measurements such as X/K-band observations.

The phase shift shown in [17.1] induces a change in the group delay, phase delay and phase delay rate given by

$$\tau^{cp} \equiv \frac{\partial \phi^{cp}}{\partial \omega} = \frac{k(t)}{\omega^2} \qquad [17.2a]$$

$$\tau_p^{cp} \equiv \frac{\phi^{cp}}{\omega} = -\frac{k(t)}{\omega^2} \qquad [17.2b]$$

$$\dot{\tau}_p^{cp} \equiv \frac{\partial \tau_p^{cp}}{\partial t} = -\frac{\dot{k}(t)}{\omega^2}. \qquad [17.2c]$$

Dual Frequency Calibration

The single-frequency expressions given by [17.2] can be used to combine the total observables from two frequencies into a single observable, free of dispersive effects. The S-band group delay in the presence of charged particles is given by

$$\begin{aligned} \tau_S &= \bar{\tau} + \tau^{cp} \\ &= \bar{\tau} + \bar{k}/\omega^2_{S\tau}, \end{aligned} \qquad [17.3]$$

where $\bar{\tau}$ is the delay free of charged particle effects, $\bar{k}$ is $k(t)$ averaged over the scan duration, and $\omega^2_{S\tau}$ is an S-band reference frequency for the delay observable, derived below. The charged-particle corrected delay (or S/X corrected delay), $\tau_{S/X}$, can be formed with a weighted linear sum of the S and X-band delays. If $C_{S\tau}$ and $C_{X\tau}$ are the S and X-band delay weights, using equation [17.3] gives:

$$\begin{aligned} \tau_{S/X} &= C_{S\tau}\tau_S + C_{X\tau}\tau_X \\ &= C_{S\tau}(\bar{\tau} + \bar{k}/\omega^2_{S\tau}) + C_{X\tau}(\bar{\tau} + \bar{k}/\omega^2_{X\tau}) \\ &= \bar{\tau}(C_{S\tau} + C_{X\tau}) + \bar{k}(C_{S\tau}/\omega^2_{S\tau} + C_{X\tau}/\omega^2_{X\tau}), \end{aligned} \qquad [17.4]$$

where τ_S and τ_X are the total S and X-band BWS delays. The S/X corrected delay can be made equal to $\bar{\tau}$ only if the following two equations hold:

$$\begin{aligned} C_{S\tau} + C_{X\tau} &= 1, \\ \frac{C_{S\tau}}{\omega^2_{S\tau}} + \frac{C_{X\tau}}{\omega^2_{X\tau}} &= 0. \end{aligned} \qquad [17.5]$$

This leads to expressions for the delay weights in terms of the reference frequencies:

$$C_{S\tau} = \frac{-\omega^2_{S\tau}}{\omega^2_{X\tau} - \omega^2_{S\tau}} \qquad C_{X\tau} = \frac{\omega^2_{X\tau}}{\omega^2_{X\tau} - \omega^2_{S\tau}}. \qquad [17.6]$$

The other linear combination similar to [17.4] can be used to estimate $\bar{k}$:

$$\begin{aligned} \bar{k}_{S/X} &= C_{Sk}\tau_S + C_{Xk}\tau_X \\ &= \bar{\tau}\Big(C_{Sk} + C_{Xk}\Big) + \bar{k}\Big(C_{Sk}/\omega^2_{S\tau} + C_{Xk}/\omega^2_{X\tau}\Big). \end{aligned} \qquad [17.7]$$

where $\bar{k}_{S/X}$ is the calculated estimate of $\bar{k}$, just as $\tau_{S/X}$ is the calculated estimate of $\bar{\tau}$. For $\bar{k}_{S/X}$ to be equal to $\bar{k}$, the following must hold

$$C_{Sk} + C_{Xk} = 0, \qquad [17.8]$$
$$\frac{C_{Sk}}{\omega^2_{S\tau}} + \frac{C_{Xk}}{\omega^2_{X\tau}} = 1.$$

This leads to

$$C_{Sk} = \frac{\omega^2_{S\tau}\omega^2_{X\tau}}{\omega^2_{X\tau} - \omega^2_{S\tau}} \qquad C_{Xk} = \frac{-\omega^2_{S\tau}\omega^2_{X\tau}}{\omega^2_{X\tau} - \omega^2_{S\tau}}. \qquad [17.9]$$

The phase delay rate equivalent of equations [17.4] and [17.7],

$$\dot{\tau}_{S/X} = C_{S\dot{\tau}}\,\dot{\tau}_S + C_{X\dot{\tau}}\,\dot{\tau}_X \qquad [17.10]$$

$$\bar{\dot{k}}_{S/X} = C_{S\dot{k}}\,\dot{\tau}_S + C_{X\dot{k}}\,\dot{\tau}_X, \qquad [17.11]$$

and the equivalent of [17.3] lead to similar expressions for the S/X corrected phase delay rate and time averaged $\dot{k}(t)$ weights:

$$C_{S\dot{\tau}} = \frac{-\omega^2_{S\dot{\tau}}}{\omega^2_{X\dot{\tau}} - \omega^2_{S\dot{\tau}}} \qquad C_{X\dot{\tau}} = \frac{\omega^2_{X\dot{\tau}}}{\omega^2_{X\dot{\tau}} - \omega^2_{S\dot{\tau}}} \qquad [17.12]$$

$$C_{S\dot{k}} = \frac{-\omega^2_{S\dot{\tau}}\omega^2_{X\dot{\tau}}}{\omega^2_{X\dot{\tau}} - \omega^2_{S\dot{\tau}}} \qquad C_{X\dot{k}} = \frac{\omega^2_{S\dot{\tau}}\omega^2_{X\dot{\tau}}}{\omega^2_{X\dot{\tau}} - \omega^2_{S\dot{\tau}}}, \qquad [17.13]$$

where $\omega^2_{S\dot{\tau}}$ and $\omega^2_{X\dot{\tau}}$ are the S and X-band reference frequencies for the phase delay rate observable, derived later. The phase delay equivalents of [17.4], [17.7] and [17.3] lead to the phase delay weights, and a second expression for the $\bar{k}$ weights:

$$C_{S\tau^p} = \frac{-\omega^2_{S\tau^p}}{\omega^2_{X\tau^p} - \omega^2_{S\tau^p}} \qquad C_{X\tau^p} = \frac{\omega^2_{X\tau^p}}{\omega^2_{X\tau^p} - \omega^2_{S\tau^p}} \qquad [17.14]$$

$$C_{Sk^p} = \frac{-\omega^2_{S\tau^p}\omega^2_{X\tau^p}}{\omega^2_{X\tau^p} - \omega^2_{S\tau^p}} \qquad C_{Xk^p} = \frac{\omega^2_{X\tau^p}\omega^2_{S\tau^p}}{\omega^2_{X\tau^p} - \omega^2_{S\tau^p}}, \qquad [17.15]$$

These two expressions are given for completeness, but [17.14] is only needed for phase connection (see section 18) and [17.15] is not usually useful.

Consider Analysis:

Dispersive, Tropospheric and Manual Phase Calibration Effects

The effects on the S/X corrected delay, phase delay rate, and phase observables caused by dispersive and tropospheric media effects as well as manual phase calibration processing effects are calculated here. The last subsection of section 5 derives the expression for the model phase, given by [5.31], which includes these effects. Equation [5.31] must be modified to include the counterrotation procedure given in section 11, by subtracting ϕ^a_{ij} from it. The residual model phase just before fitting (section 14) is given by

$$\begin{aligned}\phi^r_{ij} = &\left[\phi_0 - \phi^*_0 + \omega_0(\bar{\tau}^t - \bar{\tau}^{t*}) - \Delta\omega_0\left(\tau^*_{cl} - \frac{\bar{k}^*}{\omega^{*2}_\tau}\right) - \phi^a_0\right] \qquad [17.16]\\ &+ (\tau - \tau^*_{cl} + \bar{\tau}^t - \bar{\tau}^{t*} + \frac{\bar{k}^*}{\omega^{*2}_\tau} - \tau^a)(\omega_i - \omega_0) + (\dot{\tau} + \bar{\dot{\tau}}^t - \dot{\tau}^a)\omega_i(t_j - t_0)\\ &- \frac{\bar{k} - \bar{k}^*}{\omega_i} - \bar{\dot{k}}\frac{(t_j - t_0)}{\omega_i} + \bar{\dot{k}}^*\frac{t^*_{1i}}{\omega_i} + \omega^{*2}_0\frac{t^*_{2i}}{\omega_i} - \omega_i(t^*_{3i} + t^*_{5i} - t^*_{6i}) - \frac{k^r_j}{\omega_i} + \omega_i\tau^{tr}_j,\end{aligned}$$

where $\Delta\omega_0$ is given by [5.32] and ω^*_τ, derived later, is [17.29] evaluated for the manual phase calibration (MPC) scan. Note that ϕ_0, τ and $\dot{\tau}$ represent the total residuals (residuals about the correlator model) without media, instrumental or manual phase calibration effects. The effect on the total band observables induced by combining many time/frequency points can be calculated by substituting the above equation into the linear least-squares formalism, given by equations [14.3], [14.14] and [14.15]. It will be shown below that minimizing the dispersive effects on the final S/X corrected observables leads to expressions for $\omega^2_{S\tau}$, $\omega^2_{S\dot{\tau}}$, $\omega^2_{S\tau P}$ and their X-band counterparts. The phase fit is used in this consider analysis because it is used for the high SNR scans; observable variances from low SNR scans are presumably dominated by system noise and are insensitive to the small difference in consider errors between the phase and phasor models.

Equation [17.16] is substituted into the $\mathcal{A}^T\mathcal{W}\mathcal{F}$ matrix shown in [14.14]. Note that i in [14.14] implicitly runs over all time and frequency points while i and j run over these

points in [17.16]. The parameter estimates are derived by multiplying this by [14.8] to give

$$\begin{pmatrix} \phi_0^r \\ \tau^r \\ \dot{\tau}^r \end{pmatrix} = \frac{1}{S_{d0}} \begin{pmatrix} \vec{S}_\phi^c \cdot [\vec{S}_{s1} + \omega_0 \vec{S}_{s2} + \omega_0 t_0 \vec{S}_{s3}] \\ \vec{S}_\phi^c \cdot [\vec{S}_{s2} + t_0 \vec{S}_{s3}] \\ \vec{S}_\phi^c \cdot \vec{S}_{s3} \end{pmatrix}, \qquad [17.17]$$

where $\vec{S}_\phi^c$ is similar to $\vec{S}_\phi$ in [C.8] except the phase in the expressions for S_a, S_b and S_c in [C.2] is given by [17.16]. Expanding gives

$$\begin{aligned} \vec{S}_\phi^c = & \Big[\phi_0 - \phi_0^* + \omega_0(\bar{\tau}^t - \bar{\tau}^{t*}) - \Delta\omega_0\Big(\tau_{c1}^* - \frac{\bar{k}^*}{\omega_\tau^{*2}}\Big) - \phi_0^a\Big]\vec{S}_{V1} \qquad [17.18] \\ & + (\tau - \tau_{c1}^* + \bar{\tau}^t - \bar{\tau}^{t*} + \frac{\bar{k}^*}{\omega_\tau^{*2}} - \tau^a)(\vec{S}_{V2} - \omega_0 \vec{S}_{V1}) \\ & + (\dot{\tau} + \bar{\dot{\tau}}^t - \dot{\tau}^a)(\vec{S}_{V3} - t_0 \vec{S}_{V2}) \\ & - (\bar{k} - \bar{k}^*)\vec{S}_{V5} - \bar{\dot{k}}(\vec{S}_{V4} - t_0 \vec{S}_{V5}) + \bar{\dot{k}}^* \vec{S}_{t1} \\ & + \omega_0^2 \vec{S}_{t2} - \vec{S}_{t3} - \vec{S}_{t5} + \vec{S}_{t6} - \vec{S}_{Vk} + \vec{S}_{V\tau} \end{aligned}$$

and the $\vec{S}$ terms are given by [C.6] and [C.12]. Note the last six terms correspond to the non-linear part of the dispersive and tropospheric models. Substituting this into [17.17] and using [C.9] gives

$$\begin{aligned} \phi_0^r + \phi_0^a &= [\phi_0 - \phi_0^* + \omega_0(\bar{\tau}^t - \bar{\tau}^{t*}) - \Delta\omega_0\tau_{c1}^*] - \bar{k}\,S_{k\phi} + \bar{k}^* S_{k^*\phi} - \bar{\dot{k}} S_{\dot{k}\phi} + \bar{\dot{k}}^* S_{\dot{k}^*\phi} + S_{a\phi} \qquad [17.19] \\ \tau^r + \tau^a &= [\tau - \tau_{c1}^* + (\bar{\tau}^t - \bar{\tau}^{t*})] + \bar{k}\,S_{k\tau} - \bar{k}^* S_{k^*\tau} + \bar{\dot{k}} S_{\dot{k}\tau} - \bar{\dot{k}}^* S_{\dot{k}^*\tau} + S_{a\tau} \\ \dot{\tau}^r + \dot{\tau}^a &= (\dot{\tau} + \bar{\dot{\tau}}^t) - \bar{k}\,S_{k\dot{\tau}} + \bar{k}^* S_{k^*\dot{\tau}} - \bar{\dot{k}} S_{\dot{k}\dot{\tau}} + \bar{\dot{k}}^* S_{\dot{k}^*\dot{\tau}} + S_{a\dot{\tau}}. \end{aligned}$$

Undefined quantities are given by equations [C.13]. The first group of terms in each equation shows the effects on the parameter values from a linear troposphere model, the second and third terms give the effects from a constant dispersive model, the fourth and fifth terms show the linear dispersive effects and the last term includes the non-linear effects from both the troposphere and dispersion models. The signs of the dispersive terms in the delay equation of [17.19] are different from those in the other two equations, reflecting

the sign difference in the rightmost terms of equations [17.2]. Note the a priori values passed through the least-squares analysis correctly, indicating the counterrotation given by [11.2] is done correctly (actually, this had to be the case since the design matrix, [14.4], is the matrix of partials of [14.1] which has the same form as [11.2]). Also note the delay and phase are affected by the difference in the average tropospheric delay between the MPC scan and the scan being analyzed, while the phase delay rate is only affected by the troposphere rate of the analyzed scan and contains no $\bar{\dot{\tau}}^{t*}$ term; this is desired so the time derivative of the delay effect is equal to the phase delay rate effect.

Care is needed in maintaining the two sign conventions coming together here: the Block II, station 1 minus station 2, system and the Modest, station 2 minus station 1, system. Residual variables, which include those calculated up through section 15 in this report, are in the Block II convention. Total variables, those with the correlator model restored as described in the last section, are in the Modest convention. All expressions in this section are valid in either sign convention as long as all quantities are used in the same convention. To avoid considerable switching between systems, all variables in the remainder of this section are to be interpreted as being in the Modest sign convention. To form total observables here, the left side of [17.19] is *added* to the correlator model values. This is equivalent to [16.6] if the minus signs are absorbed into the residual and a priori observables with the troposphere and dispersive modeling, [5.21], by interpreting these to be in the Modest convention. Thus, $\bar{k}$, $\bar{\dot{k}}$, k_j^r, $\bar{\tau}^t$, $\bar{\dot{\tau}}^r$, τ_j^{tr}, and τ_{cl}^*, along with all residual and a priori variables, are assumed to be in the Modest convention for the remainder of this section.

Adding the correlator model to equations [17.19] so they can be expressed in terms of total S and X-band observables gives:

$$\begin{aligned}
\phi_S &= \tilde{\phi}_{0S} - \phi_{0S}^* + \omega_{0S}(\bar{\tau}^t - \bar{\tau}^{t*}) - \Delta\omega_{0S}\tau_{\mathrm{cl(S)}}^* - \bar{k}\,S_{k\phi} + \bar{k}^* S_{k^*\phi} - \bar{\dot{k}} S_{\dot{k}\phi} + \bar{\dot{k}}^* S_{\dot{k}^*\phi} + S_{a\phi} \quad [17.20]\\
\tau_S &= \tilde{\tau} - \tau_{\mathrm{cl(S)}}^* + (\bar{\tau}^t - \bar{\tau}^{t*}) \qquad + \bar{k}\,S_{k\tau} - \bar{k}^* S_{k^*\tau} + \bar{\dot{k}} S_{\dot{k}\tau} - \bar{\dot{k}}^* S_{\dot{k}^*\tau} + S_{a\tau}\\
\dot{\tau}_S &= \tilde{\dot{\tau}} + \bar{\dot{\tau}}^t \qquad - \bar{k}\,S_{k\dot{\tau}} + \bar{k}^* S_{k^*\dot{\tau}} - \bar{\dot{k}} S_{\dot{k}\dot{\tau}} + \bar{\dot{k}}^* S_{\dot{k}^*\dot{\tau}} + S_{a\dot{\tau}}
\end{aligned}$$

$$\phi_X = \tilde{\phi}_{0X} - \phi^*_{0X} + \omega_{0X}(\bar{\tau}^t - \bar{\tau}^{t*}) - \Delta\omega_{0X}\tau^*_{\mathrm{cl(X)}} - \bar{k}\,X_{k\phi} + \bar{k}^*X_{k^*\phi} - \bar{\dot{k}}X_{\dot{k}\phi} + \bar{\dot{k}}^*X_{\dot{k}^*\phi} + X_{a\phi} \quad [17.21]$$

$$\tau_X = \tilde{\tau} - \tau^*_{\mathrm{cl(X)}} + (\bar{\tau}^t - \bar{\tau}^{t*}) + \bar{k}\,X_{k\tau} - \bar{k}^*X_{k^*\tau} + \bar{\dot{k}}X_{\dot{k}\tau} - \bar{\dot{k}}^*X_{\dot{k}^*\tau} + X_{a\tau}$$

$$\dot{\tau}_X = \tilde{\dot{\tau}} + \bar{\dot{\tau}}^t - \bar{k}\,X_{k\dot{\tau}} + \bar{k}^*X_{k^*\dot{\tau}} - \bar{\dot{k}}X_{\dot{k}\dot{\tau}} + \bar{\dot{k}}^*X_{\dot{k}^*\dot{\tau}} + X_{a\dot{\tau}},$$

where $\Delta\omega_{0S}$ and $\Delta\omega_{0X}$ are the S and X-band $\Delta\omega_0$ defined by equation [5.32]. The variable on the left and the first term on the right of each equation above are total observables. The total observables with a tilde indicate quantities without media, instrumental or MPC effects:

$$\tilde{\phi}_{0S} \equiv \omega_{0S}\tau_b^{mr} + \phi_{0S} + 2\pi N_S \quad [17.22]$$

$$\tilde{\phi}_{0X} \equiv \omega_{0X}\tau_b^{mr} + \phi_{0X} + 2\pi N_X$$

$$\tilde{\tau} \equiv \tau_b^{mr} + \tau$$

$$\tilde{\dot{\tau}} \equiv \dot{\tau}_b^{mr} + \dot{\tau},$$

ϕ_{0S} is, for example, the S-band ϕ_0, τ_b^{mr} is the correlator model given by [16.10], and N_S and N_X are the integer number of S and X-band cycles needed for phase connection (see next section). Equations [17.20] and [17.21] can be substituted into the linear combinations such as [17.4] to remove dispersive effects:

$$\tau_{S/X} - \tilde{\tau} = (\bar{\tau}^t - \bar{\tau}^{t*}) - \tau^*_{\mathrm{cl(S)}} - \frac{\omega^2_{X\tau}\Delta\tau^*_{\mathrm{cl}}}{\omega^2_{X\tau} - \omega^2_{S\tau}} \quad [17.23a]$$

$$+ \frac{1}{\omega^2_{X\tau} - \omega^2_{S\tau}}\Big[(\bar{k} - \bar{k}^*)(\omega^2_{X\tau}X_{k\tau} - \omega^2_{S\tau}S_{k\tau}) + \bar{k}^*(\omega^2_{X\tau}/\omega^{*2}_{X\tau} - \omega^2_{S\tau}/\omega^{*2}_{S\tau})$$

$$+ \bar{\dot{k}}(\omega^2_{X\tau}X_{\dot{k}\tau} - \omega^2_{S\tau}S_{\dot{k}\tau}) - \bar{\dot{k}}^*(\omega^2_{X\tau}X_{\dot{k}^*\tau} - \omega^2_{S\tau}S_{\dot{k}^*\tau}) + (\omega^2_{X\tau}X_{a\tau} - \omega^2_{S\tau}S_{a\tau})\Big]$$

$$\dot{\tau}_{S/X} - \tilde{\dot{\tau}} = \bar{\dot{\tau}}^t + \frac{1}{\omega^2_{X\dot{\tau}} - \omega^2_{S\dot{\tau}}}\Big[-(\bar{k} - \bar{k}^*)(\omega^2_{X\dot{\tau}}X_{k\dot{\tau}} - \omega^2_{S\dot{\tau}}S_{k\dot{\tau}}) - \bar{\dot{k}}(\omega^2_{X\dot{\tau}}X_{\dot{k}\dot{\tau}} - \omega^2_{S\dot{\tau}}S_{\dot{k}\dot{\tau}}) \quad [17.23b]$$

$$+ \bar{\dot{k}}^*(\omega^2_{X\dot{\tau}}X_{\dot{k}^*\dot{\tau}} - \omega^2_{S\dot{\tau}}S_{\dot{k}^*\dot{\tau}}) + (\omega^2_{X\dot{\tau}}X_{a\dot{\tau}} - \omega^2_{S\dot{\tau}}S_{a\dot{\tau}})\Big]$$

where $S_{k^*\tau} \equiv S_{k\tau} - 1/\omega_{S\tau}^{*2}$ and $S_{k^*\dot{\tau}} \equiv S_{k\dot{\tau}}$ (see [C.13]) are used for simplification, and

$$\Delta\tau_{\mathrm{cl}}^{*} \equiv \tau_{\mathrm{cl(X)}}^{*} - \tau_{\mathrm{cl(S)}}^{*} \qquad [17.24]$$

(see [5.30]). The phase delay equivalent of [17.23a] is derived from the phase expressions in [17.20] and [17.21] but is not shown here because cycle ambiguities, the N_S and N_X in [17.22], are not known a priori. Typically, the dominant dispersive terms in the phase expressions are eliminated directly to resolve cycle ambiguities, making phase delay S/X corrections unnecessary. The other linear combination of delays and rates, [17.7] and [17.11], can be used to obtain the following:

$$\bar{k}_{S/X} = \bar{k}^{*}\left(\frac{\omega_{X\tau}^{*2} - \omega_{S\tau}^{*2}}{\omega_{X\tau}^{2} - \omega_{S\tau}^{2}}\right)\left(\frac{\omega_{X\tau}^{2}\omega_{S\tau}^{2}}{\omega_{X\tau}^{*2}\omega_{S\tau}^{*2}}\right) + \frac{\omega_{S\tau}^{2}\omega_{X\tau}^{2}}{\omega_{X\tau}^{2} - \omega_{S\tau}^{2}}\Big[\Delta\tau_{\mathrm{cl}}^{*} + (\bar{k} - \bar{k}^{*})(S_{k\tau} - X_{k\tau}) \qquad [17.25a]$$
$$+ \bar{\dot{k}}(S_{\dot{k}\tau} - X_{k\tau}) - \bar{\dot{k}}^{*}(S_{\dot{k}^{*}\tau} - X_{\dot{k}^{*}\tau}) + (S_{a\tau} - X_{a\tau})\Big]$$

$$\bar{\dot{k}}_{S/X} = \frac{\omega_{S\dot{\tau}}^{2}\omega_{X\dot{\tau}}^{2}}{\omega_{X\dot{\tau}}^{2} - \omega_{S\dot{\tau}}^{2}}\Big[(\bar{k} - \bar{k}^{*})(S_{k\dot{\tau}} - X_{k\dot{\tau}}) + \bar{\dot{k}}(S_{\dot{k}\dot{\tau}} - X_{k\dot{\tau}}) \qquad [17.25b]$$
$$- \bar{\dot{k}}^{*}(S_{\dot{k}^{*}\dot{\tau}} - X_{\dot{k}^{*}\dot{\tau}}) - (S_{a\dot{\tau}} - X_{a\dot{\tau}})\Big]$$

In the absence of media and processing effects, the right side of equations [17.23] should be zero. Minimizing the largest term in each equation leads to definitions of the reference frequencies. The dominant term in [17.23a] is the one proportional to $(\bar{k} - \bar{k}^{*})$. This term can be eliminated by choosing

$$\omega_{S\tau}^{2} = 1/S_{k\tau} \qquad \omega_{X\tau}^{2} = 1/X_{k\tau}. \qquad [17.26]$$

Similarly, the $\bar{\dot{k}}$ term is the dominant dispersive term in [17.23b] and can be eliminated by choosing

$$\omega_{S\dot{\tau}}^{2} = 1/S_{\dot{k}\dot{\tau}} \qquad \omega_{X\dot{\tau}}^{2} = 1/X_{\dot{k}\dot{\tau}}. \qquad [17.27]$$

Finally, the dominant term in the phase delay equivalent of [17.23a] (not shown) is proportional to $(\bar{k} - \bar{k}^*)$ and can be eliminated by setting

$$\omega^2_{S\tau^p} = 1/S_{k\tau^p} \qquad \omega^2_{X\tau^p} = 1/X_{k\tau^p}. \tag{17.28}$$

These expressions can be written in their more expanded form using [C.13]

$$\omega^2_{S\tau} = \frac{S_{d0}}{S_{d5} - t_0 S_{d6}} \tag{17.29}$$

$$\omega^2_{S\dot{\tau}} = \frac{S_{d0}}{S_{d3} - t_0 S_{d6}} \tag{17.30}$$

$$\omega^2_{S\tau^p} = \frac{\omega_{0S} S_{d0}}{S_{d4} - \omega_{0S} S_{d5} + t_0 \omega_{0S} S_{d6}}, \tag{17.31}$$

with similar expressions for X-band. With these definitions and those of [C.14], equations [17.23] and [17.25] become

$$\tau_{S/X} = \tilde{\tau} + (\bar{\tau}^t - \bar{\tau}^{t*}) - \tau^*_{\mathrm{cl(S)}} - C_{X\tau}\Delta\tau^*_{\mathrm{cl}} + \bar{\dot{k}} R_{\dot{k}\tau} - \bar{\dot{k}}^* R_{\dot{k}^*\tau} + R_{a\tau} \tag{17.32a}$$

$$\dot{\tau}_{S/X} = \tilde{\dot{\tau}} + \bar{\dot{\tau}}^t - (\bar{k} - \bar{k}^*) R_{k\dot{\tau}} + \bar{\dot{k}}^* R_{\dot{k}^*\dot{\tau}} + R_{a\dot{\tau}} \tag{17.32b}$$

$$\bar{k}_{S/X} = \bar{k} + C_{Sk}\Delta\tau^*_{\mathrm{cl}} - \bar{k}^* Q_{k^*k} + \bar{\dot{k}} R_{\dot{k}k} - \bar{\dot{k}}^* R_{\dot{k}^*k} + R_{ak} \tag{17.32c}$$

$$\bar{\dot{k}}_{S/X} = \bar{\dot{k}} + (\bar{k} - \bar{k}^*) R_{k\dot{k}} - \bar{\dot{k}}^* R_{\dot{k}^*\dot{k}} - R_{a\dot{k}} \tag{17.32d}$$

These expressions are exact, given their model assumptions. The first two quantities (the S/X corrected delay and phase delay rate) are passed to Modest for further analysis.

The first term on the right side of equations [17.32] shows the uncorrupted observable and the terms that follow are consider error terms which can introduce systematic effects in the S/X-corrected quantities. The second term on the right of [17.32a] and [17.32b] shows the effects from the average tropospheric delay and rate, and appears to be the dominant error term in these expressions at present. An external calibration (for example, Water Vapor Radiometer (WVR) data) is needed to eliminate these systematic effects.

The last three terms in equations [17.32] can be regarded as data drop-out effects; these terms would be zero if $\sigma_{\phi_{ij}}$ were constant in time, for each bin ($\sigma_{\phi_{ij}} = \sigma_{\phi_i}$). Fit evaluates the first two drop-out terms shown (16-byte precision is necessary in this calculation). Because they are usually negligibly small, Fit does not use them to correct the S/X observables at present. The $\bar{\dot{k}} R_{\dot{k}\tau}$ and $\bar{\dot{k}}^* R_{\dot{k}^*\tau}$ terms in [17.32a] are usually on the order of 10^{-14} seconds, though $\bar{\dot{k}} R_{\dot{k}\tau}$ may contribute on the order of a picosecond. The $(\bar{k} - \bar{k}^*) R_{k\dot{\tau}}$ term in [17.32b] is typically on the order of 10^{-17}, but can be of order 10^{-16}; the $\bar{\dot{k}}^* R_{\dot{k}^*\dot{\tau}}$ term is about three orders of magnitude smaller. The $\bar{\dot{k}} R_{\dot{k}k}$ and $\bar{k}^* Q_{k^*k}$ terms in [17.32c] contribute on the order of 10^8 cyc^2/sec, which typically represents about a 0.1% correction to $\bar{k}_{S/X}$; $\bar{\dot{k}}^* R_{\dot{k}^*k}$ is about three orders of magnitude smaller. The $(\bar{k} - \bar{k}^*) R_{k\dot{k}}$ term in [17.32d] is on the order of 10^2 cyc^2/sec^2, which is about a 0.01% correction to $\bar{\dot{k}}_{S/X}$; the $\bar{\dot{k}}^* R_{\dot{k}^*\dot{k}}$ term is about an order of magnitude smaller. The last drop-out term in each expression is not evaluated by Fit. These terms represent a number of negligible effects, the largest of which is probably the one proportional to $\vec{S}_{Vk}$ (see last group of equations in [C.13]). Fit does not attempt the calculation of $\vec{S}_{Vk}$ from the k_j^r time series, which is calculated from the time series of residual S and X-band delays (Fit calculates for plotting purposes), because it is dominated by system noise.

The remaining error terms in [17.32a], not discussed immediately above, are due to differences in the S and X-band clocks. This effect, also discussed in section 5, is written as two terms: a constant clock-like term, $\tau^*_{\mathrm{cl(S)}}$, which is usually absorbed at the Modest stage of analysis by a clock parameter, and a term proportional to the S and X-band clock difference, $C_{X\tau} \Delta\tau^*_{\mathrm{cl}}$, where $C_{X\tau}$ is given by [17.6] and $\Delta\tau^*_{\mathrm{cl}}$ is given by [17.24] and [5.30] and assumed to be constant during the experiment. Changes from scan to scan in $C_{X\tau}$ imply a changing delay term which cannot be absorbed by a Modest clock parameter. The size of this effect has not been studied thoroughly at this time but may border on being significant. Presumably, $\Delta\tau^*_{\mathrm{cl}}$ could be estimated in Modest since it is assumed to be constant and $C_{X\tau}$ is known for each scan.

The formal errors of the four quantities in [17.32] are given by

$$\sigma^2_{\tau_{S/X}} = C^2_{S\tau}\sigma^2_{\tau_s} + C^2_{X\tau}\sigma^2_{\tau_x} \qquad [17.33a]$$

$$\sigma^2_{\dot{\tau}_{S/X}} = C^2_{S\dot{\tau}}\sigma^2_{\dot{\tau}_s} + C^2_{X\dot{\tau}}\sigma^2_{\dot{\tau}_x} \qquad [17.33b]$$

$$\sigma^2_{\bar{k}_{S/X}} = C^2_{Sk}\sigma^2_{\tau_s} + C^2_{Xk}\sigma^2_{\tau_x} \qquad [17.33c]$$

$$\sigma^2_{\dot{\bar{k}}_{S/X}} = C^2_{S\dot{k}}\sigma^2_{\dot{\tau}_s} + C^2_{X\dot{k}}\sigma^2_{\dot{\tau}_x}, \qquad [17.33d]$$

where σ_{τ_s} and $\sigma_{\dot{\tau}_s}$ are given by [14.10b] and [14.10c], and similar expressions hold for the X-band quantities. The formal errors for the delay and phase delay rate, [17.33a] and [17.33b], are also passed to Modest for further analysis.

Section 18

Phase Connection

This section summarizes the expressions needed for phase connection. Phase connection is the process by which the estimated phase, given by [14.16a], [10.2] and [12.4], is used to form a phase delay observable. Since only the fractional number of cycles of the total phase is measured, the integer part must be determined from other information such as the BWS delay and/or model delays. Fit does not attempt phase connection at present but passes the necessary information to the Modest binary file where software independent of Fit can be used to study cycle ambiguity resolution.

The residual phase, ϕ_0^r, given by [14.16a], and the a priori residual phase, ϕ_0^a, given by [10.2] and [12.4], are determined only to a fraction of a cycle; the true residual phase is given by $2\pi N + \phi_0^a + \phi_0^r$, where N is an integer. This true residual phase, divided by the reference band frequency ω_0, gives the residual phase delay. If the correlator model contains no dispersive effects, it can be applied to the residual phase delay in the same manner as the group delay (see [16.9]). The total phase delay for S-band observations, τ_S^p, can be written

$$\tau_S^p = \tau_b^{mr} + \frac{\phi_{0S}^a + \phi_{0S}^r + 2\pi N_S}{\omega_{0S}} \qquad [18.1]$$

$$\equiv \tau_{\mathrm{Fit}(S)}^p + \frac{2\pi N_S}{\omega_{0S}}$$

where ϕ_{0S}^a and ϕ_{0S}^r are in the Modest sign convention, τ_b^{mr} is the correlator model delay given by [16.10], N_S is an unknown integer, and

$$\tau_{\mathrm{Fit}(S)}^p \equiv \tau_b^{mr} + \frac{\phi_{0S}^a + \phi_{0S}^r}{\omega_{0S}} \qquad [18.2]$$

is the quantity Fit passes to Modest as the S-band phase delay (S-band is assumed here and throughout this section, but similar equations hold for X-band).

The S-band phase delay, considering dispersive, tropospheric and manual phase calibration effects as presented in the last subsection of section 17, is given by (see [17.20])

$$\tau_S^p = \tilde{\tau}_S^p - \frac{\phi_{0S}^*}{\omega_{0S}} + (\bar{\tau}^t - \bar{\tau}^{t*}) - \frac{\Delta\omega_{0S}}{\omega_{0S}}\tau_{\mathrm{cl(S)}}^* - \bar{k}S_{k\tau^p} + \bar{k}^* S_{k^*\tau^p} \qquad [18.3]$$
$$- \dot{\bar{k}}S_{\dot{k}\tau^p} + \dot{\bar{k}}^* S_{\dot{k}^*\tau^p} + S_{a\tau^p}.$$

Here, $\tilde{\tau}_S^p \equiv \tilde{\phi}_{0S}/\omega_{0S}$ is the phase delay without propagation or processing effects, $\tilde{\phi}_{0S}$ is given by [17.22] and $\Delta\omega_{0S} \equiv \omega_{0S} - \omega_{0S}^*$ (see [5.32]). The last three terms of [18.3] are usually negligible and will be dropped ($\dot{\bar{k}}S_{\dot{k}\tau^p}$ and $\dot{\bar{k}}^* S_{\dot{k}^*\tau^p}$ contribute on the order of 10^{-5} cycles divided by the band reference frequency). The second, fourth and sixth terms of this equation depend directly on ω_{0S}. If all scans are processed with the same ω_{0S}, the second term will represent a constant, clock-like effect, the fourth term will vanish and the sixth term will simplify. Equating [18.3] to [18.1], assuming a constant ω_{0S} for all scans, $\bar{\omega}_{0S}$, and expanding $S_{k\tau^p}$ and $S_{k^*\tau^p}$ gives

$$\tau_{\mathrm{Fit}(S)}^p + \frac{2\pi N_S}{\bar{\omega}_{0S}} = \tilde{\tau}_S^p - \tau_{\mathrm{cl}}^{p*} + (\bar{\tau}^t - \bar{\tau}^{t*}) - \frac{(\bar{k} - \bar{k}^*)}{\omega_{S\tau^p}^2}, \qquad [18.4]$$

where

$$\tau_{\mathrm{cl}}^{p*} \equiv \frac{\phi_{0S}^*}{\bar{\omega}_{0S}}, \qquad [18.5]$$

and $\omega_{S\tau^p}^2$ is given by [17.28] and [17.31].

Equation [18.4] can be rearranged to give

$$\tau_{\mathrm{Fit}(S)}^p + \frac{(\bar{k} - \bar{k}^*)}{\omega_{S\tau^p}^2} + \frac{2\pi N_S}{\bar{\omega}_{0S}} = \tilde{\tau}_S^p - \tau_{\mathrm{cl}}^{p*} + (\bar{\tau}^t - \bar{\tau}^{t*}) \qquad [18.6]$$
$$\simeq \tau_{\mathrm{Mod}}^m,$$

where τ_{Mod}^m is the Modest delay estimate which includes clock and tropospheric modeling. This can be rewritten as

$$\tau_{\mathrm{Fit}(S)}^p + \frac{(\bar{k} - \bar{k}^*)}{\omega_{S\tau^p}^2} - \tau_{\mathrm{Mod}}^m + \frac{2\pi N_S}{\bar{\omega}_{0S}} = \frac{2\pi F_S}{\bar{\omega}_{0S}}, \qquad [18.7]$$

where F_S is introduced to make a strict equality. If $\bar{k}$ and $\bar{k}^*$ are approximated by $\bar{k}_{S/X}$ and $\bar{k}^*_{S/X}$ (given by [17.32c]), then

$$\tau^p_{\text{Fit}(S)} + \frac{(\bar{k}_{S/X} - \bar{k}^*_{S/X})}{\omega^2_{S\tau^p}} - \tau^m_{\text{Mod}} + \frac{2\pi N_S}{\bar{\omega}_{0S}} \simeq \frac{2\pi F_S}{\bar{\omega}_{0S}}, \qquad [18.8]$$

All quantities, except N_S, on the left side of this equation are known, so N_S can be chosen to minimize the right side. This defines F_S to be a number of cycles between -1/2 and +1/2. With N_S determined, the right side of [18.6] gives the S-band phase delay. The formal error in F_S, which can be easily derived from [18.8], [14.10a] and [17.33c], is

$$\sigma^2_{F_S} = \frac{\sigma^2_{\phi_0}}{4\pi^2} + \frac{\omega^2_{0S}}{\omega^4_{S\tau^p}}(\sigma^2_{\bar{k}_{S/X}} + \sigma^2_{\bar{k}^*_{S/X}}), \qquad [18.9]$$

if σ_{F_S} has units of cycles, and σ_{ϕ_0} has units of radians. A standard check that the assigned N_S is meaningful is to plot F_S for many scans; each F_S should be near zero (because the Modest clock parameter should remove any constant bias) and their errors should be a small fraction of a cycle.

Section 19

Modest Interface

This section summarizes those quantities passed from Fit to Modest; Table 19.1 summarizes all such data. As stated at the beginning of this report, the goal of this analysis is to derive the charged particle calibrated delay, phase delay rate and phase delay. Fit passes three delays and phase delay rates (and their formal errors) to Modest: those for S and X band given by [16.9] and the final S/X corrected values given by [17.4] and [17.6] for the delay and [17.10] and [17.12] for the phase delay rate. The phase delay for S and X band, given by [18.2], is passed but the S/X calibrated phase delay is not because phase connection, which Fit does not attempt, is needed first. The amplitude and its formal error, given by [14.17], are also passed for both bands. The reference time given by [3.1] is added to the scan start time to give the absolute scan reference time. This time, along with the reference frequencies given by [3.2], [17.29], [17.30] and [17.31] for both bands, is also passed. Finally, the source name, station names, scan length and scan duration are passed to Modest.

Quantity	Reference	Fortran Storage
Source Name		$C*12$
Station Names		$2(C*8)$
Reference Date		$I*4$
Reference Time	[3.1]+Scan Start	$R*8$
Observation Number		$I*2$
Reference Frequencies	[3.2] [17.29–31]	$8(R*8)$
Scan Length		$R*4$
Amplitude	[14.17] [2.16c]	$2(R*4)$
Amplitude Error		$2(R*4)$
Group Delay	[16.9] [17.4]	$3(R*8)$
Phase Delay Rate	[16.9] [17.10]	$3(R*8)$
Phase Delay	[18.2]	$3(R*8)$
Group Delay Error	[14.10b]	$3(R*4)$
Phase Delay Rate Error	[14.10c]	$3(R*4)$
Phase Delay Error	[14.10a]	$3(R*4)$

Table 19.1 Size and order of data passed from Fit to Modest. The reference column lists the relevant equations from the text when applicable. An additional $I*2$ record descriptor is written to Modest before these data.

Appendix A

Phase and Amplitude Probability Distributions

The phase and amplitude probability distributions for a complex phasor, along with their means and variances, are derived from the Gaussian distributions of the x and y phasor components. The phase distribution is derived first by defining the following transformation and its inverse:

$$\begin{aligned}(x, y) &\rightarrow (w, w \tan\phi), \\ (\phi, w) &\rightarrow (\text{arctan2}(y, x), x),\end{aligned} \qquad [A.1]$$

where ϕ is the angle to a given x–y point, w is a dummy variable which will be eliminated by integration, and the function $\text{arctan2}(y, x)$ is defined by

$$\text{arctan2}(y, x) \equiv \begin{cases} \tan^{-1}\frac{y}{x} & x > 0 \\ \tan^{-1}\frac{y}{x} + \text{sign}(y) \cdot \pi & x < 0 \\ \text{sign}(y) \cdot \frac{\pi}{2} & x = 0. \end{cases} \qquad [A.2]$$

Figure A.1 illustrates the transformation. From this figure, $w > 0$ implies $|\phi| < \frac{\pi}{2}$ and $w < 0$ implies $|\phi| > \frac{\pi}{2}$; the other, blank regions correspond to the transformation $\phi = \text{arctan2}(y, x) + \pi$.

The ϕ probability distribution is obtained by integrating $H(\phi, w)$, the two-dimensional probability distribution, over w. The infinitesimals in the two coordinate systems can be equated:

$$H(\phi, w)\, d\phi\, dw = f(x)\, g(y)\, dx\, dy, \qquad [A.3]$$

where f and g are the Gaussian x and y distributions. The ϕ probability distribution, $P(\phi)$, can now be written as

$$P(\phi) = \int_{-\infty}^{\infty} H(\phi, w)\, dw \qquad [A.4]$$

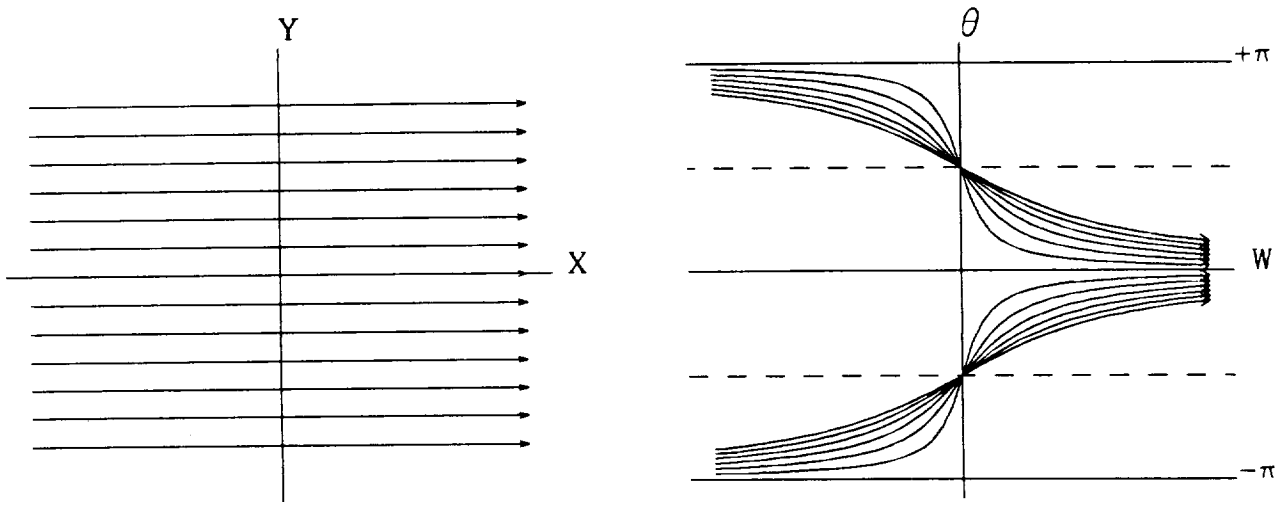

Fig. A.1 The two-dimensional transformation between the x–y plane and the w–ϕ plane for the function given by [A.1]. The horizontal lines with arrows show the transformation. The regions in the w–ϕ plane free of such lines have no corresponding point in the x–y plane; these areas correspond to the function $\phi = \text{atan2}(y, x) + \pi$.

$$= \begin{cases} \int_0^\infty H(\phi, w)\, dw & |\phi| < \frac{\pi}{2} \\ \int_{-\infty}^0 H(\phi, w)\, dw & |\phi| > \frac{\pi}{2} \end{cases}$$

$$= \begin{cases} \int_0^\infty f(x)\, g(y)\, |J|\, dw & |\phi| < \frac{\pi}{2} \\ \int_{-\infty}^0 f(x)\, g(y)\, |J|\, dw & |\phi| > \frac{\pi}{2} \end{cases}$$

where $|J|$ is the Jacobian of the transformation ([A.1]):

$$J \equiv \det \begin{pmatrix} \frac{\partial x}{\partial w} & \frac{\partial y}{\partial w} \\ \frac{\partial x}{\partial \phi} & \frac{\partial y}{\partial \phi} \end{pmatrix} \qquad [A.5a]$$

$$= x \sec^2 \phi. \qquad [A.5b]$$

Substituting [A.5b] and eliminating the absolute value signs in [A.4] leads to

$$P(\phi) = \begin{cases} \sec^2\phi \int_0^\infty f(w)\, g(w\tan\phi)\, w\, dw & |\phi| < \frac{\pi}{2} \\ \sec^2\phi \int_0^\infty f(-w)\, g(-w\tan\phi)\, w\, dw & |\phi| > \frac{\pi}{2}. \end{cases} \qquad [A.6]$$

Using the Gaussian distributions for x and y, with means $\bar{x}$ and $\bar{y}$, and variances σ_x^2 and σ_y^2,

$$f(x) = \frac{1}{\sqrt{2\pi}\sigma_x} e^{\frac{-(x-\bar{x})^2}{2\sigma_x^2}} \qquad g(y) = \frac{1}{\sqrt{2\pi}\sigma_y} e^{\frac{-(y-\bar{y})^2}{2\sigma_y^2}}, \qquad [A.7]$$

leads to

$$P(\phi) = \frac{\sec^2\phi}{2\pi\sigma_x\sigma_y} \int_0^\infty \exp - \left[\frac{(\pm w - \bar{x})^2}{2\sigma_x^2} + \frac{(\pm w\tan\phi - \bar{y})^2}{2\sigma_y^2}\right] w\, dw \qquad [A.8]$$

$$= \frac{e^{-c}}{2\pi\sigma_x\sigma_y\cos^2\phi} \int_0^\infty e^{-aw^2 \pm bw} w\, dw,$$

where

$$a \equiv \frac{1}{2}\left(\frac{1}{\sigma_x^2} + \frac{\tan^2\phi}{\sigma_y^2}\right) = \frac{1}{2\cos^2\phi}\left(\frac{\cos^2\phi}{\sigma_x^2} + \frac{\sin^2\phi}{\sigma_y^2}\right) \qquad [A.9]$$

$$b \equiv \frac{\bar{x}}{\sigma_x^2} + \frac{\bar{y}\tan\phi}{\sigma_y^2} = \frac{1}{\cos\phi}\left(\frac{\bar{x}\cos\phi}{\sigma_x^2} + \frac{\bar{y}\sin\phi}{\sigma_y^2}\right)$$

$$c \equiv \frac{1}{2}\left(\frac{\bar{x}^2}{\sigma_x^2} + \frac{\bar{y}^2}{\sigma_y^2}\right).$$

The upper sign in [A.8] corresponds to $|\phi| < \frac{\pi}{2}$ and the lower sign to $|\phi| > \frac{\pi}{2}$; this will be the case for all such equations below. Making a change of variables from w to $r = \sqrt{a}(w \mp \frac{b}{2a})$ leads to

$$P(\phi) = \frac{e^{k'^2 - c}}{2\pi\sigma_x\sigma_y\, a\cos^2\phi} \int_{\mp k'}^\infty e^{-r^2}(r \pm k')\, dr, \qquad [A.10]$$

where

$$k' \equiv \frac{b}{2\sqrt{a}} \qquad [A.11]$$

$$= \frac{\text{sign}(\cos\phi)}{\sqrt{2}} \frac{\left(\frac{\bar{x}\cos\phi}{\sigma_x^2} + \frac{\bar{y}\sin\phi}{\sigma_y^2}\right)}{\sqrt{\frac{\cos^2\phi}{\sigma_x^2} + \frac{\sin^2\phi}{\sigma_y^2}}}.$$

Define $k \equiv k'\text{sign}(\cos\phi) = \pm k'$ (using the sign convention noted above) so that

$$P(\phi) = \frac{e^{k^2-c}}{2\pi\sigma_x\sigma_y a\cos^2\phi} \int_{-k}^{\infty} e^{-r^2}(r-k)\,dr \qquad \text{(for all } \phi\text{).} \qquad [A.12]$$

Evaluating the integral and substituting in the expressions for a and c gives the final probability distribution for ϕ as

$$P(\phi) = \frac{\sigma_x\sigma_y e^{-\frac{1}{2}\left(\frac{\bar{x}^2}{\sigma_x^2}+\frac{\bar{y}^2}{\sigma_y^2}\right)}}{2\pi(\sigma_x^2\sin^2\phi + \sigma_y^2\cos^2\phi)}[1 + \sqrt{\pi}\,k\,e^{k^2}(1+\text{erf}\,k)] \qquad [A.13]$$

$$k = \frac{1}{\sqrt{2}} \frac{\left(\frac{\bar{x}\cos\phi}{\sigma_x^2} + \frac{\bar{y}\sin\phi}{\sigma_y^2}\right)}{\sqrt{\frac{\cos^2\phi}{\sigma_x^2} + \frac{\sin^2\phi}{\sigma_y^2}}}.$$

Equation [A.13] was derived for general x and y Gaussian distributions, but as indicated by equation [2.9], the variances of the x and y components are approximately equal. Equation [A.13] can be simplified using $\sigma_x = \sigma_y = \sigma$ to give

$$P(\phi) = \frac{1}{2\pi} e^{\frac{-R^2}{2\sigma^2}}\,[1 + \sqrt{\pi}\,k\,e^{k^2}(1+\text{erf}\,k)], \qquad [A.14]$$

$$k = \frac{R}{\sqrt{2}\,\sigma}\cos(\phi - \bar{\phi}),$$

where R and ϕ are defined by $\bar{x} \equiv R\cos\bar{\phi}$ and $\bar{y} \equiv R\sin\bar{\phi}$. This should be compared to equation [2.15a].

The mean of ϕ is seen to be unbiased by evaluating

$$\begin{aligned}\langle\phi\rangle &= \int_{\bar{\phi}-\pi}^{\bar{\phi}+\pi} \phi\, P(\phi)\, d\phi \qquad [A.15]\\ &= \int_{-\pi}^{\pi} (\alpha+\bar{\phi})\, P(\alpha+\bar{\phi})\, d\alpha \\ &= \int_{-\pi}^{\pi} \alpha\, P(\alpha+\bar{\phi})\, d\alpha + \bar{\phi}\int_{-\pi}^{\pi} P(\alpha+\bar{\phi})\, d\alpha \\ &= \bar{\phi},\end{aligned}$$

where $\alpha \equiv \phi - \bar{\phi}$ and the last two integrals are zero and one respectively, because the first is odd with even integration limits and the second is the distribution normalization. The phase variance is given by

$$\begin{aligned}\mathrm{Var}(\phi) &= \int_{-\pi}^{\pi} (\phi - \langle\phi\rangle)^2\, P(\phi)\, d\phi \qquad [A.16]\\ &= \int_{-\pi-\bar{\phi}}^{\pi-\bar{\phi}} \phi^2\, P(\phi+\bar{\phi})\, d\phi \\ &= \int_{-\pi}^{\pi} \phi^2\, P(\phi+\bar{\phi})\, d\phi \\ &= \frac{\pi^2}{3} e^{\frac{-R^2}{2\sigma^2}} + \frac{1}{\sqrt{2\pi}}\frac{R}{\sigma}\int_0^{\pi} \phi^2 \cos\phi\, e^{\frac{-R^2\sin^2\phi}{2\sigma^2}} \left(1 + \mathrm{erf}\,\frac{R\cos\phi}{\sqrt{2}\sigma}\right) d\phi.\end{aligned}$$

Equations [A.15] and [A.16] are equivalent to [2.15b] and [2.15c].

The Amplitude Probability Distribution

The amplitude probability distribution can be obtained with the transformation

$$\begin{aligned}(x,y) &\rightarrow (w, \sqrt{A^2 - w^2}) \qquad [A.17]\\ (A,w) &\rightarrow (\sqrt{x^2+y^2}, x),\end{aligned}$$

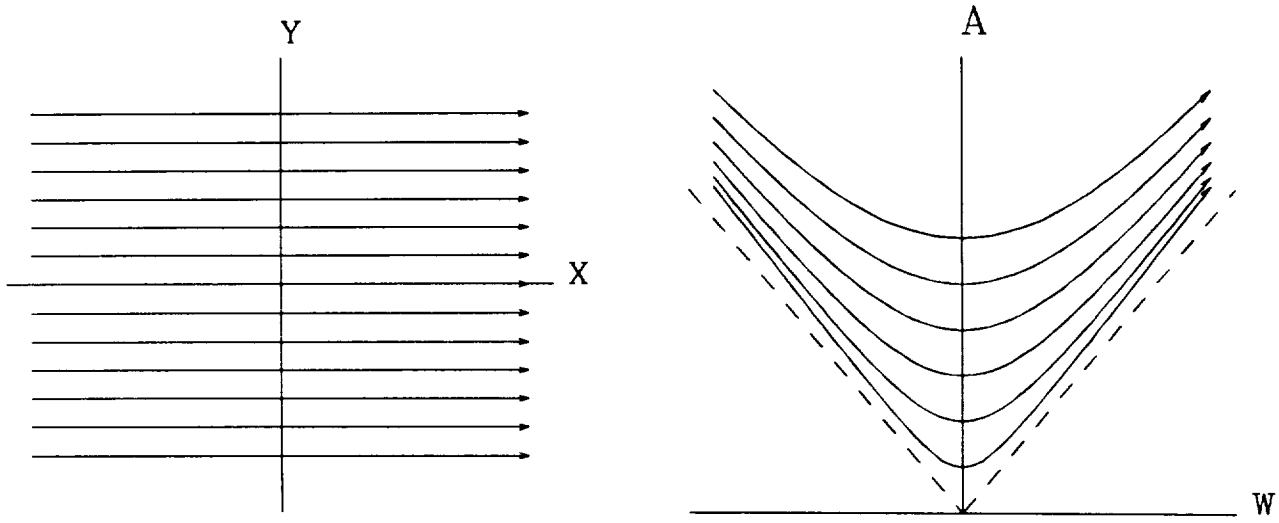

Fig. A.2 The two-dimensional transformation between the x–y plane and the w–A plane for the function given by [A.17]. The horizontal lines with arrows show the transformation. The dashed lines in the w–A plane show $A = \pm w$.

where A is the amplitude. Figure A.2 illustrates this transformation. Because both signs of y transform to the same A–w point, this transformation is not one-to-one; this is handled explicitly by a separate integration for each sign of y. The amplitude probability distribution can now be written

$$P(A) = \int_{-\infty}^{\infty} H(A,w)\,dw \qquad [A.18]$$
$$= \int_{-\infty}^{\infty} f(x)\,g(y)\,|J|\,dw + \int_{-\infty}^{\infty} f(x)\,g(-y)\,|J|\,dw,$$

where J, given by [A.5a] with ϕ replaced with A, is $A/\sqrt{A^2 - w^2}$. Substituting this into [A.18] and simplifying gives

$$P(A) = \frac{A}{2\pi\sigma^2} e^{\frac{-(R^2+A^2)}{2\sigma^2}} \int_{-A}^{A} \left[\exp\left(\frac{\bar{x}\,w + \bar{y}\,\sqrt{A^2 - w^2}}{\sigma^2} \right) + \right. \qquad [A.19]$$
$$\left. \exp\left(\frac{\bar{x}\,w - \bar{y}\,\sqrt{A^2 - w^2}}{\sigma^2} \right) \right] \frac{dw}{\sqrt{A^2 - w^2}},$$

where R is defined above.

Using $\bar{x} \equiv R\cos\bar{\phi}$ and $\bar{y} \equiv R\sin\bar{\phi}$ as above, and changing variables from w to β with $w \equiv A\cos\beta$, leads to

$$P(A) = \frac{A}{2\pi\sigma^2} e^{\frac{-(R^2+A^2)}{2\sigma^2}} \int_0^{\pi} \left(e^{\frac{RA}{\sigma^2}\cos(\beta-\bar{\phi})} + e^{\frac{RA}{\sigma^2}\cos(\beta+\bar{\phi})} \right) d\beta \qquad [A.20]$$

$$= \frac{A}{2\pi\sigma^2} e^{\frac{-(R^2+A^2)}{2\sigma^2}} \int_{-\bar{\phi}}^{\pi-\bar{\phi}} \left(e^{\frac{RA}{\sigma^2}\cos\alpha} + e^{\frac{RA}{\sigma^2}\cos\alpha} \right) d\alpha$$

$$= \frac{A}{\pi\sigma^2} e^{\frac{-(R^2+A^2)}{2\sigma^2}} \int_0^{\pi} e^{\frac{RA}{\sigma^2}\cos\alpha}\, d\alpha,$$

where $\alpha \equiv \beta - \bar{\phi}$. Using the integral representation of the Modified Bessel function[10]

$$I_0(x) = \frac{1}{\pi} \int_0^{\pi} e^{\pm x\cos\beta}\, d\beta, \qquad [A.21]$$

leads to the final expression for the amplitude probability distribution (see equation [2.16a])

$$P(A) = \frac{A}{\sigma^2} e^{\frac{-(R^2+A^2)}{2\sigma^2}} I_0\left(\frac{RA}{\sigma^2}\right). \qquad [A.22]$$

The amplitude mean and variance can be derived in the same manner as the phase mean and variance. The amplitude mean is given by

$$\langle A \rangle = \int_{-\infty}^{\infty} A\, P(A)\, dA \qquad [A.23]$$

$$= \frac{1}{\sigma^2} e^{\frac{-R^2}{2\sigma^2}} \int_0^{\infty} A^2\, e^{\frac{-A^2}{2\sigma^2}} I_0\left(\frac{RA}{\sigma^2}\right) dA.$$

The solution to this integral is given in reference 11, giving equation [2.16b]. The amplitude variance is calculated using

$$\mathrm{Var}(A) = \int_{-\infty}^{\infty} (A - \langle A \rangle)^2\, P(A)\, dA \qquad [A.24]$$

$$= \int_{-\infty}^{\infty} A^2\, P(A)\, dA - \langle A \rangle^2$$

$$= \langle A^2 \rangle - \langle A \rangle^2,$$

where $\langle A^2 \rangle$ is also given in reference 11 as

$$\langle A^2 \rangle = R^2 + 2\sigma^2. \qquad [A.25]$$

Substituting this and [A.23] into [A.24] leads to the final expression for the amplitude variance, given by [2.16c].

Appendix B

Effects of Time and Frequency FFTs on Data Phasors and A Priori Estimates

This section presents a detailed accounting of the data phasors through the time FFT, the rescaling operation and the frequency FFT. The goal is to derive an expression for the final, transformed phasors in terms of the original data phasors given by equation [10.1].

The standard FFT transforms a matrix $\vec{a}(i)$ into the matrix $\vec{b}(k)$, each having m phasors. These matrices are related by

$$\vec{b}(k) = \sum_{i=1}^{m} \vec{a}(i)\, e^{2\pi \mathrm{i} \frac{(i-1)(k-1)}{m}} \qquad i,k = 1,2,\cdots,m. \qquad [B.1]$$

By padding the input FFT array with additional zero-amplitude phasors, the output array will have more entries, corresponding to a finer discrete sampling of the transform function. If m data phasors are padded with zero-amplitude phasors resulting in a total of n phasors, the equation relating the data and transformed arrays is

$$\vec{b}(k) = \sum_{i=1}^{m} \vec{a}(i)\, e^{2\pi \mathrm{i} \frac{(i-1)(k-1)}{n}} \qquad \begin{cases} i = 1,2,\cdots,m \\ k = 1,2,\cdots,n. \end{cases} \qquad [B.2]$$

From this equation, it can be seen that no approximation or inaccuracy results from padding the FFT arrays; the padding simply increases the sampling density of the transformed phasors.

The first FFT performed by Fit is over the phasor time series of each bin. If $\vec{\rho}_{kl}$ is the data phasor for the kth time point and lth bin, then the transformed array, $\vec{F}(i,l)$, is given by

$$\vec{F}(i,l) = \sum_{k=1}^{n_r} \vec{\rho}_{kl} \exp 2\pi \mathrm{i} \frac{(k-1)(i-1)}{n_t}, \qquad [B.3]$$

where n_r is the number of data time points, and n_t is the total number of phasors in the FFT after padding, and is selected to be the lowest power of two that at least doubles n_r.

The time FFT is shown schematically in Figure B.1a. The lower numbers in the figure indicate the elements of the FFT output array, and the upper numbers represent the fringe frequency corresponding to the given array element. The first array element corresponds to zero fringe frequency. The second element corresponds to fringe frequency $\Delta \equiv 1\,(\text{cycle})/n_t\,t_c$ Hz, where t_c is the number of seconds between points in the time series, usually two seconds with the Block II correlator. Each successive array element corresponds to a fringe frequency Δ higher than the previous element. The sampling rate of $1\,(\text{cycle})/t_c$ Hz limits the fringe frequency to $\pm 1\,(\text{cycle})/2t_c$; actual fringe frequencies outside this range will appear in it through aliasing (r in the figure corresponds to this highest frequency; $r \equiv 1\,(\text{cycle})/2t_c$). Thus, array elements in the second half of the array should be interpreted as negative fringe frequencies, increasing from the largest negative fringe frequency $-r$ Hz to $-\Delta$ Hz.

Because the fringe frequency in Figure B.1a is discontinuous at the midpoint, Fit swaps the array halves, as shown in Figure B.1b. Equation [B.3] must be modified to reflect this change in array ordering. Replacing i with $i - n_t/2$, the swapped array of transformed phasors, $\vec{F}'(i,l)$, can be written in terms of the original phasors as

$$\vec{F}'(i,l) = \sum_{k=1}^{n_r} \vec{\rho}_{kl} \exp 2\pi \mathrm{i} \frac{(k-1)(i - n_t/2 - 1)}{n_t}. \qquad [B.4]$$

Fit next interpolates and rescales the transformed phasors. The resulting density is half that found in a hypothetical bin having frequency ω_0. For the purpose at hand, this can be broken into two stages: the interpolation, followed by the rescaling. If $\vec{F}''(i,l)$ is a matrix element after interpolation, then

$$\begin{aligned} \vec{F}''(i,l) &= \vec{F}'(2i,l) \qquad [B.5] \\ &= \sum_{k=1}^{n_r} \vec{\rho}_{kl} \exp 2\pi \mathrm{i} \frac{(k-1)(2i - n_t/2 - 1)}{n_t}. \end{aligned}$$

This operation is shown schematically in Figure B.1c, where $\Delta' = 2\Delta$. The rescaling results in the nominal fringe rate being multiplied by ω_l/ω_0. If $\vec{F}'''$ is the matrix after

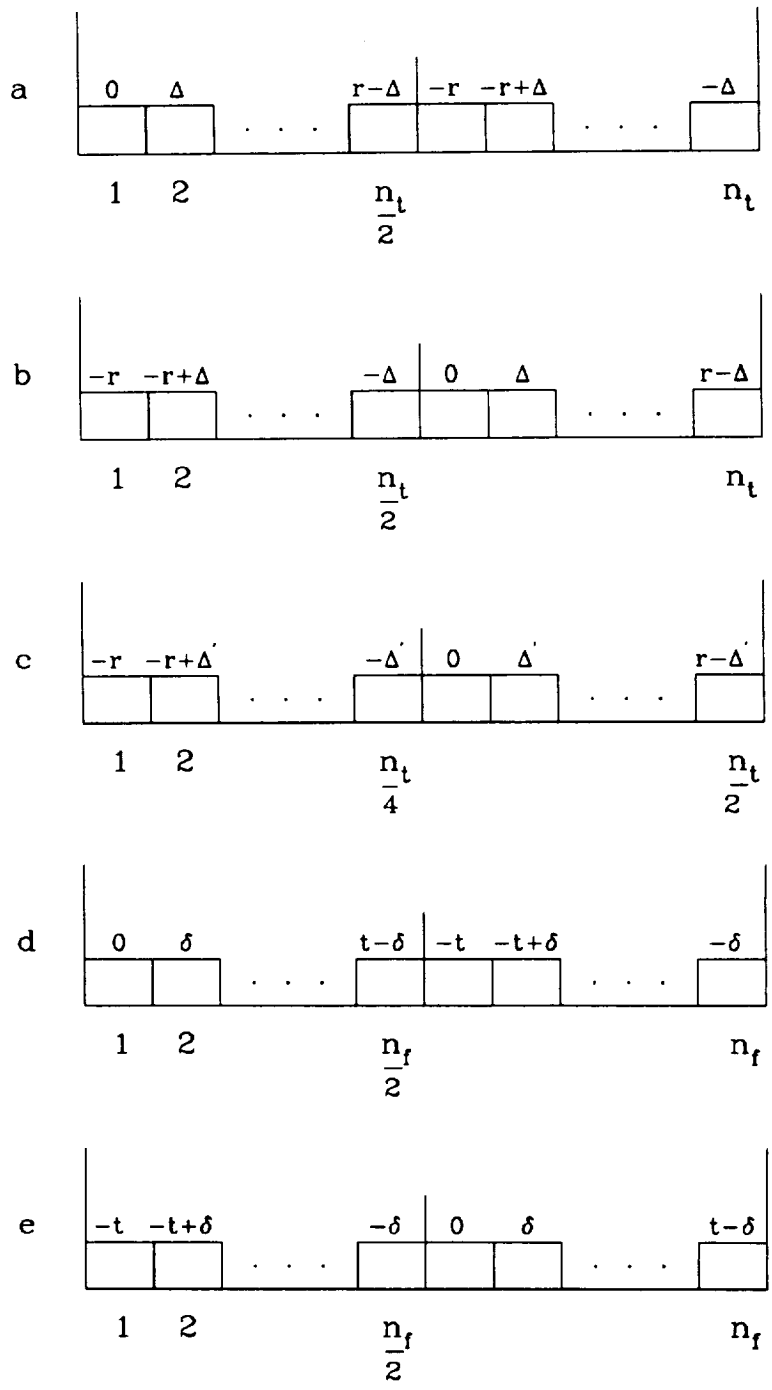

Fig. B.1 Schematic representations of the FFT arrays at various stages of the analysis. The lower numbers are the FFT array elements and the upper numbers are the corresponding fringe frequency (a–c) or BWS delay (d–e).

rescaling then

$$\vec{F}'''(i,l) = \sum_{k=1}^{n_r} \vec{\rho}_{kl} \exp 2\pi \mathrm{i} \frac{(k-1)(2i - n_t/2 - 1)}{n_t} \frac{\omega_l}{\omega_0}. \qquad [B.6]$$

Figure B.1c still applies after rescaling if r and Δ are assumed to be scaled by ω_l/ω_0.

Fit next performs the frequency FFT. This FFT not only has zero-amplitude phasors padding the end of the array, but also has them between channels when BWS is used to increase the bandwidth. If $\vec{G}(i,j)$ is a phasor after performing the frequency FFT, then

$$\vec{G}(i,j) = \sum_{l=1}^{n_b} \vec{F}'''(i,l) \exp 2\pi \mathrm{i} \frac{(T(l)-1)(j-1)}{n_f} \qquad [B.7]$$

$$= \sum_{l=1}^{n_b} \sum_{k=1}^{n_r} \vec{\rho}_{kl} \exp 2\pi \mathrm{i} \left[\frac{(k-1)(2i - n_t/2 - 1)}{n_t} \frac{\omega_l}{\omega_0} + \frac{(T(l)-1)(j-1)}{n_f} \right],$$

where n_b is the number of bins, and n_f is the lowest power of two that at least doubles the number of possible bins across the observing band. The $T(l)$ array maps the sequential bin number to a hypothetical bin number assuming the observing band is packed as densely as possible:

$$T(l) = \frac{\omega_l - \omega_1}{\omega_b} + 1, \qquad [B.8]$$

where ω_b is the width of a single bin and ω_1 is the frequency of the first bin. Figure B.1d shows the frequency FFT in a similar manner to Figure B.1a. Here, $\delta \equiv 1\,(\text{cycle})/n_f\,\omega_b$ seconds is the phasor spacing in delay, and $\pm t$ is the range of BWS delays, where $t \equiv 1\,(\text{cycle})/2\omega_b$ seconds. The final operation Fit performs is to swap the array halves in the frequency direction to eliminate the discontinuity at the array center. This is the same as replacing j with $j - n_f/2$ in [B.7]. Substituting [B.8] leads to the final form of the transformed phasor, $\vec{T}_{ij}$,

$$\vec{T}_{ij} = \sum_{l=1}^{n_b} \sum_{k=1}^{n_r} \vec{\rho}_{kl} \exp 2\pi \mathrm{i} \left[\frac{(k-1)(2i - n_t/2 - 1)}{n_t} \frac{\omega_l}{\omega_0} + \frac{(\omega_l - \omega_1)(j - n_f/2 - 1)}{\omega_b\, n_f} \right], \qquad [B.9]$$

which is also shown schematically in Figure B.1e (compare to [10.1]).

Calculation of A Priori Estimates

The maximum amplitude phasor among those obtained from the FFTs corresponds to a discrete i–j point near the true maximum phasor. An iterative search in i–j space is performed near this maximum FFT phasor to obtain the i–j point giving the true maximum amplitude; call this point (x_i, x_j) and call the phase of the transformed phasor at this point $\phi_{\max} \equiv \arg \vec{T}(x_j, x_i)$. At the maximum amplitude point, the data phasors have the same phase to the best approximation of any point in the delay–rate space. If Θ_{ijkl} is the phase of the exponent in [B.9] and Φ_{kl} is the phase of the data phasor, $\vec{\rho}_{kl}$, then on average

$$\Phi_{kl} + \Theta_{x_i x_j kl} = \phi_{\max}. \qquad [B.10]$$

Rewrite $\Theta_{x_i x_j kl}$ as

$$\Theta_{x_i x_j kl} = \frac{2\pi(k-1)(2x_i - n_t/2 - 1)}{n_t}\frac{\omega_l}{\omega_0} + \frac{2\pi(\omega_l - \omega_1)(x_j - n_f/2 - 1)}{\omega_b n_f} \qquad [B.11]$$

$$= 2\pi(k-1)\frac{\omega_l}{\omega_0}\bar{x}_i + \frac{2\pi}{\omega_b}(\omega_l - \omega_1)\bar{x}_j$$

$$= \frac{2\pi}{t_c}(t_k - t_1)\frac{\omega_l}{\omega_0}\bar{x}_i + \frac{2\pi}{\omega_b}(\omega_l - \omega_1)\bar{x}_j,$$

where

$$\bar{x}_i \equiv \frac{2x_i - n_t/2 - 1}{n_t} \qquad \bar{x}_j \equiv \frac{x_j - n_f/2 - 1}{n_f}, \qquad [B.12]$$

and $(k-1) \equiv (t_k - t_1)/t_c$ are used. To obtain the a priori estimates, replace the data phases, Φ_{kl}, with the model phase given by [6.2]. Substituting [B.11] and [6.2] into [B.10] leads to

$$\phi_{\max} = \tau\omega_l - \tau\omega_0 + \dot{\tau}\omega_l t_k - \dot{\tau}\omega_l t_0 + \phi_0 + \frac{2\pi}{t_c}\frac{\omega_l}{\omega_0}\bar{x}_i(t_k - t_1) + \frac{2\pi}{\omega_b}\bar{x}_j(\omega_l - \omega_1) \qquad [B.13]$$

$$= (\dot{\tau} + \frac{2\pi}{\omega_0 t_c}\bar{x}_i)\omega_l t_k + (\tau - \dot{\tau}t_0 - \frac{2\pi}{\omega_0 t_c}t_1\bar{x}_i + \frac{2\pi}{\omega_b}\bar{x}_j)\omega_l + (\phi_0 - \tau\omega_0 - \frac{2\pi}{\omega_b}\omega_1\bar{x}_j),$$

where all k and l dependence has been placed outside the parentheses. For this equation to hold for all k and l, the quantities inside the first two sets of parentheses must be zero. Thus, the following equations must hold

$$0 = \dot{\tau} + \frac{2\pi}{\omega_0 t_c}\bar{x}_i \qquad [B.14]$$

$$0 = \tau - \dot{\tau}t_0 - \frac{2\pi}{\omega_0 t_c}t_1\bar{x}_i + \frac{2\pi}{\omega_b}\bar{x}_j$$

$$\phi_{\max} = \phi_0 - \tau\omega_0 - \frac{2\pi}{\omega_b}\omega_1\bar{x}_j.$$

Solving these equations for τ, $\dot{\tau}$ and ϕ_0 gives

$$\tau = -\frac{2\pi}{\omega_0 t_c}(t_0 - t_1)\bar{x}_i - \frac{2\pi}{\omega_b}\bar{x}_j \qquad [B.15]$$

$$= \dot{\tau}(t_0 - t_1) - \frac{2\pi}{\omega_b}\bar{x}_j$$

$$\dot{\tau} = -\frac{2\pi}{\omega_0 t_c}\bar{x}_i$$

$$\phi_0 = \phi_{\max} - \frac{2\pi}{t_c}(t_0 - t_1)\bar{x}_i - \frac{2\pi}{\omega_b}(\omega_0 - \omega_1)\bar{x}_j$$

$$= \phi_{\max} + \tau(\omega_0 - \omega_1) + \dot{\tau}\omega_1(t_0 - t_1),$$

which are also equations [10.2], as desired.

Appendix C

Time and Frequency Summations and Expressions

This section defines time and frequency summations, and combinations of these, which are used extensively in the least-squares analysis found in section 14 and the charged particle and tropospheric consider analysis given in section 17. Some simplifying expressions are also included here which are useful in deriving some of the equations in those sections. For the sums that follow, i runs over all bins in the band with bin frequencies ω_i, j runs over all time points, t_j, σ_{ij}^2 is given by [2.15c], and ϕ_{ij} is the phase of the data phasors. S-band expressions are given here; X_1 would be the X-band counterpart to S_1, for example.

$$S_m^j \equiv \sum_i^{(S)} \frac{1}{\omega_i \sigma_{ij}^2} \qquad S_m \equiv \sum_j S_m^j = \sum_{ij}^{(S)} \frac{1}{\omega_i \sigma_{ij}^2} \qquad [C.1]$$

$$S_0^j \equiv \sum_i^{(S)} \frac{1}{\sigma_{ij}^2} \qquad S_0 \equiv \sum_j S_0^j = \sum_{ij}^{(S)} \frac{1}{\sigma_{ij}^2}$$

$$S_1^j \equiv \sum_i^{(S)} \frac{\omega_i}{\sigma_{ij}^2} \qquad S_1 \equiv \sum_j S_1^j = \sum_{ij}^{(S)} \frac{\omega_i}{\sigma_{ij}^2}$$

$$S_2^j \equiv \sum_i^{(S)} \frac{\omega_i^2}{\sigma_{ij}^2} \qquad S_2 \equiv \sum_j S_2^j = \sum_{ij}^{(S)} \frac{\omega_i^2}{\sigma_{ij}^2}$$

$$S_3 \equiv \sum_j t_j S_m^j = \sum_{ij}^{(S)} \frac{t_j}{w_i \sigma_{ij}^2}$$

$$S_4 \equiv \sum_j t_j S_0^j = \sum_{ij}^{(S)} \frac{t_j}{\sigma_{ij}^2}$$

$$S_5 \equiv \sum_j t_j S_1^j = \sum_{ij}^{(S)} \frac{\omega_i t_j}{\sigma_{ij}^2}$$

$$S_6 \equiv \sum_j t_j S_2^j = \sum_{ij}^{(S)} \frac{\omega_i^2 t_j}{\sigma_{ij}^2}$$

$$S_7 \equiv \sum_j t_j^2 S_0^j = \sum_{ij}^{(S)} \frac{t_j^2}{\sigma_{ij}^2}$$

$$S_8 \equiv \sum_j t_j^2 S_1^j = \sum_{ij}^{(S)} \frac{\omega_i t_j^2}{\sigma_{ij}^2}$$

$$S_9 \equiv \sum_j t_j^2 S_2^j = \sum_{ij}^{(S)} \frac{\omega_i^2 t_j^2}{\sigma_{ij}^2}$$

The following expressions contain the interferometer phase:

$$S_a^j \equiv \sum_i^{(S)} \frac{\phi_{ij}}{\sigma_{ij}^2} \qquad S_a \equiv \sum_j S_a^j = \sum_{ij}^{(S)} \frac{\phi_{ij}}{\sigma_{ij}^2} \qquad [C.2]$$

$$S_b^j \equiv \sum_i^{(S)} \frac{\omega_i \phi_{ij}}{\sigma_{ij}^2} \qquad S_b \equiv \sum_j S_b^j = \sum_{ij}^{(S)} \frac{\omega_i \phi_{ij}}{\sigma_{ij}^2}$$

$$S_c \equiv \sum_j t_j S_b^j = \sum_{ij}^{(S)} \frac{\omega_i t_j \phi_{ij}}{\sigma_{ij}^2}$$

The following combinations are defined in terms of the summations given by [C.1]:

$$S_{02} \equiv S_0 S_2 - S_1^2 \qquad [C.3]$$

$$S_{06} \equiv S_0 S_6 - S_1 S_5$$

$$S_{16} \equiv S_1 S_6 - S_2 S_5$$

$$S_{09} \equiv S_0 S_9 - S_5^2$$

$$S_{19} \equiv S_1 S_9 - S_5 S_6$$

$$S_{29} \equiv S_2 S_9 - S_6^2.$$

More complicated combinations are given by

$$S_{d0} \equiv +\mathrm{Det}\begin{vmatrix} S_0 & S_1 & S_5 \\ S_1 & S_2 & S_6 \\ S_5 & S_6 & S_9 \end{vmatrix} = S_5 S_{16} - S_6 S_{06} + S_9 S_{02} \qquad [C.4]$$

$$S_{d1} \equiv +\mathrm{Det}\begin{vmatrix} S_3 & S_4 & S_7 \\ S_1 & S_2 & S_6 \\ S_5 & S_6 & S_9 \end{vmatrix} = S_3 S_{29} - S_4 S_{19} + S_7 S_{16}$$

$$S_{d2} \equiv -\mathrm{Det}\begin{vmatrix} S_0 & S_1 & S_5 \\ S_3 & S_4 & S_7 \\ S_5 & S_6 & S_9 \end{vmatrix} = S_3 S_{19} - S_4 S_{09} + S_7 S_{06}$$

$$S_{d3} \equiv +\mathrm{Det}\begin{vmatrix} S_0 & S_1 & S_5 \\ S_1 & S_2 & S_6 \\ S_3 & S_4 & S_7 \end{vmatrix} = S_3 S_{16} - S_4 S_{06} + S_7 S_{02}$$

$$S_{d4} \equiv +\mathrm{Det}\begin{vmatrix} S_m & S_0 & S_4 \\ S_1 & S_2 & S_6 \\ S_5 & S_6 & S_9 \end{vmatrix} = S_m S_{29} - S_0 S_{19} + S_4 S_{16}$$

$$S_{d5} \equiv -\mathrm{Det}\begin{vmatrix} S_0 & S_1 & S_5 \\ S_m & S_0 & S_4 \\ S_5 & S_6 & S_9 \end{vmatrix} = S_m S_{19} - S_0 S_{09} + S_4 S_{06}$$

$$S_{d6} \equiv +\mathrm{Det}\begin{vmatrix} S_0 & S_1 & S_5 \\ S_1 & S_2 & S_6 \\ S_m & S_0 & S_4 \end{vmatrix} = S_m S_{16} - S_0 S_{06} + S_4 S_{02}$$

When each of the quantities above is normalized to the same units by using the appropriate factors of ω_0 and t_0, it is found that

$$2\frac{S_{d0}}{\omega_0^2} \approx \frac{S_{d1}}{t_0\omega_0} \approx \frac{S_{d2}}{t_0} \approx 2S_{d3} \approx \frac{S_{d4}}{\omega_0} \approx 2S_{d5} \qquad [C.5]$$

and S_{d6}, in these normalized units, is five to six orders of magnitude smaller than the above variables. With these definitions, all the above quantities are positive except S_{d6}, which can have either sign.

The following vectors can be defined

$$\vec{S}_{V1} \equiv (S_0, S_1, S_5) \qquad [C.6]$$
$$\vec{S}_{V2} \equiv (S_1, S_2, S_6)$$
$$\vec{S}_{V3} \equiv (S_5, S_6, S_9)$$
$$\vec{S}_{V4} \equiv (S_3, S_4, S_7)$$
$$\vec{S}_{V5} \equiv (S_m, S_0, S_4)$$

$$\vec{S}_{S1} \equiv (S_{29}, -S_{19}, S_{16}) \qquad [C.7]$$
$$\vec{S}_{S2} \equiv (-S_{19}, S_{09}, -S_{06})$$
$$\vec{S}_{S3} \equiv (S_{16}, -S_{06}, S_{02})$$

$$\vec{S}_{\phi} \equiv (S_a, S_b, S_c). \qquad [C.8]$$

With these definitions, the following hold:

$$\begin{array}{lll} \vec{S}_{S1} \cdot \vec{S}_{V1} = S_{d0} & \vec{S}_{S2} \cdot \vec{S}_{V1} = 0 & \vec{S}_{S3} \cdot \vec{S}_{V1} = 0 \\ \vec{S}_{S1} \cdot \vec{S}_{V2} = 0 & \vec{S}_{S2} \cdot \vec{S}_{V2} = S_{d0} & \vec{S}_{S3} \cdot \vec{S}_{V2} = 0 \\ \vec{S}_{S1} \cdot \vec{S}_{V3} = 0 & \vec{S}_{S2} \cdot \vec{S}_{V3} = 0 & \vec{S}_{S3} \cdot \vec{S}_{V3} = S_{d0} \\ \vec{S}_{S1} \cdot \vec{S}_{V4} = S_{d1} & \vec{S}_{S2} \cdot \vec{S}_{V4} = -S_{d2} & \vec{S}_{S3} \cdot \vec{S}_{V4} = S_{d3} \\ \vec{S}_{S1} \cdot \vec{S}_{V5} = S_{d4} & \vec{S}_{S2} \cdot \vec{S}_{V5} = -S_{d5} & \vec{S}_{S3} \cdot \vec{S}_{V5} = S_{d6}. \end{array} \qquad [C.9]$$

Definitions containing t_0 are:

$$S_{t1} \equiv S_{06} - t_0\, S_{02} \qquad [C.10]$$
$$S_{t2} \equiv S_{09} - t_0\, S_{06}$$
$$S_{t3} \equiv S_{19} - t_0\, S_{16}$$
$$S_{t0} \equiv S_{t2} - t_0\, S_{t1}$$
$$= S_{09} - 2\, t_0\, S_{06} + t_0^2\, S_{02}.$$

The following identities are useful for simplifying expressions:

$$
\begin{aligned}
S_{02}S_{09} - S_{06}^2 &= S_0 S_{d0} \\
S_{02}S_{19} - S_{06}S_{16} &= S_1 S_{d0} \\
S_{02}S_{29} - S_{16}^2 &= S_2 S_{d0} \\
S_{06}S_{19} - S_{09}S_{16} &= S_5 S_{d0} \\
S_{06}S_{29} - S_{16}S_{19} &= S_6 S_{d0} \\
S_{09}S_{29} - S_{19}^2 &= S_9 S_{d0}.
\end{aligned}
\qquad [C.11]
$$

The following are defined for the consider analysis in section 17 (see [5.27] for the t^* definitions):

$$
\vec{S}_{t1} \equiv \left(\sum_{ij}^{(S)} \frac{t_{1i}^*}{\omega_i \sigma_{ij}^2}, \sum_{ij}^{(S)} \frac{t_{1i}^*}{\sigma_{ij}^2}, \sum_{ij}^{(S)} \frac{t_j t_{1i}^*}{\sigma_{ij}^2} \right) \qquad [C.12]
$$

$$
\vec{S}_{t2} \equiv \left(\sum_{ij}^{(S)} \frac{t_{2i}^*}{\omega_i \sigma_{ij}^2}, \sum_{ij}^{(S)} \frac{t_{2i}^*}{\sigma_{ij}^2}, \sum_{ij}^{(S)} \frac{t_j t_{2i}^*}{\sigma_{ij}^2} \right)
$$

$$
\vec{S}_{t3} \equiv \left(\sum_{ij}^{(S)} \frac{\omega_i t_{3i}^*}{\sigma_{ij}^2}, \sum_{ij}^{(S)} \frac{\omega_i^2 t_{3i}^*}{\sigma_{ij}^2}, \sum_{ij}^{(S)} \frac{\omega_i^2 t_j t_{3i}^*}{\sigma_{ij}^2} \right)
$$

$$
\vec{S}_{t5} \equiv \left(\sum_{ij}^{(S)} \frac{\omega_i t_{5i}^*}{\sigma_{ij}^2}, \sum_{ij}^{(S)} \frac{\omega_i^2 t_{5i}^*}{\sigma_{ij}^2}, \sum_{ij}^{(S)} \frac{\omega_i^2 t_j t_{5i}^*}{\sigma_{ij}^2} \right)
$$

$$
\vec{S}_{t6} \equiv \left(\sum_{ij}^{(S)} \frac{\omega_i t_{6i}^*}{\sigma_{ij}^2}, \sum_{ij}^{(S)} \frac{\omega_i^2 t_{6i}^*}{\sigma_{ij}^2}, \sum_{ij}^{(S)} \frac{\omega_i^2 t_j t_{6i}^*}{\sigma_{ij}^2} \right)
$$

$$
\vec{S}_{Vk} \equiv \left(\sum_{ij}^{(S)} \frac{k_j^r}{\omega_i \sigma_{ij}^2}, \sum_{ij}^{(S)} \frac{k_j^r}{\sigma_{ij}^2}, \sum_{ij}^{(S)} \frac{t_j k_j^r}{\sigma_{ij}^2} \right)
$$

$$
\vec{S}_{V\tau} \equiv \left(\sum_{ij}^{(S)} \frac{\omega_i \tau_j^{tr}}{\sigma_{ij}^2}, \sum_{ij}^{(S)} \frac{\omega_i^2 \tau_j^{tr}}{\sigma_{ij}^2}, \sum_{ij}^{(S)} \frac{\omega_i^2 t_j \tau_j^{tr}}{\sigma_{ij}^2} \right)
$$

Several simplifying expressions are defined as:

$$
\begin{aligned}
S_{k\phi} &\equiv (S_{d4} - \omega_0 S_{d5} + \omega_0 t_0 S_{d6})/S_{d0} \\
S_{k\tau} &\equiv (S_{d5} - t_0 S_{d6})/S_{d0} \\
S_{k\dot{\tau}} &\equiv S_{d6}/S_{d0} \\
S_{k\tau^p} &\equiv S_{k\phi}/\omega_0
\end{aligned}
\qquad [C.13]
$$

$$
\begin{aligned}
S_{k^*\phi} &\equiv S_{k\phi} + \Delta\omega_0/\omega_{S\tau}^{*2} \\
S_{k^*\tau} &\equiv S_{k\tau} - 1/\omega_{S\tau}^{*2} \\
S_{k^*\dot{\tau}} &\equiv S_{k\dot{\tau}} \\
S_{k^*\tau^p} &\equiv S_{k^*\phi}/\omega_0
\end{aligned}
$$

$$
\begin{aligned}
S_{\dot{k}\phi} &\equiv [(S_{d1} - \omega_0 S_{d2} + \omega_0 t_0 S_{d3}) - t_0(S_{d4} - \omega_0 S_{d5} + \omega_0 t_0 S_{d6})]/S_{d0} \\
S_{\dot{k}\tau} &\equiv [(S_{d2} - t_0 S_{d3}) - t_0(S_{d5} - t_0 S_{d6})]/S_{d0} \\
S_{\dot{k}\dot{\tau}} &\equiv (S_{d3} - t_0 S_{d6})/S_{d0} \\
S_{\dot{k}\tau^p} &\equiv S_{\dot{k}\phi}/\omega_0
\end{aligned}
$$

$$
\begin{aligned}
S_{\dot{k}^*\phi} &\equiv \vec{S}_{t1} \cdot (\vec{S}_{S1} + \omega_0 \vec{S}_{S2} + \omega_0 t_0 \vec{S}_{S3})/S_{d0} \\
S_{\dot{k}^*\tau} &\equiv -\vec{S}_{t1} \cdot (\vec{S}_{S2} + t_0 \vec{S}_{S3})]/S_{d0} \\
S_{\dot{k}^*\dot{\tau}} &\equiv (\vec{S}_{t1} \cdot \vec{S}_{S3})/S_{d0} \\
S_{\dot{k}^*\tau^p} &\equiv S_{\dot{k}^*\phi}/\omega_0
\end{aligned}
$$

$$
\begin{aligned}
S_{a\phi} &\equiv (\omega_0^2 \vec{S}_{t2} - \vec{S}_{t3} - \vec{S}_{t5} + \vec{S}_{t6} - \vec{S}_{Vk} + \vec{S}_{V\tau}) \cdot (\vec{S}_{S1} + \omega_0 \vec{S}_{S2} + \omega_0 t_0 \vec{S}_{S3})/S_{d0} \\
S_{a\tau} &\equiv (\omega_0^2 \vec{S}_{t2} - \vec{S}_{t3} - \vec{S}_{t5} + \vec{S}_{t6} - \vec{S}_{Vk} + \vec{S}_{V\tau}) \cdot (\vec{S}_{S2} + t_0 \vec{S}_{S3})/S_{d0} \\
S_{a\dot{\tau}} &\equiv (\omega_0^2 \vec{S}_{t2} - \vec{S}_{t3} - \vec{S}_{t5} + \vec{S}_{t6} - \vec{S}_{Vk} + \vec{S}_{V\tau}) \cdot \vec{S}_{S3}/S_{d0} \\
S_{a\tau^p} &\equiv S_{a\phi}/\omega_0.
\end{aligned}
$$

The following are simplifying ratios:

$$R_{\dot{k}\tau} \equiv \left(\frac{X_{k\tau}S_{\dot{k}\tau} - S_{k\tau}X_{\dot{k}\tau}}{X_{k\tau} - S_{k\tau}}\right) \qquad R_{\dot{k}k} \equiv \left(\frac{X_{\dot{k}\tau} - S_{\dot{k}\tau}}{X_{k\tau} - S_{k\tau}}\right) \qquad [C.14]$$

$$R_{\dot{k}^*\tau} \equiv \left(\frac{X_{k\tau}S_{\dot{k}^*\tau} - S_{k\tau}X_{\dot{k}^*\tau}}{X_{k\tau} - S_{k\tau}}\right) \qquad R_{\dot{k}^*k} \equiv \left(\frac{X_{\dot{k}^*\tau} - S_{\dot{k}^*\tau}}{X_{k\tau} - S_{k\tau}}\right)$$

$$R_{a\tau} \equiv \left(\frac{X_{k\tau}S_{a\tau} - S_{k\tau}X_{a\tau}}{X_{k\tau} - S_{k\tau}}\right) \qquad R_{ak} \equiv \left(\frac{X_{a\tau} - S_{a\tau}}{X_{k\tau} - S_{k\tau}}\right)$$

$$R_{k\dot{\tau}} \equiv \left(\frac{X_{\dot{k}\dot{\tau}}S_{k\dot{\tau}} - S_{\dot{k}\dot{\tau}}X_{k\dot{\tau}}}{X_{\dot{k}\dot{\tau}} - S_{\dot{k}\dot{\tau}}}\right) \qquad R_{kk} \equiv \left(\frac{X_{k\dot{\tau}} - S_{k\dot{\tau}}}{X_{\dot{k}\dot{\tau}} - S_{\dot{k}\dot{\tau}}}\right)$$

$$R_{\dot{k}^*\dot{\tau}} \equiv \left(\frac{X_{\dot{k}\dot{\tau}}S_{\dot{k}^*\dot{\tau}} - S_{\dot{k}\dot{\tau}}X_{\dot{k}^*\dot{\tau}}}{X_{\dot{k}\dot{\tau}} - S_{\dot{k}\dot{\tau}}}\right) \qquad R_{\dot{k}^*k} \equiv \left(\frac{X_{\dot{k}^*\dot{\tau}} - S_{\dot{k}^*\dot{\tau}}}{X_{\dot{k}\dot{\tau}} - S_{\dot{k}\dot{\tau}}}\right)$$

$$R_{a\dot{\tau}} \equiv \left(\frac{X_{\dot{k}\dot{\tau}}S_{a\dot{\tau}} - S_{\dot{k}\dot{\tau}}X_{a\dot{\tau}}}{X_{\dot{k}\dot{\tau}} - S_{\dot{k}\dot{\tau}}}\right) \qquad R_{ak} \equiv \left(\frac{X_{a\dot{\tau}} - S_{a\dot{\tau}}}{X_{k\dot{\tau}} - S_{k\dot{\tau}}}\right)$$

$$R_{\dot{k}\tau^p} \equiv \left(\frac{X_{k\phi}S_{\dot{k}\phi} - S_{k\phi}X_{\dot{k}\phi}}{X_{k\phi} - S_{k\phi}}\right) \qquad R_{\dot{k}k^p} \equiv \left(\frac{X_{\dot{k}\phi} - S_{\dot{k}\phi}}{X_{k\phi} - S_{k\phi}}\right)$$

$$R_{\dot{k}^*\tau^p} \equiv \left(\frac{X_{k\phi}S_{\dot{k}^*\phi} - S_{k\phi}X_{\dot{k}^*\phi}}{X_{k\phi} - S_{k\phi}}\right) \qquad R_{\dot{k}^*k^p} \equiv \left(\frac{X_{\dot{k}^*\phi} - S_{\dot{k}^*\phi}}{X_{k\phi} - S_{k\phi}}\right)$$

$$R_{a\tau^p} \equiv \left(\frac{X_{k\phi}S_{a\phi} - S_{k\phi}X_{a\phi}}{X_{k\phi} - S_{k\phi}}\right) \qquad R_{ak^p} \equiv \left(\frac{X_{a\phi} - S_{a\phi}}{X_{k\phi} - S_{k\phi}}\right)$$

$$Q_{k^*k} \equiv 1 - \left(\frac{\omega_{X\tau}^{*2} - \omega_{S\tau}^{*2}}{\omega_{X\tau}^2 - \omega_{S\tau}^2}\right)\left(\frac{\omega_{X\tau}^2\omega_{S\tau}^2}{\omega_{X\tau}^{*2}\omega_{S\tau}^{*2}}\right)$$

Appendix D

Variable Definitions

The variables used in this report, except for those found in the appendices, are given below along with their definitions. The equation number next to each variable gives the definition or first occurrence of the given variable; a − or + preceding the equation number indicates the variable is defined just before or after the indicated equation, respectively. Variables are ordered alphabetically by the primary symbol, with Roman characters first, followed by Greek symbols.

a_i	−[10.4]	Coefficient i (i between 1 and 5) for 2-D parabolic fit
A	−[2.15]	Generic phasor amplitude
A_i	[15.6]	Phasor amplitude of time-bin point i
A_{ij}	+[14.17]	Phasor amplitude of bin i at time point j
A'_{ij}	[14.17]	Bandpass corrected phasor amplitude of bin i at time point j
$\langle A \rangle$	[2.16b]	Mean phasor amplitude
A_{t_i}	[2.19]	Station i's tone phasor amplitude
$\mathcal{A}$	[14.4]	Design matrix for least-squares analysis
A_b	[6.1]	Band amplitude
$\check{A}_b$	[15.2]	Trial band amplitude
A_i^{ft}	[7.3]	Model FFT phasor amplitude
A^m	[10.4]	FFT phasor amplitude
A^t	[7.1]	Test amplitude
A_k^t	[7.2]	Test amplitude for phase rate k
$\mathcal{A}_I$	[15.9]	Imaginary part of design matrix $\mathcal{A}$
$\mathcal{A}_R$	[15.9]	Real part of design matrix $\mathcal{A}$

b	[2.1]	Bin index
B	[2.8]	Average blanking counts: $B \equiv (B_x + B_y)/2$
$\hat{B}$	$-$[2.12]	Average Block II blanking counts: $\hat{B} \equiv (\hat{B}_x + \hat{B}_y)/2$
B_i	+[14.17]	Bandpass amplitude correction for channel bin i
B_x	[2.5]	Real (cosine) blanking counts
B_y	[2.5]	Imaginary (sine) blanking counts
$\hat{B}_x$	$-$[2.12]	Real (cosine) Block II blanking counts
$\hat{B}_y$	$-$[2.12]	Imaginary (sine) Block II blanking counts
$\hat{B}_I$	[12.2]	Average integrated Block II blanking counts
c	[16.1]	Speed of light = 2.9979×10^8 m/sec
$\hat{C}$	[2.13]	Like-sign cosine (real) Block II counts in bin mode
$\hat{C}_I$	[12.1]	Integrated like-sign cosine (real) Block II counts in bin mode
$\hat{C}_{t_i}$	[4.1]	Like-sign tone cosine (real) Block II counts for station i
$C_{S\tau}$	[17.4]	S-band delay weight for dual frequency calibration
$C_{X\tau}$	[17.4]	X-band delay weight for dual frequency calibration
$C_{S\dot{\tau}}$	[17.10]	S-band phase delay rate weight for dual frequency calibration
$C_{X\dot{\tau}}$	[17.10]	X-band phase delay rate weight for dual frequency calibration
$C_{S\tau^p}$	[17.14]	S-band phase delay weight for dual frequency calibration
$C_{X\tau^p}$	[17.14]	X-band phase delay weight for dual frequency calibration
C_{Sk}	[17.7]	S-band Total Electron Content (TEC) weight
C_{Xk}	[17.7]	X-band TEC weight
$C_{S\dot{k}}$	[17.11]	S-band TEC rate weight
$C_{X\dot{k}}$	[17.11]	X-band TEC rate weight

C_{Sk^P}	[17.15]	S-band TEC weight (from phase delay)
C_{Xk^P}	[17.15]	X-band TEC weight (from phase delay)
D_i	[5.4]	Weighted phase average for bin i
$\bar{D}_i$	[5.7]	Weighted phase average for bin i after model subtraction
E_i	[5.4]	Time weighted phase average for bin i
$\bar{E}_i$	[5.7]	Time weighted phase average for bin i after model subtraction
$\mathcal{F}$	[14.3]	Matrix of observations for least-squares analysis
$\mathcal{F}_R$	[15.9]	Real part of observation matrix $\mathcal{F}$
$\mathcal{F}_I$	[15.9]	Imaginary part of observation matrix $\mathcal{F}$
F_S	[18.7]	Fractional number of cycles to connect phase
F_i	[5.24]	Special summation involving residual TEC
G_i	[5.24]	Special summation involving residual TEC
h	[8.2]	Ratio used for phasor interpolation
i		Index, often used to index bin numbers
I	[2.11]	Invalid counts
$\hat{I}$	−[2.12]	Block II invalid counts
$\hat{I}_I$	[12.1]	Block II integrated invalid counts
$\hat{I}_{t_i}$	[2.18]	Block II tone invalid counts for station i
I_0	[2.16]	Modified Bessel function of order zero
I_1	[2.16]	Modified Bessel function of order one
j		Index, often used to index time points
k_j	[5.20]	Proportional to baseline TEC at time t_j
$\bar{k}$	[5.21]	Average k_j: proportional to scan TEC

$\bar{\dot{k}}$	[5.21]	Averaged k_j rate: proportional to scan TEC rate
k_j^r	[5.21]	Residual of k_j after subtracting linear model
$\bar{k}^*$	[5.26]	Average k_j for the MPC scan
$\bar{\dot{k}}^*$	[5.26]	Averaged k_j rate for the MPC scan
$k(t)$	[17.1]	Proportional to baseline TEC at time t
$\dot{k}(t)$	[17.2c]	Proportional to baseline TEC rate at time t
k_s	$-$[17.1]	Proportional to station Total Electron Content (TEC)
$\bar{k}_{S/X}$	[17.7]	Estimate of $\bar{k}$ using S and X-band BWS delays
$\bar{\dot{k}}_{S/X}$	[17.11]	Estimate of $\bar{\dot{k}}$ using S and X-band phase delay rates
$\hat{k}$	[16.1]	Unit vector in direction of wave propagation
l	[2.1]	Lag index
L_x	[2.5]	Real (cosine) like-sign counts
L_y	[2.5]	Imaginary (sine) like-sign counts
$\hat{L}_x$	[2.12]	Real (cosine) Block II like-sign counts
$\hat{L}_y$	[2.12]	Imaginary (sine) Block II like-sign counts
M	+[2.12]	Block II normalization factor
M_i	[5.24]	Special summation involving residual tropospheric delay
M_{t_i}	+[4.1]	Block II tone normalization factor for station i
$\vec{M}_i$	[15.1]	Model phasor for ith time-bin point
$\check{\vec{M}}_i$	[15.3]	Trial model phasor for ith time-bin point
n_b	[10.1]	Number of bins in band
n_f	[10.1]	Number of BWS delay points in FFT
n_r	[10.1]	Number of time points

n_t	[10.1]	Number of phase delay rate points in FFT
N	$-$[2.11]	Number of bits summed per dump
N_i	[5.24]	Special summation involving residual tropospheric delay
N_L	[2.1]	Number of lags per channel
N_I	[12.1]	Number of bits summed per integrated dump
N_S	[17.22]	Number of S-band cycles needed for phase connection
N_X	[17.22]	Number of X-band cycles needed for phase connection
O	[16.3]	Combination of terms of this order
$P(A)$	[2.16a]	Phasor amplitude probability distribution
$P(\phi)$	[2.15a]	Phasor phase probability distribution
$\vec{P}_{ij}^{m}$	[6.1]	Phasor model for bin i at time point j
r_e	$-$[17.1]	Classical electron radius $= 2.8179 \times 10^{-15}$ m
$\vec{r}_i(t)$	[16.1]	Location of station i at time t
R	$-$[2.16]	Location of phasor probability distribution's center in polar coordinates: (R, ϕ^R)
S_i	[5.4]	Special MPC sum for bin i
$\hat{S}$	[2.13]	Like-sign sine (imaginary) Block II counts in bin mode
$\hat{S}_I$	[12.1]	Integrated like-sign sine (imaginary) Block II counts in bin mode
$\hat{S}_{t_i}$	[4.1]	Like-sign tone sine (imaginary) Block II counts for station i
t		Time
t_0	[3.1]	Scan reference time
t_1	[10.2]	Time tag of first time point
t_j	[3.1]	Time tag of jth time point
t_j^b	[2.3]	Time tag of jth bit

t_c	[10.2]	Time between adjacent time points
t_0'	[12.3]	Recalculated scan reference time
t_{ni}^*	[5.27]	Special time expression number n for bin i used in MPC analysis
T_i	[5.4]	Special MPC sum for bin i
T_{ij}	[10.1]	Transformed (by 2-D FFT) phasor for ith phase delay rate point and jth BWS delay point
U_x	[2.5]	Real (cosine) unlike-sign counts
U_y	[2.5]	Imaginary (sine) unlike-sign counts
U_i	[5.4]	Special MPC sum for bin i
V	[2.3]	Valid counts
V_I	[12.2]	Integrated valid counts
V_{t_i}	[2.17]	Valid tone counts for station i
$\mathcal{W}$	[14.5]	Weight matrix for least-squares analysis (inverse of observation covariance)
x_i	[10.3]	Real variable corresponding to integer phasor index i
x_j	[10.3]	Real variable corresponding to integer phasor index j
$\bar{x}_i$	[10.3]	Linear function of x_i
$\bar{x}_j$	[10.3]	Linear function of x_j
$\mathcal{X}$	[14.2]	Parameter matrix for least-squares analysis
$\hat{\mathcal{X}}$	[14.2]	Matrix of minimum variance, unbiased estimates of parameters in $\mathcal{X}$ for least-squares analysis
Z_x	+[2.12]	DC bias for Block II cosine accumulator
Z_i	[5.11]	Combination of special MPC sums for bin i
$\beta_l(t_j^b)$	[2.3]	Lag l's single-bit correlation coefficient at bit time t_j^b
θ	[2.15c]	Dummy phase variable used for integration

ν	[4.3]	Calibrated variance scale factor
$\vec{\rho}_b(t)$	[2.1]	Frequency-domain complex correlation coefficient for bin b at time t
$\vec{\rho}_l(t)$	[2.1]	Lag-domain complex correlation coefficient for lag l at time t
$\vec{\rho}_{t_i}(t)$	[2.17]	Tone complex correlation coefficient for station i at time t
$\vec{\rho}$	[8.2]	Generic data phasor
ρ_x	[2.13]	X-component (also real-component or cosine-component) of $\vec{\rho}_b$
ρ_y	[2.13]	Y-component (also imaginary-component or sine-component) of $\vec{\rho}_b$
$\vec{\rho}_1$	[8.2]	Generic data phasor
$\vec{\rho}_2$	[8.2]	Generic data phasor
$\vec{\rho}_I$	[12.1]	Integrated complex correlation coefficient
$\vec{\rho}_{ij}$	[10.1]	Complex correlation coefficient $\vec{\rho}_b$ for bin i at time point j
$\vec{\rho}^{\,c}_{ij}$	[11.1]	Counterrotated complex correlation coefficient for bin i at time point j (after a priori model is removed)
$\vec{\rho}^{\,cc}$	[14.18]	Counterrotated complex correlation coefficient for bin i at time point j (after residual model is removed)
$\rho_{\phi\tau}$	[14.10d]	Phase-BWS delay correlation coefficient
$\rho_{\phi\dot{\tau}}$	[14.10e]	Phase-phase delay rate correlation coefficient
$\rho_{\tau\dot{\tau}}$	[14.10f]	BWS delay-BWS delay correlation coefficient
σ^2	[2.9]	Variance of either component of complex correlation coefficient
σ_I^2	[12.2]	Variance of either integrated phasor component
$\sigma_{t_i}^2$	[2.17]	Variance of either tone phasor component
σ_ϕ^2	[2.15c]	Variance of phasor phase
$\sigma_{\phi_i}^2$	[14.5]	Variance of phasor phase for ith time-frequency point
$\sigma_{\phi_{ij}}^2$	[3.1]	Variance of phasor phase for bin i at time point j

σ_A^2	[2.16c]	Variance of phasor amplitude
$\sigma_{A_{ij}}^2$	+[14.7]	Variance of phasor amplitude for bin i at time point j
$\sigma_{A_{ij}}^{2\prime}$	[14.7]	Variance of bandpass corrected phasor amplitude for bin i at time point j
$\sigma_{A_b}^2$	[14.17]	Variance of band amplitude
$\sigma_{\phi_0}^2$	[14.10a]	Variance of ϕ_0 parameter
σ_τ^2	[14.10b]	Variance of τ parameter
$\sigma_{\dot{\tau}}^2$	[14.10c]	Variance of $\dot{\tau}$ parameter
$\sigma_{\tau_{S/X}}^2$	[17.33a]	Variance of S/X BWS delay
$\sigma_{\dot{\tau}_{S/X}}^2$	[17.33b]	Variance of S/X phase delay rate
$\sigma_{\bar{k}_{S/X}}^2$	[17.33c]	Variance of S/X corrected $\bar{k}$
$\sigma_{\dot{\bar{k}}_{S/X}}^2$	[17.33d]	Variance of S/X corrected $\dot{\bar{k}}$
$\sigma_{F_S}^2$	[18.9]	Variance of F_S
τ	[5.13]	BWS delay for generic band
τ^a	[6.2]	A priori BWS delay
$\tau^{a\prime}$	[12.3]	A priori BWS delay corresponding to recalculated t_0 and ω_0
τ^r	[14.1]	Residual BWS delay
τ_b	[16.6]	Symmetric baseline delay
τ_b^r	[16.1]	Retarded baseline delay
τ_b^m	[16.6]	Model symmetric baseline delay
τ_b^{mr}	[16.10]	Model retarded baseline delay
τ_{s_i}	[16.7]	Symmetric station delay for station i
$\tau_{s_i}^m$	[16.2]	Model symmetric station delay for station i
$\tau_{s_i}^{mr}$	[16.2]	Model retarded station delay for station i

τ_S	[17.3]	S-band BWS delay
τ_X	[17.4]	X-band BWS delay
$\bar{\tau}$	[17.3]	BWS delay without media, instrumental or MPC effects
$\bar{\tau}^t$	[5.21]	Scan averaged tropospheric delay
$\bar{\tau}^{t*}$	[5.26]	Scan averaged tropospheric delay for MPC scan
$\check{\tau}$	[15.2]	Trial BWS delay
$\tilde{\tau}$	[17.22]	Total BWS delay without media, instrumental or MPC effects
τ^*	[5.19]	BWS delay from MPC scan
τ^{cp}	[17.2a]	BWS delay change induced by charged particle effects
τ_p^{cp}	[17.2b]	Phase delay change induced by charged particle effects
τ_S^p	[18.1]	S-band phase delay
$\tilde{\tau}_S^p$	[18.3]	S-band phase delay without media, instrumental, or MPC effects
$\tau_{S/X}$	[17.4]	S/X corrected BWS delay
τ_j^t	[5.20]	Tropospheric delay at time point j
τ_j^{tr}	[5.21]	Residual tropospheric delay at time point j after subtracting linear model
τ^{lt}	[14.20]	Linear tropospheric model delay
τ_{BSA}	[5.12]	Band-averaged bitstream alignment (BSA) delay
τ_{BSA}^*	[5.26]	Band-averaged bitstream alignment (BSA) delay for the MPC scan
$\bar{\tau}_{\mathrm{BSA}}^*$	[5.28]	Band-averaged bitstream alignment (BSA) delay for the MPC scan without dispersive effects
τ_{cl}^*	[5.30]	Clock error for given band, assumed constant for all scans including MPC scan
$\tau_{\mathrm{cl(S)}}^*$	[17.20]	S-band clock error, assumed constant for all scans including MPC scan
$\tau_{\mathrm{cl(X)}}^*$	[17.21]	X-band clock error, assumed constant for all scans including MPC scan

$\tau^{p*}_{\mathrm{cl(S)}}$	[18.5]	S-band clock-like term used in phase connection, assumed constant for all scans including MPC scan
τ^{*}_{cor}	[5.28]	Small delay correction term
$\bar{\tau}^{m}_{\mathrm{Mod}}$	[18.6]	Modest model delay
$\bar{\tau}^{p}_{\mathrm{Fit(S)}}$	[18.2]	S-band phase delay calculated by Fit
$\Delta\tau^{*}_{\mathrm{cl}}$	[17.24]	Difference between S and X-band clock errors
$\dot{\tau}^{\mathrm{mpc}}$	[5.1]	Band phase delay rate estimate for MPC analysis
$\dot{\tau}$	[5.13]	Phase delay rate
$\dot{\tau}^{a}$	[6.2]	A priori phase delay rate
$\dot{\tau}^{a\prime}$	[12.3]	A priori phase delay rate corresponding to recalculated t_0 and ω_0
$\dot{\tau}^{r}$	[14.1]	Residual phase delay rate
$\dot{\tau}_S$	[17.10]	S-band phase delay rate
$\dot{\tau}_X$	[17.10]	X-band phase delay rate
$\dot{\tau}_{S/X}$	[17.10]	S/X corrected phase delay rate
$\overset{\mathrm{v}}{\dot{\tau}}$	[15.2]	Trial phase delay rate
$\tilde{\dot{\tau}}$	[17.22]	Total phase delay rate without media, instrumental or MPC effects
$\bar{\dot{\tau}}$	[17.22]	Phase delay rate without media, instrumental or MPC effects
$\bar{\dot{\tau}}^{t}$	[5.21]	Scan averaged tropospheric delay rate
$\bar{\dot{\tau}}^{t*}$	+[17.19]	Scan averaged tropospheric delay rate for the MPC scan
$\dot{\tau}^{\mathrm{cp}}_{p}$	[17.2c]	Phase delay rate change induced by charged particle effects
ϕ	−[2.15]	Generic phasor phase
$\langle\phi\rangle$	[2.15b]	Mean phasor phase
ϕ_{t_i}	[4.2]	Tone phasor phase for station i

ϕ^R	−[2.16]	Location of phasor probability distribution's center in polar coordinates: (R, ϕ^R)
ϕ_{ij}	[5.2]	Phase for bin i at time point j
$\bar{\phi}_{ij}$	[5.6]	Counterrotated phase for MPC calibration for bin i at time point j
ϕ'_{ij}	[5.18]	MPC corrected phase for bin i at time point j
ϕ^a_{ij}	[6.2]	A priori phase model for bin i at time point j
$\phi^{a\,\prime}_{ij}$	[12.3]	A priori phase model, corresponding to recalculated t_0 and ω_0, for bin i at time point j
ϕ^r_{ij}	[14.1]	Residual phase model for bin i at time point j
ϕ_0	[5.13]	Band phase
ϕ^a_0	[6.2]	A priori band phase
$\phi^{a\prime}_0$	[12.3]	A priori band phase corresponding to recalculated t_0 and ω_0
ϕ^r_0	[14.1]	Residual band phase
ϕ^*_0	[5.19]	Band phase for MPC scan
$\check{\phi}_0$	[15.2]	Trial band phase
ϕ_i	[14.3]	Phasor phase for ith time-frequency point
ϕ^*_i	[5.12]	Bin phase offsets for bin i; output of MPC analysis
ϕ^b_i	[5.6]	Model residual fringe phase for bin i
$\check{\phi}_i$	[15.2]	Trial phasor phase for ith time-frequency point
ϕ_{0S}	[17.22]	Total S-band phase
ϕ_{0X}	[17.22]	Total X-band phase
ϕ^*_{0S}	[17.20]	Total S-band phase from MPC scan
ϕ^*_{0X}	[17.21]	Total X-band phase from MPC scan
$\tilde{\phi}_{0S}$	[17.20]	Total S-band phase without media, instrumental or MPC effects

$\tilde{\phi}_{0X}$	[17.21]	Total X-band phase without media, instrumental or MPC effects
ϕ_{ij}^{m}	[5.20]	Model phase for bin i at time point j assuming instrumental, dispersive and tropospheric phase offsets
ϕ_{ij}^{Im}	[5.13]	Model phase for bin i at time point j assuming only instrumental phase offsets
ϕ^{lm}	$-$[7.1]	Linear model phase
ϕ_{ij}^{tm}	[14.19]	Model phase for bin i at time point j
$\phi_{\max}$	[10.2]	Phase of the maximum amplitude phasor after FFTs
ϕ_{ij}^{mpc}	[5.1]	MPC model phase for bin i at time point j
ϕ_{0i}^{mpc}	[5.1]	MPC bin i reference phase
ϕ^{cp}	[17.1]	Phase change induced by charged particle effects
ϕ_i^I	[5.13]	Instrumental phase offset for bin i
ϕ_i^{Im}	[2.3]	Model fringe phase corresponding to bit time t_j^b
$\dot{\phi}$	[8.1]	Band phase rate $\equiv \omega_0 \dot{\tau}$
φ_j	[13.1]	Bin-averaged phase for phase tracking at time j
χ^2	[5.2]	Chi-squared for MPC analysis
ψ_i	[8.1]	Rescaling scale factor
ω	$-$[17.1]	Generic observation frequency
ω_i	[3.1]	Observation frequency of bin i
ω_0	$+$[3.2]	Band reference frequency
ω_1	[10.1]	Observation frequency of lowest frequency bin in band
ω_b	[10.2]	Bandwidth of single bin (nominally 0.5 Mhz)
ω_0'	[12.3]	Recalculated band reference frequency
ω_{0S}	$+$[3.2]	Band reference frequency for S-band

ω_{0X}	[3.2]	Band reference frequency for X-band
ω_0^*	[5.26]	Band reference frequency for MPC scan
$\Delta\omega_0$	[5.32]	Difference between scan and MPC scan reference frequency $\equiv \omega_0 - \omega_0^*$
$\Delta\omega_{0S}$	[17.20]	S-Band $\Delta\omega_0$
$\bar{\omega}_{0S}$	$-$[18.4]	Common S-Band reference frequency for all scans
ω_i^b	[5.6]	Model residual fringe frequency for bin i
ω_i^f	$-$[8.1]	Residual fringe frequency for bin i
ω_τ^*	[5.28]	MPC scan's $\omega_{S\tau}$ (without the band subscript) for a generic band
$\omega_{S\tau}$	[17.3]	S-band reference frequency for S/X BWS delay calculation
$\omega_{X\tau}$	[17.4]	X-band reference frequency for S/X BWS delay calculation
$\omega_{S\dot{\tau}}$	[17.12]	S-band reference frequency for S/X phase delay rate calculation
$\omega_{X\dot{\tau}}$	[17.12]	X-band reference frequency for S/X phase delay rate calculation
$\omega_{S\tau^p}$	[17.14]	S-band reference frequency for S/X phase delay calculation
$\omega_{X\tau^p}$	[17.14]	X-band reference frequency for S/X phase delay calculation
Ω	$-$[7.1]	Trial fringe rate
Ω_k	[7.2]	Trial fringe rate number k

References

1. Sovers, O. J., and Fanselow, J. L., "Observation Model and Parameter Partials for the JPL VLBI Parameter Estimation Software 'MASTERFIT'-1987," JPL Publication 83-39, Rev. 3, Jet Propulsion Laboratory, Pasadena, California, December, 1987.

2. Thomas, J. B., "Interferometry Theory for the Block II Processor," JPL Publication 87-29, Jet Propulsion Laboratory, Pasadena, California, October, 1987.

3. O'Connor, T., "Introduction to Block II VLBI Correlator Hardware," Jet Propulsion Laboratory, Pasadena, California, April, 1989 (internal document).

4. Thomas, J. B., "System Noise Effects in VLBI Measurements," JPL Engineering Memorandum 315.6, Jet Propulsion Laboratory, Pasadena, California, October, 1976 (internal document).

5. Jacobs, C. S., "Expected Noise on Phase Calibration Tones Extracted with the Block II," JPL-IOM 335.3-91, 1991, in press (internal document).

6. Thomas, J. B., "An Analysis of Radio Interferometry with the Block 0 System," JPL Publication 81-49, Jet Propulsion Laboratory, Pasadena, California, December, 1981.

7. Sigman, E. H., "Phase Calibration Generator," TDA Progress Report 42-92, Jet Propulsion Laboratory, Pasadena, California, February 1988, pp. 89-104.

8. Hamilton, W. C., "Statistics in Physical Science," The Ronald Press Company, New York, 1964.

9. Coker, R. F., "Mark III Correlated Flux Densities on the DSN," JPL-IOM 335.6-91-028, December 1991 (internal document).

10. Abramowitz, M., and Stegun, I., "Handbook of Mathematical Functions," Dover Publications Inc., New York, 1965.

11. Thompson, A. R., Moran J. M., and Swenson, G. W., Jr., "Interferometry and Synthesis in Radio Astronomy," John Wiley and Sons, New York, 1986.